การสังเคราะห์ทินไดออกไซด์ที่มีรูพรุนขนาดเมโซโดยใช้เรซอซินอล ฟอร์มาลดิไฮด์เจลช่วย

นางสาวกรกมล บรรเจิดธีรกุล

วิทยานิพนธ์นี้เป็นส่วนหนึ่งของการศึกษาตามหลักสูตรปริญญาวิศวกรรมศาสตรมหาบัณฑิต

สาขาวิชาวิศวกรรมเคมี ภาควิชาวิศวกรรมเคมี

คณะวิศวกรรมศาสตร์ จุฬาลงกรณ์มหาวิทยาลัย

ปีการศึกษา 2556

SYNTHESIS OF MESOPOROUS TIN DIOXIDE ASSISTED BY RESORCINOL-FORMALDEHYDE GEL

Miss Kornkamol Banjerdteerakul

A Thesis Submitted in Partial Fulfillment of the Requirements
for the Degree of Master of Engineering Program in Chemical Engineering
Department of Chemical Engineering
Faculty of Engineering
Chulalongkorn University
Academic Year 2013

Thesis Title	SYNTHESIS OF MESOPOROUS TIN DIOXIDE ASSISTED BY RESORCINOL-FORMALDEHYDE GEL
By	Miss Kornkamol Banjerdteerakul
Field of Study	Chemical Engineering
Thesis Advisor	Assistant Professor Varong Pavarajarn, Ph.D.

Accepted by the Faculty of Engineering, Chulalongkorn University in Partial Fulfillment of the Requirements for the Master's Degree

.....Dean of the Faculty of Engineering
(Professor Bundhit Eua-Arporn, Ph.D.)

THESIS COMMITTEE

.....Chairman
(Professor Suttichai Assabumrungrat , Ph.D.)

.....Thesis Advisor
(Assistant Professor Varong Pavarajarn, Ph.D.)

.....Examiner
(Assistant Professor Apinan Soottitantawat, D.Eng.)

.....External Examiner
(Pamornrat Chantam, D.Eng.)

กรกมล บรรเจิดธีรกุล : การสังเคราะห์ทินไดออกไซด์ที่มีรูพรุนขนาดเมโซโดยใช้เรซอซินอล ฟอร์มาลดิไฮด์เจลช่วย. (SYNTHESIS OF MESOPOROUS TIN DIOXIDE ASSISTED BY RESORCINOL-FORMALDEHYDE GEL) อ.ที่ปรึกษาวิทยานิพนธ์หลัก : ผศ.ดร.วรงค์ ปวราจารย์, 105 หน้า.

ทินไดออกไซด์ที่มีรูพรุนขนาดเมโซถูกสังเคราะห์ โดยวิธีการโซลเจลโดยใช้เรโซซินอลฟอร์มาลดิไฮด์เจล (อาร์เอฟเจล) เป็นแม่แบบ การใช้อาร์เอฟเจลเป็นแม่แบบดีกว่าการใช้สารลดแรงตึงผิวเป็นแม่แบบเนื่องจากค่าใช้จ่ายในกระบวนการต่ำและสามารถทำได้ง่าย ตัวแม่แบบถูกเตรียมจากปฏิกิริยาพอลิคอนเดนเซชันของสารละลายผสมระหว่างเรโซซินอลและฟอร์มาลดิไฮด์ อย่างไรก็ตามทินเตตระคลอไรด์เพนตะไฮเดรตหรือสารตั้งต้นของทินจะไม่ถูกใส่ลงในสารละลายอาร์เอฟเจลโดยตรง เนื่องจากการใส่สารตั้งต้นของทินโดยตรงจะทำให้เกิดการแข็งตัวอย่างรวดเร็ว การสังเคราะห์ทินไดออกไซด์จะเริ่มจากเตรียมทินโซลโดยการผสมสารตั้งต้นของทินเข้ากับฟอร์มาลดิไฮด์ นอกจากนี้ เพื่อป้องกันการไม่เป็นเนื้อเดียวกันของเจลที่ได้ ตัวทำละลายที่ใช้สำหรับการทำอาร์เอฟเจลเช่น เอทานอล จึงถูกนำมาใช้ในการสังเคราะห์วัสดุชนิดนี้ จากผลการทดลองพบว่า การใช้แม่แบบในการสังเคราะห์ทำให้ผลิตภัณฑ์มีโครงสร้างที่เป็นรูพรุนขนาดเมโซ และมีปริมาณพื้นที่ผิวสูงกว่าผลิตภัณฑ์ที่ไม่ได้ใช้แม่แบบ สภาวะในการเตรียมเป็นปัจจัยสำคัญที่มีผลต่อลักษณะและสมบัติของผลิตภัณฑ์ ตัวอย่างเช่น การเพิ่มเวลาที่ใช้ในการบ่มอาร์เอฟเจลเป็นผลให้ได้ผลิตภัณฑ์ที่มีพื้นที่ผิวสูงขึ้นและขนาดอนุภาคทินไดออกไซด์ที่เชื่อมต่อกันมีขนาดเล็กลง ความเข้มข้นของสารตั้งต้นที่ใช้ ได้แก่ สัดส่วนโมลของทินต่อฟอร์มาลดีไฮด์ และทินต่อเรโซซินอล มีผลต่อรูปสัณฐานและสมบัติของผลิตภัณฑ์ที่ได้ นอกจากนี้ยังมีการศึกษาผลของตัวแปรอื่นๆ ได้แก่ สัดส่วนโมลของเรโซซินอลต่อตัวเร่งปฏิกิริยา เวลาที่ใช้ในการบ่มทินโซล เวลาที่ใช้ในการบ่มเจลที่ผสมแล้ว ชนิดของตัวทำละลายที่ใช้ในการเจือจางอาร์เอฟเจล และกระบวนการที่ใช้ทำให้เจลแห้ง โดยพบว่าการทำปฏิกิริยาระหว่างทินโซลและอาร์เอฟเจลเป็นปัจจัยสำคัญที่ส่งผลต่อความเป็นรูพรุนขนาดเมโซของทินไดออกไซด์

ภาควิชา วิศวกรรมเคมี ลายมือชื่อนิสิต .....

สาขาวิชา วิศวกรรมเคมี ลายมือชื่อ อ.ที่ปรึกษาวิทยานิพนธ์หลัก .....

ปีการศึกษา 2556

5570519821 : MAJOR CHEMICAL ENGINEERING
KEYWORDS : MESOPOROUS TIN DIOXIDE / RESORCINOL-FORMALDEHYDE GEL / SOL-GEL POLYCONDENSATION

KORNKAMOL BANJERDTEERAKUL : SYNTHESIS OF MESOPOROUS TIN DIOXIDE ASSISTED BY RESORCINOL-FORMALDEHYDE GEL. ADVISOR : ASST. PROF. VARONG PAVARAJARN, Ph.D., 105 pp.

Mesoporous tin dioxide was synthesized by sol-gel method using resorcinol-formaldehyde gel (RF gel) as a template. Using RF gel as a template is better than surfactant template due to low cost and easy to handle. The template was prepared by sol-gel polycondensation of the mixture between resorcinol and formaldehyde. Tin tetrachloride pentahydrate ($SnCl_4.5H_2O$) or tin precursor was not directly added into RF-gel due to rapid solidification. First, the preformed tin sol was formed by mixing tin precursor and formaldehyde. In order to prevent non-homogeneous of the mixed gel, diluting solvent such as ethanol was applied to fabricate this material. The results showed that when the template was used, the product has mesoporous structure and higher surface area than the product without assisting template. Process conditions were found to be the important factors that affect the morphology and properties of the product. For example, increasing the aging time of RF-gel resulted in enhanced surface area and smaller connected tin dioxide particles. Concentration of reactants, i.e., tin-to-formaldehyde molar ratio (Sn/F) and tin-to-resorcinol resorcinol molar ratio (Sn/R) significantly affect both the morphology and properties of the obtained product. Moreover, the effect of other parameters, namely, resorcinol-to-catalyst molar ratio (R/C), tin sol aging time, aging time for mixed gel, type of diluting solvent and drying process, were also studied. It was found that interaction between tin sol and RF gel is the important factor affecting mesoporous structure of tin dioxide.

Department : Chemical Engineering Student's Signature .....
Field of Study : Chemical Engineering Advisor's Signature .....
Academic Year : 2013

ACKNOWLEDGEMENTS

I would like to express my gratitude to my advisor, my committee members, my fellow students, my parents and my university for their many supports.

First, I would like to extend my sincere appreciation to my thesis advisor, Assistant Professor Varong Pavarajarn for his guidance, supports and generosity. His advices help me accomplish the research including his effort to comment and revise my research report.

I would also like to express my appreciation to my committee members, Professor Suttichai Assabumrungrat, Assistant Professor Apinan Soottitantawat and Dr. Pamornrat Chantam for their recommendation and feedback about this work.

Special thanks to my fellow students at Center of Excellent in Particle Technology, Department of Chemical Engineering, Chulalongkorn University for their assistance.

Moreover, I would like to express my deepest gratitude to my parents for their supports and encouragement through the year that I studied and conducted this research.

Most of all, I would like to thank Chulalongkorn University for giving me an opportunity to study and doing the research with high technology equipments.

CONTENTS

Page

Page

LIST OF TABLES

Table **Page**

Page

LIST OF FIGURES

Figure **Page**

Page

Page

Page

Page

CHAPTER I

INTRODUCTION

Nowadays, porous materials have attracted many attentions due to their wide range of usage, for example, the applications in adsorption, separation, catalysis and sensors because of outstanding characteristics of these materials especially their large surface area [1]. Ceramic is one kind of materials which plays important role in many industries. With high strength, high thermal and chemical stability, ceramic has been widely used [2]. The development of ceramic into porous material causes further remarkable characteristic, i.e., low density, low thermal conductivity, low specific heat, high surface area and high permeability [3, 4]. Accordingly, porous ceramic is practically usable as a filter [5, 6], catalyst support [7, 8], gas sensor [9, 10] and thermal insulation [3].

Tin dioxide has been considered as one of the most important oxide semiconductor (n-type) owning to its wide energy band gap (3.6-3.8 eV) [11], relatively high gas sensing properties and high chemical stability [12, 13]. From the above reasons, it has been applied in many fields such as catalysts [14], chemical sensors [15, 16], photo-electrochemical cells [17] and lithium battery anodes [18]. Recently, the synthesis of mesoporous tin dioxide has been popular because of its large surface area. It is believed that by having large surface area or by increasing the surface area, the activity of the particles such as having more surface sites available for gas adsorption can be improved [19-21]. Various techniques have been used for synthesis the mesoporous tin dioxide, for instance, hydrothermal [18, 22], spray pyrolysis [23], chemical vapor deposition [24], sonochemical [17], precipitation [25] and sol-gel method [17, 26, 27]. Sol-gel technique is also one of the methods that is very promising for fabricating the mesoporous tin dioxide because it is able to operate at room temperature in an air, easy to handle and specially low cost [28, 29]. Furthermore, many efforts have been made to prepare mesoporous tin dioxide by using surfactants such as cetyltrimethylammonium bromide (CTAB) [30, 31], dodecylamine [32], tetradecylamine [33] and sodium diosulfosuccinate (AOT) [34, 35]. However, the syntheses of tin dioxide using those surfactants were not successful as expected because pore structure collapses after removing the surfactant. Thus, during calcination process, the template that can preserve pore structure at the high temperature is essentially required.

In 1989, Pekala et al. accomplished in synthesizing resorcinol formaldehyde gel (RF gel) from polymerization of resorcinol and formaldehyde using sodium carbonate as the

catalyst [36]. The RF gel can be transformed to carbon aerogel which has special features, namely, open-cell structure, small pore size (less than 50 nm.), high surface area (400-1000 m^2/g) and moreover its decomposition takes place at high temperature as estimated as 500^OC [37, 38]. Thus, using RF gel as a template is good alternative for the fabrication of the mesoporous tin dioxide.

In this study, RF gel was used as a template to synthesize mesoporous tin dioxide according to the method proposed by Pekala [36]. Tin dioxide was synthesized with and without RF-gel in order to verify that RF gel assists the product to have mesoporous structure. The interaction between tin precursor and RF gel were also investigated to study the mechanism of formation mesoporous tin dioxide.

The effect of various factors, i.e., molar ratio of tin to formaldehyde (Sn/F ratio), molar ratio of resorcinol to catalyst (R/C ratio), molar ratio of tin to resorcinol (Sn/R ratio), type of diluting solvent, aging time of preformed Sn sol, aging time of RF gel, aging time of mixed gel, drying process and calcination temperature, were also studied by BET, FT-IR, SEM, TGA and XRD techniques.

The thesis is divided into five chapters. Chapter I is introduction that describes motivation, objective and scope of this work. Chapter II is theory and literature reviews corresponding to characteristic of tin dioxide, sol-gel process, resorcinol formaldehyde gel, porous material and summary of previous research about synthesis of mesoporous tin dioxide. Chapter III is experimental. This chapter describes experimental procedure and detail of characterization techniques that were used in this study. Chapter IV is results and discussion. The last chapter is overall conclusions and recommendation for future work.

Objective of the research:

The objective of the research is to synthesize mesoporous tin dioxide and to investigate formation mechanism of the mesoporous tin dioxide.

Scope of the research:

- Mesoporous tin dioxide was fabricated by using RF gel as a template, according to the procedure of Pekala et al., via sol-gel method.

  Condition for the synthesis of mesoporous tin dioxide

  - Molar ratio of tin to formaldehyde: 0.003-0.060

- Molar ratio of resorcinol to catalyst: 50-300
- Molar ratio of tin to resorcinol: 0.03-0.10
- Type of diluting solvent: water and ethanol
- Aging time of preformed tin sol: 0-120 h
- Aging time of RF gel: 1-4 h
- Aging time of mixed gel: 2-5 days
- Drying process: conventional drying at 100^{o}C and freeze drying
- Calcination temperature: 400-700 ^{o}C

- Characterizations of tin dioxide were done by
  - BET (Brunauer, Emmett and Teller) method for estimating surface area and pore size distribution.
  - FT-IR (Fourier Transform Infrared Spectroscopy) for specifying functional groups.
  - SEM (Scanning Electron Microscopy) for observing particle morphology.
  - TGA (Thermogravimetric Analysis) for studying thermal decomposition of the particles.
  - XRD (X-ray diffraction) for identifying phase composition.

CHAPTER II

THEORY AND LITERATURE REVIEW

In this chapter, theory and literature review corresponding to synthesis of mesoporous tin dioxide, including classification and property of tin dioxide, sol gel method, RF gel and porous material, are described as followed.

2.1 Tin dioxide

Tin dioxide (SnO_2) was firstly produced and patented in 1962 [39, 40]. Tin dioxide is a crystal of white color. It has density of 7.0096 g/cm^3 and its melting point is about 2000°C. The tin dioxide has amorphous or polycrystalline structure with a tetragonal lattice of rutile with parameters a = b = 0.4737 nm, c = 0.3185 nm. [41, 42]. For crystalline tin dioxide, there are two tin atoms and four oxygen atoms in one unit cell. From the previous study, under high vacuum, the calcination temperatures were investigated by X-ray diffraction (XRD) demonstrating that no phase transitions was occurred when the calcination temperatures are below 300^{o}C [43]. It is noted that the phase transformation arose approximately at 400^{o}C and Sn_3O_4 is an intermediate phase during the phase transformation from SnO to SnO_2 in the temperature range between 400 and 500 °C. When increasing the temperature higher than 500 °C, the Sn_3O_4 phase is transformed into the rutile SnO_2 phase. A temperature higher than 700 ^{o}C, the rutile phase is the only appeared phase in XRD pattern [44].

Moreover, the effect of parameter such a pressure on the phase transition was also investigated both in experiments and theories. Experimentally, it was found that the sequence of phase transformation is from rutile-type to $CaCl_2$-type to α-PbO_2-type to modified fluorite-type occurring at 11.8, 12 and 21 GPa, respectively [45]. In theoretical study, it was found using equations of states and density functional theory at the B3LYP level that the sequence of phase transition is from the rutile-type to $CaCl_2$-type, α-PbO_2-type, pyrite type, ZrO_2-type, fluorite-type and cotunnite-type at 12,17,18,24 and 33 GPa, respectively [46].

There are various techniques that can synthesize nanosized tin dioxide particle, for example, sol gel method, chemical vapor decomposition, sputtering method, gas phase condensation, flame synthesis, pulsed laser ablation and mechanochemical processing. The key factors often used to choose the synthesis technique include the required scale of the product, purity of the tin dioxide product materials, toxicity, repeatability of the tin dioxide properties, handling considerations of the tin dioxide precursor materials, continuous or batch

processing, cost of materials and procedures required, and complexity and waste of the tin dioxide fabrication step. The most widely used technique is sol gel method owing to inexpensive, narrow size distribution of the product, good homogeneity, easy to process and low operating temperature [47]. However, tin dioxide produced from the sol gel technique may be contaminated with chloride when tin chloride is used as precursor because it is cheap comparing to the granulated tin and tin alkoxide [47, 48]. According to Zhang and Gao, the problem about the chloride contamination can be resolved so that the tin dioxides formed from the sol gel method are free from chloride impurities [49].

The outstanding properties of SnO_2 are optical, electrical and mechanical properties [46]. Tin dioxide has been considered as a versatile material due to widely usage e.g. for gas sensor applications, for catalyst in the oxidation of organic compounds, being a main component in rechargeable Li batteries, being a major portion in opto-electronic devices and being a pigment in the glasses enamels and in ceramic glazes industry [50-52].

In gas sensing applications, tin dioxide, an n-type semiconductor with broad-band gap (3.6-3.8 eV) [11], is the most vital material due to high sensitivity to small concentration of gases (at ppm levels) and low processing costs [39, 47]. The tin dioxide used in gas sensor application is frequently the tetragonal cassiterite phase. Many carbon monoxide alarms are produced by using tin dioxide as an active component [47]. In addition, there has been many attempts to apply tin dioxide as a detector for other gases including toxic gases [13, 53]. The performance of the gas sensors depends on their characteristics, i.e, particle size, particle connections and compositional characteristics. It is found that both reducing particle size and adding additives (nobel metals or other metal oxides) to create nanocomposite materials can improve the performance of the tin dioxide sensor [47].

The mechanism of tin dioxide sensor response is shown in Figure 2.1. This sensor response is resulted from surface interactions between the tin dioxide and the surrounding gases (oxidizing and reducing gases). First, oxygen gas in air is adsorbed onto the tin dioxide surface and then electrons from tin dioxide surface are transferred to the adsorbed oxygen. This results in the formation of an electron-depleted region (also known as the space charge layer) near the tin dioxide surface, where is an area of high resistance.

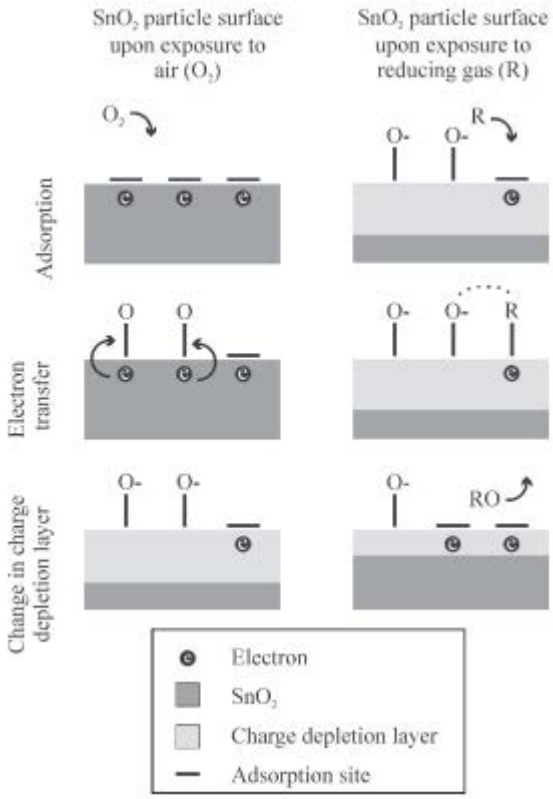

Figure 2.1 The mechanisms of SnO_2 sensor response to oxidizing and reducing gases [47].

After exposing to a reducing gas like CO, the electrons are released back to the surface. Therefore the resistance of the space charge layer will be decreased. The surface reactions are shown in the equation 2.1and 2.2 [47].

$$CO + O^-_{ads} \longrightarrow CO_2 + e^- \qquad (2.1)$$

$$2CO + O^-_{2,ads} \longrightarrow 2CO_2 + e^- \qquad (2.2)$$

2.2 Sol-gel processing

Sol-gel is a synthesis method that many researchers used to apply in their investigations because of its advantage such as low cost, easy to perform and can be operated at room temperature [28, 29]. This method has been applied to fabricate various materials, for instance, ceramics and organic-inorganic hybrids. There are two corresponding reactions which are hydrolysis and polycondensation. Hydrolysis reaction relates to dividing chemical bond by addition of water as illustrated in equation 2.3, and consequently metal atom (M) and methyl group (R) are separated. Two metal atoms which connects to hydroxyl group can be gathered together. In that case by-product is produced from assembling those atoms. If the by-

product is water, the process will be called “water condensation”. While if the by-product is alcohol, it will be called “alcohol condensation”. Condensation process makes the mixture be a crosslinked network or “sol”, shown in equation 2.4 and equation 2.5. The sol can be obtained from a precursor such an inorganic salt or a metal alkoxide. Metal alkoxides are popularly used as precursors because they react with water easily [54].

$$\text{M-O-R} + H_2O \longrightarrow \text{M-OH} + \text{R-OH} \qquad (2.3)$$

$$\text{M-OH} + \text{HO-M} \longrightarrow \text{M-O-M} + H_2O \qquad (2.4)$$

$$\text{M-OH} + \text{HO-M} \longrightarrow \text{M-O-M} + H_2O \qquad (2.5)$$

When crosslink network is more extensive, liquid sol will turn rigid also known as “gel”. The gel can be classified by type of bonding. Polymeric gel is formed by covalent bonding, while gelatine gel is created by entanglement of molecular chains. On the other hand, particulate gel is a gel formed by collection of particles linked by van der Waals forces [54]. The extent of crosslinking of polymeric molecules affects the amount of porosity, pore volume, pore size and thermal stability of the obtained product.

Figure 2.2 describes differences between gels of polymers with differences extent of crosslinking network. If the gel has significant branching and crosslinking, the final structure of product will mostly have macropores and mesopores, whereas the gel with little branching and cross-linking will mostly have micropores [55].

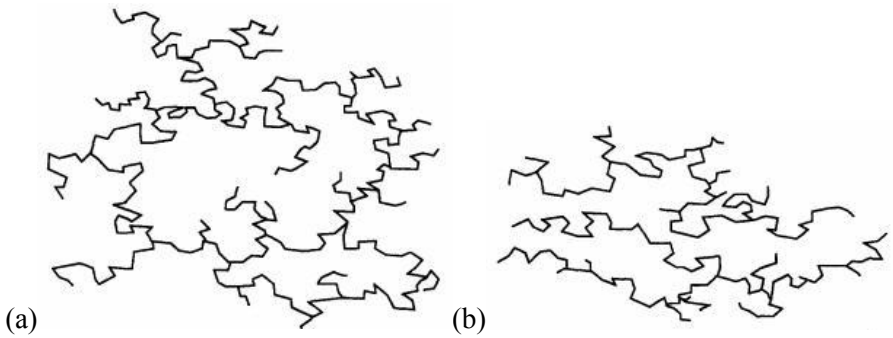

Figure 2.2 Differences between gels of polymers with (a) significant branching and cross-linking vs. (b) little branching and cross-linking [55].

During sol-gel process, the various species are formed with difference in dimensions and they are defined in different definitions as described in Figure 2.3.

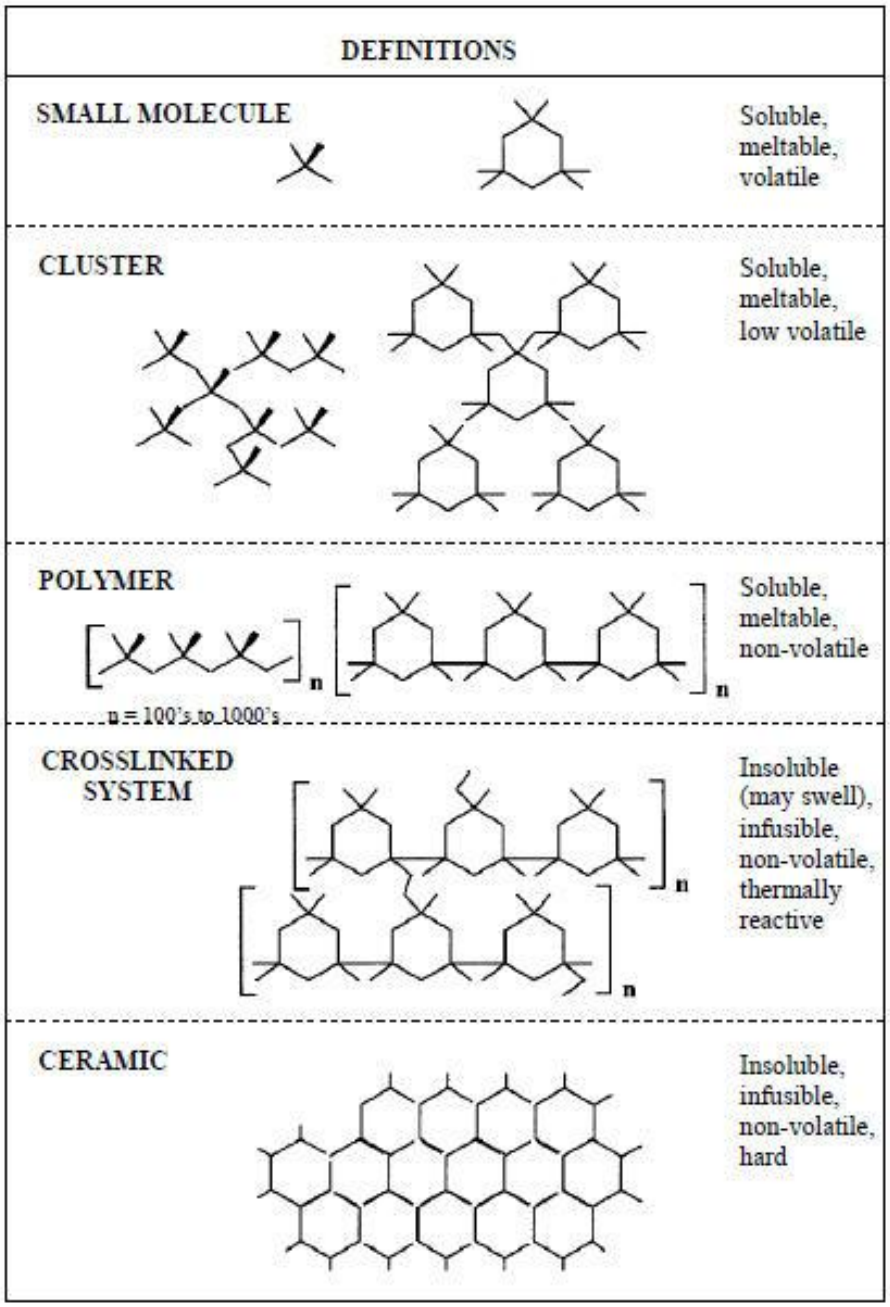

Figure 2.3 Definitions of the various species occured during sol-gel processing [56].

The properties and morphology of the synthesized product depend strongly on operating conditions such initial pH, temperature, concentration of reactant precursor, aging time, drying conditions and calcinations conditions [55].

2.3 Resorcinol-formaldehyde gel

Resorcinol or 1,3-dihydroxybenzene ($C_6H_4(OH)_2$) is a benzene ring clinged with two hydroxyl groups that are located in 1- and 3- positions, which has reaction sites in 2-, 4-, and/or 6- positions so that formaldehyde can be added to aromatic ring, as shown in Figure 2.4.

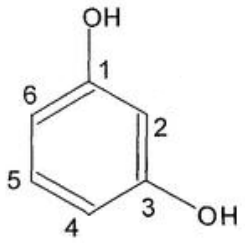

Figure 2.4 Chemical structure of resorcinol [57].

The addition of formaldehyde results in obtaining hydroxymethyl derivatives (-CH_2OH) of resorcinol. Since condensation of the hydroxymethyl derivatives (-CH_2OH) of resorcinol can take place, therefore methylene (-CH_2-) and methylene ether (-CH_2OCH_2-) bridged compounds will be occurred and this reaction will lead to generate and growth of clusters to be 3-dimensional crosslinked network called the RF hydrogel [58, 59], as demonstrated in Figure 2.5 and figure 2.6. Then, mesoporous carbon will be formed by drying the RF hydrogel, which is exchanged with an organic solvent to make a aqueous solvent out, after finishing heat treatment the gel.

1. Addition Reaction

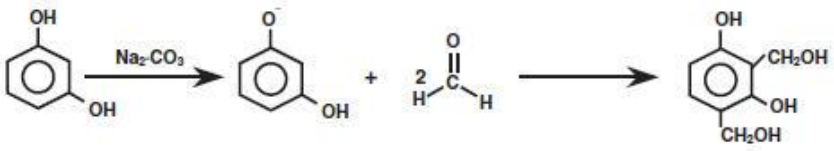

2. Condensation Reaction

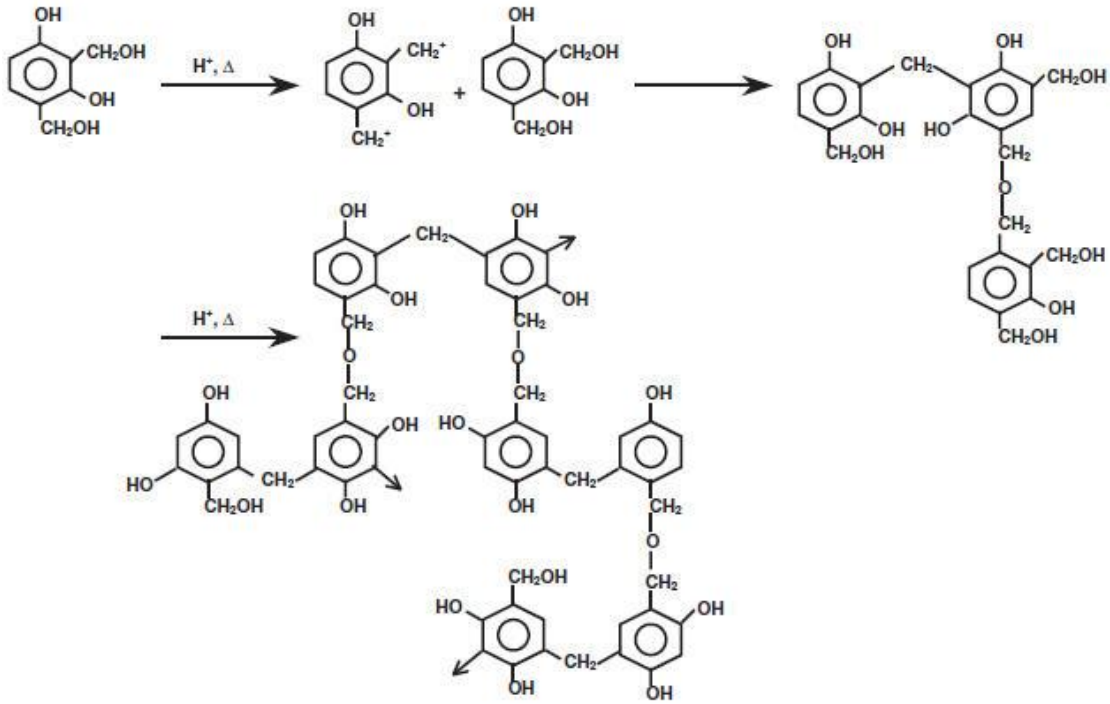

Figure 2.5 The polymerization mechanism of resorcinol with formaldehyde [60].

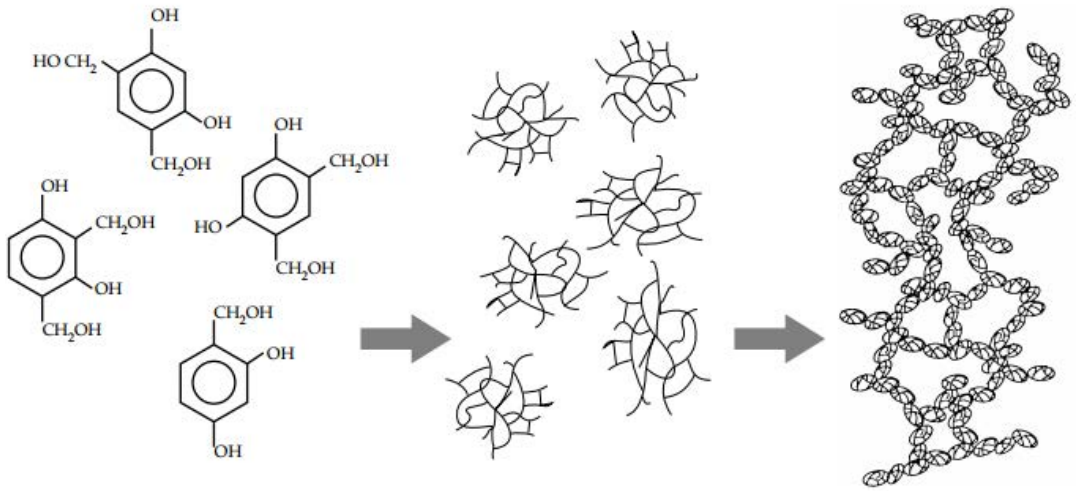

Figure 2.6 Cluster growth of resorcinol-formaldehyde monomers [61].

Resorcinol-Formaldehyde gel was firstly synthesized by Pekala et al. (1989) via sol-gel technique of resorcinol (R) and formaldehyde (F) with sodium carbonate (C) as basic catalyst [36].

The procedure to synthesize resorcinol-formaldehyde gel can be summarized as follows. At first, resorcinol (R) and formaldehyde (F) are mixed together in the presence of a basic catalyst [62] (in some case, an acidic catalyst [63]) under stirring for a short period (between 5 and 30 minutes [60, 64]) or else the mixture is homogeneous solution. Then the solution is retained in a closed container (glass or plastic) and aged until the crosslinked gel is formed. After aging, the gel is repeatly washed everyday with an organic solvent in order to assure the aqueous solvent is exchanged. Then the gel is dried at the later time in condition of subcritical or supercritical drying, at which results a carbon xerogel or aerogel, respectively. To produce highly porous carbon, the dried gel is then carbonized in nitrogen [62]. The process condition has pronounced effect on the properties and morphology of RF gels divided into 3 stages.

The first stage is about preparation of the solution, gelation and curing. In this stage, there are many factors affecting on the properties of product, for instance, concentration ratios of the different reactant, catalyst solution, gel pH, gelation and curing. The R/F molar ratio of 1:2 is commonly used ratio in the literature [62]. However, when either formaldehyde is used in excessive amount or the amount of solvent is increased, the density of the reactants will be reduced. This will result in a dilution effect which consequently increases the particle size before the gelation [65].

The gels are called aquagels or hydrogels in case deionized water is used as a solvent, whereas those are named lyogels if producing by an organic solvent (e.g., solvent, methanol, ethanol, n-propanol, or isopropanol) [63, 66].

Sodium carbonate (Na_2CO_3) is mostly used as catalyst (C) in order to activate R and makes it work as sites for monomer particles growth. The typical R/C molar ratio is between 50 and 300; but, in some cases a high ratio such as 1500 are used so that crosslinked gel microspheres are formed [67]. The surface area increases slightly when increasing R/C ratio. However, excessive R/C molar ratio will decrease the surface area. A maximum surface area appears at R/C molar ratio of 50 [68].

The initial gel pH can be controlled by using dilute acids (HNO_3 or HCl) or bases (NH_4OH) as buffers. At very low pH, the reactants become precipitated [36]. The gel pH is

typically used in range of 5.4 to 7.6 [69]. Increasing initial gel pH results in higher surface area and pore volume [70]. However, increasing initial gel pH when already reaches pH 7, the surface area will dissolve completely [71].

In gelation step, heating is required for polymerization reaction, but possible to carry this reaction at low temperature such as 30^{o}C [72]. The difference of polymerization with or without heating is gelation times. The polymerization without heating requires longer gelation time than the polymerization with heating. After gelation step, the next step is to crosslinking polymer clusters which is called "curing step". The summary of the first stage effect is shown in Table 2.1.

Table 2.1 The effect of factors during preparation of initial solution, gelation and curing on the final product [69]**.**

Factor	Effect
Decreasing reactant concentrations (equivalent to reducing R/F, R/W, or R/C ratios)	Smaller particles and pore sizes Less compaction (less void) of gel structure Increase surface area of xerogels Either reduce or increase pore volume of xerogels, depending on pH Increase electrochemical capacitance Either increases or decreases lithium ion charge and discharge capacities Depending on pyrolysis temperature and gel pH
Acidic catalyst solutions	At low RF concentrations: small, smooth, fractal aggregates of particles with wide pore size distribution At high RF concentrations: no fractal aggregates, very narrow pore size distribution, may reduce gelation time
Alkaline catalyst solutions	High concentrations: polymeric gels (small polymer particles interconnected with large necks, high surface areas, high mechanical strengths), reduce gelation time Low concentrations: colloidal gels (large particles interconnected with narrow necks, low surface areas, low mechanical strengths)
Increasing gel pH	Increase surface area and pore volume of carbon aerogels Increase electrochemical capacitance of carbon aerogels Insignificant effect on surface area of carbon xerogels Increase pore volume of carbon xerogels at high density of reactants

Table 2.1 (continued) [69]

Factor	Effect
Increasing gel pH	Either increase or decrease electrochemical capacitance of carbon xerogels, depending on concentration of reactants Either increase or decrease lithium-ion charge and discharge capacities, depending on pyrolysis temperature and reactants concentrations
Gelation and curing	Required for improving the crosslinking of polymer particles

The second stage is solvent exchange and drying process step. The solvent exchange is removing an aqueous solution with exchanging it with an organic solution. It is believed that replacing an aqueous solution is beneficial in reduction in the required time and temperature in the drying process, and moreover reduces the surface tension on the pore walls causing minimizing shrinkage [69].

There are many drying conditions that can be used, for example, subcritical drying, supercritical drying and freeze-drying. The subcritical drying or conventional evaporation of the solvent may cause the collapse of the pore due to the mechanical stresses forming from the difference between the surface tension of the vapor and liquid phases [69]. However, there are some advantages of the conventional drying such as being quick, simple and cheap method [65].

The supercritical drying can retain the pore structure, since the liquid CO_2 transforms to supercritical state condition by releasing the air little by little while filling liquid CO_2 without corresponding to the vapor-liquid interface [69]. Nevertheless, this drying process has the disadvantages such as using high pressure and being time-consuming in the solvent exchange and drying processes [73].

Freeze-drying is the drying method which avoids the formation of the vapor-liquid interface with freezing the gel and removing the solvent by sublimation. Before freezing the gel, it is important to exchange the aqueous solvent with a liquid that has no influence on the density of the gel (e.g. tert-butanol) [74, 75]. According to Tamon et al., washing the gel twice with tert-butanol is enough for exchanging the solvent [76]. If the gel is frozen without exchanging the solvent, either destruction of the gel structure or ice crystal growth will occur, thus the gel is resulted in very large pores [77]. The second stage effect is illustrated in Table 2.2.

Table 2.2 The effect of factors during in the second stage; solvent-exchange and drying process on the final product [69].

Factor	Effect
Solvent exchange	Necessary for supercritical drying with CO_2 or freeze-drying Facilitates replacement with drying media Reduction of surface tensions upon subcritical evaporation
Subcritical drying	Production of dried dense polymers called "xerogels" Causes significant shrinkage of especially wide pores Effects can be insignificant if gels were synthesized with high mechanical strength Increase lithium-ion charge and discharge capacities
Supercritical drying with CO_2	Production of dried light polymers called "aerogels" Insignificant shrinkage of pore structure High surface areas, pore volumes and, sometimes, electrochemical capacitances Requires high pressures, long times foe exchanging solvent with CO_2
Supercritical drying with acetone	Like supercritical drying with CO_2, but with lower pressures Eliminates necessity for exchanging solvent with CO_2, shortens processing time significantly Requires high tenperatures to shift acetone to supercritical conditions May cause partial thermal decomposition of dried gels
Freeze-drying	Production of dried light polymers called "cryogels" based on sublimation of frozen solvents Cryogels mostly mesoporous Density of solvents must be invariant with freezing

The third stage is pyrolysis or carbonization and activation. The pyrolysis relates to change the organic gels to carbon gels by removing any materials at a high temperature (600 to 2100 ^{o}C) in inert atmosphere [78]. Synthesizing process of the carbon aerogels can be summarized in Figure 2.7.

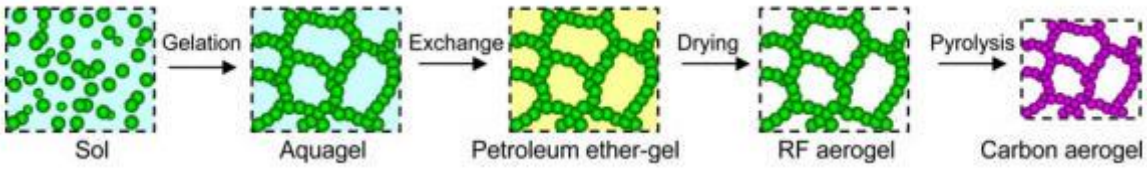

Figure 2.7 Synthesizing process of carbon aerogels [79].

Therefore, altering factors has obvious effect on the final structure and properties of the synthesized carbon aerogels. Summary of the altering those parameters in third stage is demonstrated in Table 2.3.

Table 2.3 The effect of factors during pyrolysis and activation on the product [69].

Factor	Effect
Increasing pyrolysis temperature	Reduces oxygen content Reduces surface area of carbon aerogels and xerogels Reduces pore volumes of carbon aerogels and xerogels Increases macropore size distributions Increases micropore size distributions when very low R/C ratios are used Increases electrochemical capacitance up to 850 ^{o}C, thereafter reduces it either increases or decreases lithium ion charge and discharge capacities, depending on gel pH and reactants concentrations
Increasing thermal activation time	Increases pore widths, volumes and surface areas Increases electrochemical capacitance up to 3 h, thereafter reduces the electrochemical capacitance

2.4 Porous material

The type of pores in solid can be divided based on their origin, size, state or strength as detailed in Table 2.4. Based on their origin, the pores are classified into intraparticle pores and interparticle pores. Based on their size, there are micro-, meso- and macro pores. In case of their state, the pores are splited into open- or closed pores (latent pores). At last, they are called rigid or flexible pores when based on their strength [80].

Table 2.4 Classification of pores in solid materials [80].

1) Based on their origin	
Intraparticle pores	Intrinsic intraparticle pores
	Extrinsic intraparticle pores
Interparticle pores	
2) Based on their size	
Micropore <2 nm	Ultramicropores <0.7 nm
	Supermicropores 0.7-2 nm
Mesopores 2-50 nm	
Macropores >50 nm	
3) Based on their state	
Open pores	
Closed pores (Latent pores)	
4) Based on their strength	
Rigid	
Flexible	

In this research, pores are mainly focussed based on their size, i.e., micropores (less than 2 nm. in pore diameter), mesopores (2-50 nm. in pore diameter) and macropores (greater than 50 nm. in pore diameter) [81]. The pore width, which is described as the distance between two opposite walls, is defined as a pore size [82]. Figure 2.8 shows the example of porous materials in pore size ranging from 0.5-500 nm.

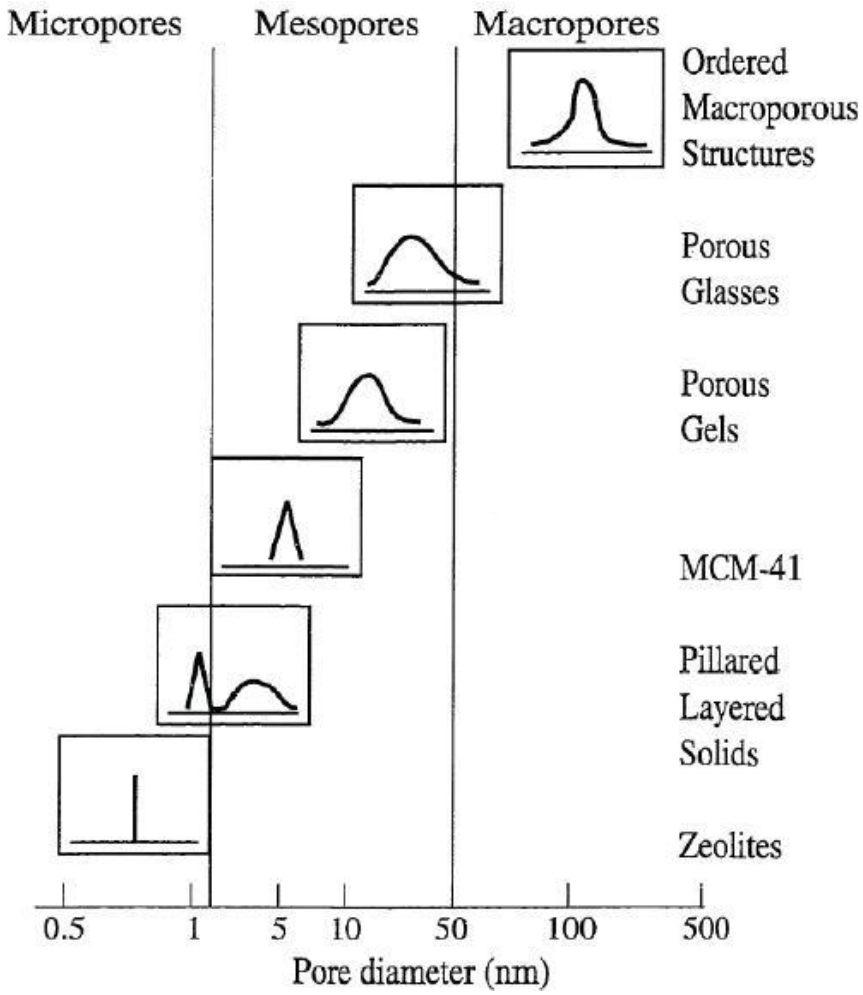

Figure 2.8 Pore size distributions of some porous materials [83].

Various techniques are used for the identification of pores as summarized in Figure 2.9. Gas adsorption is usually used to identify micropore and mesopore, mostly of N_2 at 77K. In addition, the pores are detected based on several models such as BET, DFT, t-plot, α_s-plot, BJH and HK to get the pore structure parameters, e.g., a diameter pore size, a surface area, which are necessary information for analysing these materials. Small-angle X-ray scattering is also able to identify the pores. Moreover, it has an advantage in investigating the closed pores which cannot be detected by adsorbate gas molecules. Mercury porosimetry is often utilized to examine macropores by applying various pressures in a sample that is immersed in mercury. To observe the surface of a sample, using microscopy techniques is good choice, for example, scanning tunneling microscopy (STM) and transmission electron microscopy (TEM) for exploring micropores and mesopores, scanning electron microscopy (SEM) and

optical microscopy for exploring macropores [80]. In summary, advantages and disadvantages are demonstrated in Table 2.5.

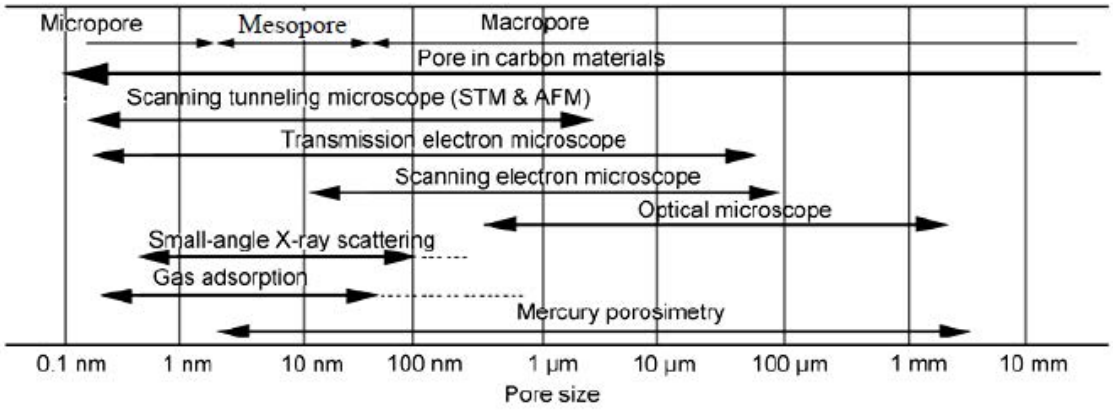

Figure 2.9 Pore size distributions of some porous materials [80].

Table 2.5 The advantages and disadvantages of characterization techniques [80].

Characterization technique	Comments (advantages and disadvantages)
Adsorption/desorption of N_2 gas at 77 K	
BET method	Give overall surface area (SS)
s plot	Give microporous and external SSs separately Give micropore volume
BJH method	Differentiate microporous and mesoporous SSs and volumes Give pore size distribution in mesopore range
DFT method	Give pore size distribution in a wide range of size
HK method	Give pore size distribution etc.
Adsorption/desorption isotherm of various gases (H_2, He, CO_2, CO)	Give the information molecular sieving performance
X-ray small-angle scattering	Detect micropores, either open or closed pores

In quantitative study, an adsorption isotherm is used to describe the amount of gas adsorbed by the porous material at a fixed temperature and various pressures. According to IUPAC, adsorption isotherms are classified into six types as shown in Figure 2.10. Type I

isotherm or Langmuir isotherm is given by the presence of micropores in a material. Type II isotherm, which is derived from non-porous or macroporous materials, indicates the multilayer adsorption process. Type III isotherm represents non-porous or macroporous materials which interact weakly with the adsorbent molecules. Type IV isotherm arises from capillary condensation in mesopores, consequently the hysteresis loop of this isotherms is appeared. Type V isotherm is similar to Type IV, but with weaker interaction with adsorbent. Type VI isotherm is stepwised multilayer adsorption which forms from a uniform non-porous surface. It is widely known that only type IV and V isotherms have hysteresis loop whose shape relates to the feature of mesoporous materials, i.e., pore size distribution, pore geometry and connectivity [84]. IUPAC classifies the hysteresis loop based on an earlier classification by De Boer as presented in Figure 2.10.

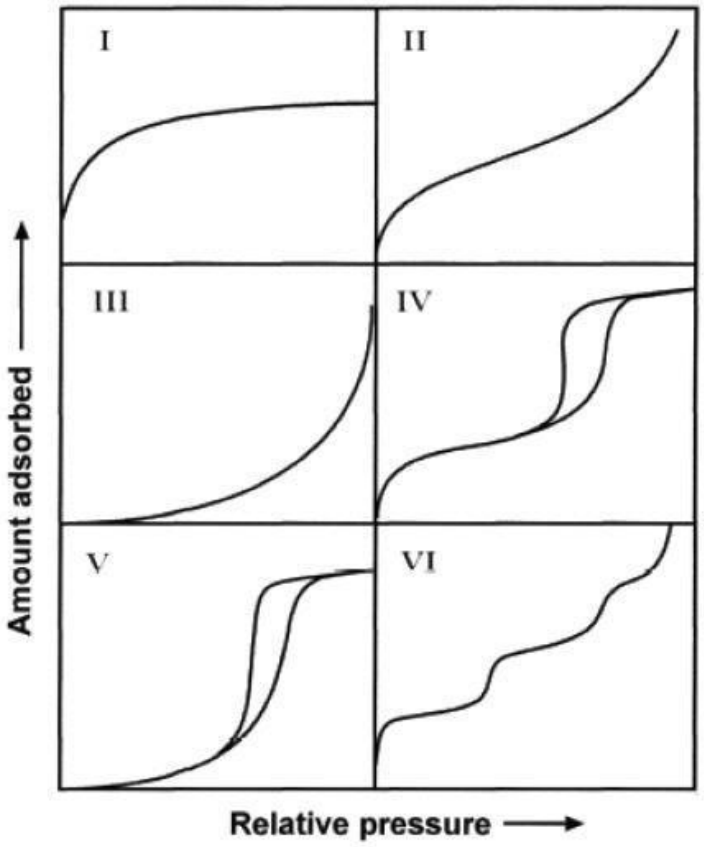

Figure 2.10 The IUPAC classification of adsorption isotherms.The hysteresis is only in types IV and V [84].

Hysteresis appearing in the adsorption-desorption isotherms is always corresponding to capillary condensation in mesoporous structures. The adsorption behavior of these

materials depends not only on the interaction between fluid and surface wall, but also the attractive interactions between the fluid molecules. Consequently, multilayer adsorption and capillary condensation in the pore occur. The unique aspect of capillary condensation is that vapor condensation occurs below the saturation vapor pressure of the pure liquid. Type H1 often concerns with porous materials composing of well-defined cylindrical-like pore channels or agglomerated uniform spheres. Type H2 frequently describes not-well defined pore channels that are disordered and also points to bottleneck constriction. Type H3 indicates a shape of pores with slit shape. At last, type H4 shows narrow slit pore inhere in the materials [84]. Types of hysteresis loops are shown in Figure 2.11.

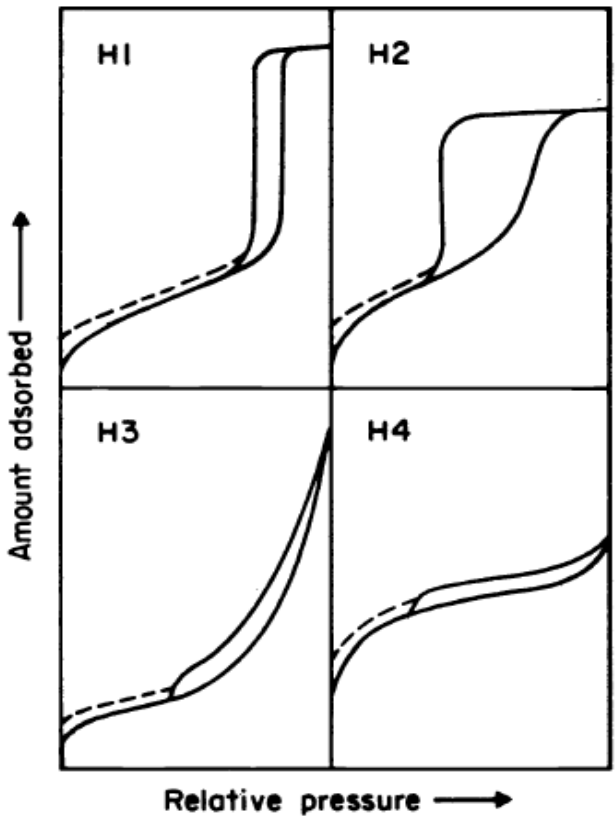

Figure 2.11 Types of hysteresis loops [84].

At the present, macropous materials is not widely used in industries because of low surface area and large non-uniform pores. Therefore, microporous and mesoporous have attracted much attention in many fields such as adsorption, separation and catalyst. However, there are some disadvantages in microporous materials. For example, zeolites are frequently representative for microporous materials which are useful in many applications including catalysis and adsorption process. Nevertheless, those applications require specific pore size,

while the microporous materials may have too small pore size. Hence, using mesoporous material may be a good alternative because mesoporous materials have wide range of pore size that can accommodate complex chemicals, molecular complexs and also biomolecular materials. Furthermore, the functionalities of large complex molecules, for example, their flexible conformational changes, motion, or diffusion, are preserved within mesopores [81].

2.5 The summary of literature surveys of synthesized mesoporous tin dioxide

The literature reviews corresponding to mesoporous tin dioxide are summarized in Table 2.6.

Table 2.6 The literature reviews of synthesized mesoporous tin dioxide.

Year	Authors	Synthesized method	Precursor	Surfactant	Calcination temperature (^oC)	Surface area (m^2/g)
1997	Li et al.	Sol-gel processing	$Na_2SnO_3.3H_2O$	N-cetyl-N,N,N-trimetylammonium bromide	450	156.8
1997	Qi et al.	Sol-gel processing	$SnCl_4$	$C_{12}S$	400	-
1998	Severin et al.	Sol-gel processing	$Sn(OPri)_4$	Tetradecylamine	400	99
2002	Yu et al.	Sol-gel processing	Tin acetate Sn(II)	Sodium dioctylsulfonate	350	-
2002	Wang et al.	Sol-gel processing	$SnCl_4.5H_2O$	Cetyltrimetylammonium bromide	400	136
2002	Srivastava et al.	Sonochemical	Tin etoxide	Cetyltrimetylammonium bromide	300	92
2003	Zhou et al.	Sol-gel processing	$SnCl_4.5H_2O$	Dodecylamine	300	359
2003	Hyodo et al.	Sol-gel processing	$Na_2SnO_3.3H_2O$	$C_{16}P_yCl$	600	374
2004	Fujihara et al.	Hydrothermal	$SnCl_4.5H_2O$	-	400	110
2006	Zhu et al.	Sol-gel processing	$SnCl_4$	Tetradecylamine	400-600	211-339
2006	Wagner et al.	Sol-gel processing	$SnCl_4.5H_2O$	Cetyltrimetylammonium bromide	350	75
2007	Cao et al.	Hydrothermal	$SnCl_4.5H_2O$	Urea	300	205

Table 2.6 (continued).

Year	Authors	Synthesized method	Precursor	Surfactant	Calcination temperature (^oC)	Surface area (m^2/g)
2007	Pan et al.	Sol-gel processing	$SnCl_4$	Pluronic F127	400-600	-
2007	Zhu et al.	Hydrothermal	$SnCl_4$	tetradecylamine	400-600	-
2009	Shon et al.	Sol-gel processing	$SnCl_2.2H_2O$	Mesoporous silica	700	84-121
2010	Che et al.	Sol-gel processing	$Na_2SnO_3.3H_2O$	$C_{16}mim^+Br^-$	700	350
2010	Dimitrov et al.	Sol-gel processing	$Sn(OC(CH_3)_3)_4$	-	225	406
2011	Yin et al.	Sol-gel processing	$SnSO_4$	-	500	43
2011	Guo et al.	Sol-gel processing	$SnCl_4$	Cetyltrimetylammonium bromide	300	347

CHAPTER III

EXPERIMENTAL

The experimental of synthesis mesoporous tin oxide, including materials and procedures will be described in this chapter. Moreover, characterizations of the obtained product are also explained thoroughly as followed.

3.1 Materials

Tin (IV) chloride pentahydrate and resorcinol with purity of 98% and 99% respectively were purchased from Sigma-Aldrich. Both formaldehyde solution with 36.5-38.0% by weight and sodium carbonate with purity of 99% were purchased from Ajax Fine Chemical. High purity ethanol with purity of 99.9% was purchased from VWR International S.A.S.

The employed chemicals are listed in Table 3.1 and details of these chemicals containing purpose of use, chemical structure and molecular formula are also shown in Table 3.1.

Table 3.1 List of the chemicals used in the research.

Chemical name	Symbol	Molecular formula	Chemical structure	Purpose of use
Resorcinol	R	$C_6H_4(OH)_2$	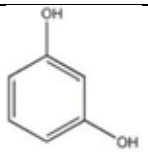	Synthesis of RF sol
Formaldehyde	F	HCOH	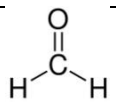	Synthesis of RF sol and Sn sol
Sodium carbonate	C	Na_2CO_3	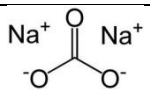	Synthesis of RF sol
Deionized water	W	H_2O	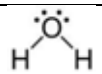	Synthesis of RF sol

Table 3.1 (continued)

Chemical name	Symbol	Molecular formula	Chemical structure	Purpose of use
Tin(IV) chloride pentahydrate	Sn	$SnCl_4.5H_2O$	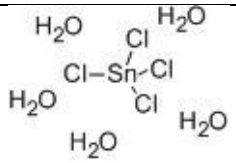	Synthesis of Sn/RF gel
Ethanol	E	C_2H_5OH	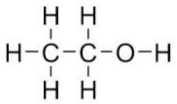	Synthesis of Sn/RF gel

3.2 Experimental procedures

3.2.1 Preparation of tin-formaldehyde preformed sol (SnF sol)

Tin (IV) chloride pentahydrate (Sn) was dissolved in formaldehyde (F) solution with varying Sn/F ratio from 0.003 to 0.060. After stirring the solution for 15 minutes, the solution was aged at room temperature. The aging time was investigated from 0 to 120 hours.

3.2.2 Preparation of resorcinol-formaldehyde gel (RF gel)

According to the method proposed by Pekala et al., RF gel was produced with fixed molar ratio of resorcinol to formaldehyde (R/F) of 0.5, resorcinol to water (R/W) of 0.15 and molar ratio of resorcinol to catalyst (R/C) ranging from 50 to 300. Before mixing sodium carbonate solution with resorcinol, resorcinol was dissolved in deionized water (W) with stirring time of 15 minutes. After adding the catalyst into the resorcinol solution, the solution was also stirred for 15 minutes. Formaldehyde solution (F) was later added into the homogeneous solution and then stirred it again for 15 minutes. The acquired solution was retained in a closed container for aging. The aging time was studied from 0 to 4 hour.

3.2.3 Preparation of tin dioxide particles

Ethanol (E) was added into the aged resorcinol-formaldehyde gel and stirred for 15 minutes with molar ratio of ethanol to resorcinol of 5. Then, the preformed tin sol was added into the solution with molar ratio of tin precursor to resorcinol (Sn/R) from 0.03 to 0.10. After the solution became homogeneous, the mixture was aged for various aging time of 2 to 5 days and then washed with tert-butyl alcohol everyday for 3 days. The washed gel was frozen in a

freezer for 24 hour and then dried by freeze drying for 24 hour. The obtained gel was calcined at 400,500,600,700^{o}C in an atmosphere condition for 6 hour with heating rate of 5^{o}C/min.

3.2.4 Characterizations

3.2.4.1 Nitrogen adsorption-desorption analysis

The specific surface area and pore size distribution of tin dioxide were determined via nitrogen adsorption and desorption analysis using the Brunauer-Emmett-Teller (BET) model and Barrett Joyner and Halenda (BJH) method, respectively. It was operated in a Belsorp mini II BEL analyzer at Center of Excellence in Particle and Technology Engineering laboratory, Chulalongkorn University.

3.2.4.2 Fourier-transform infrared spectroscopy (FT-IR)

The functional groups of the samples were identified by a Fourier transform infrared spectrometer (Nicolet 6700) at Center of Excellence in Particle and Technology Engineering laboratory, Chulalongkorn University. The infrared spectra were recorded between wavenumber of 400 and 4000 cm^{-1} with resolution of 2 cm^{-1}. The number of scan was 64 and resolution was 2 cm^{-1}.

3.2.4.3 Scanning electron microscopy (SEM)

Morphology of the obtained products was examined by a scanning electron microscope (JSM-6400, JEOL Co., Ltd.). The particle size was approximated from the micrographs, using image processing software (JEOL Semafore 5.0) at Scientific and Technological Research Equipment Center (STREC), Chulalongkorn University.

3.2.4.4 Thermal decomposition

Thermal decomposition behavior of the samples was determined by using thermogravimetric analysis on a Mettler-Toledo TGA/DSC1 STARe System at Center of Excellence in Particle and Technology Engineering laboratory, Chulalongkorn University studied with heating rate of 5°C/min in oxygen gas from temperature of 25 to 500°C. The carbon residual was also determined by this analyzer but difference in operating condition (heating rate of 10°C/min in oxygen gas from temperature of 25 to 1000°C).

3.2.4.5 X-ray diffraction analysis (XRD)

The crystalline phases of the obtaineded products were examined by using X-ray diffraction (XRD, Bruker AXS D8 Advance *)* with a CuK_{α} radiation source (wavelength =1.5406 Å) at 40 kV. The measurement was carried out in the range of 2θ = 20° – 80°. The crystallite size was calculated from the half-height width of the main diffraction peak or (110) crystalline plane of cassiterite (2θ = 27 degree), according to Scherrer's equation (equation 3.1).

$$D = \frac{k\lambda}{\beta \cos\theta} \qquad (3.1)$$

where D is crystallite size, k is a constant equal to 0.9, λ is the X-ray wavelength, β is the full width at half maximum and θ is the half diffraction angle.

CHAPTER IV

RESULTS AND DISCUSSION

This chapter is divided into 3 parts consisting of comparing tin dioxide with and without RF gel, interaction between tin sol and RF gel template and effect of various synthesis parameters. Their effects were studied by using SEM, XRD, FTIR, thermal analysis and N_2 adsorption-desorption analysis.

4.1 Tin dioxide with and without RF gel

Tin dioxide with and without RF gel were synthesized by sol-gel method. After removing the RF gel by calcination, the white powder was obtained. The color of the product without RF gel is also white. The XRD result indicated that the both products are cassiterite (See in Figure 4.1), which has tetragonal rutile structure. It was found that morphology of the obtained product with assistance of RF gel is different from the synthesized product without RF gel as shown in Figure 4.2. SEM of the product with RF gel shows porous surface area, whereas morphology of tin dioxide synthesized without RF gel is non-porous. This result combined with the result from N_2 adsorption-desorption analysis indicated that the product with RF gel has the presence of mesoporous structure with slit shape (Type IV isotherm with H3 type hysterisis loop) as illustrated in Figure 4.3. Moreover, the specific surface area of the synthesized product with RF gel (42.99 m^2/g) was higher than the product without RF gel (29.63 m^2/g). From the above results, the RF gel could be used as the template to fabricate mesoporous tin dioxide with high surface area.

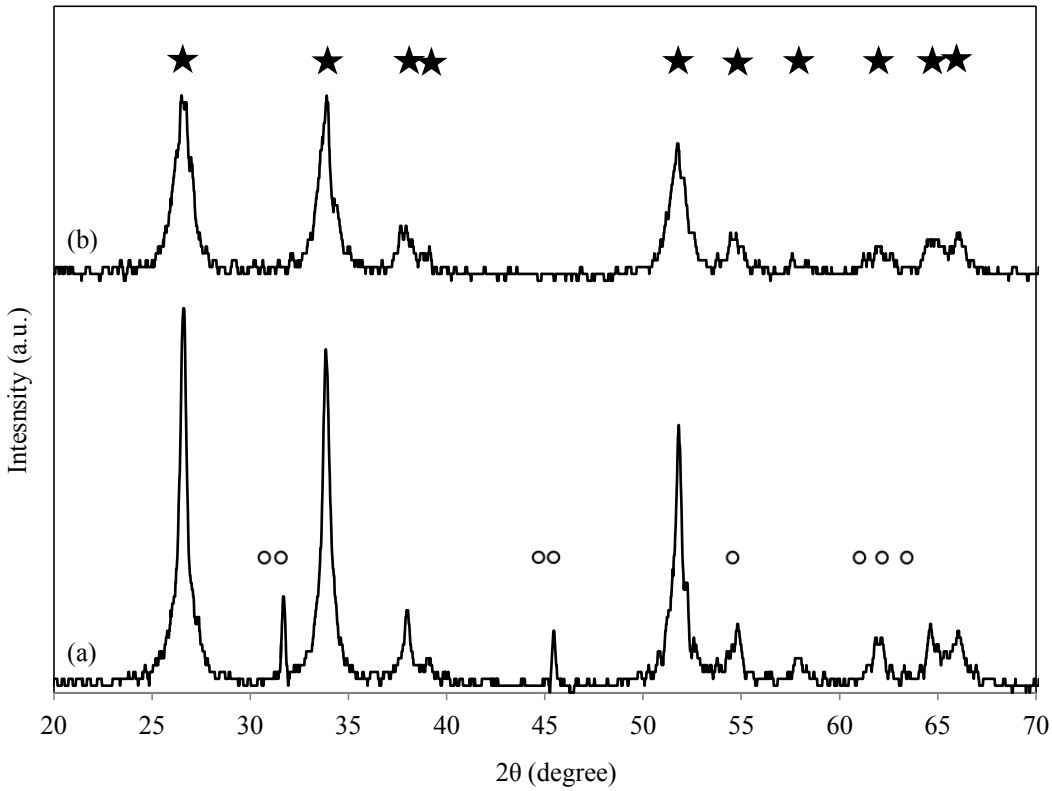

Figure 4.1 XRD patterns of the synthesized tin dioxide prepared with RF gel (a) and without RF gel (b). ○ and ★ denotes Sn phase and SnO_2, respectively.

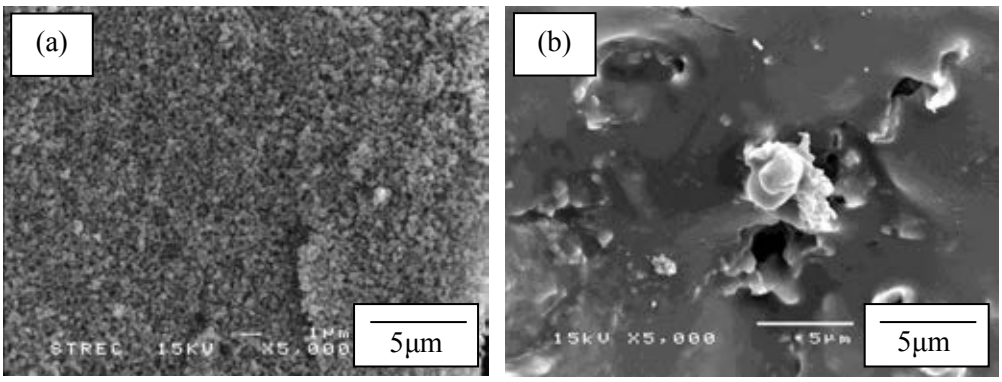

Figure 4.2 SEM micrographs of the synthesized tin dioxide with (a) and without RF gel (b).

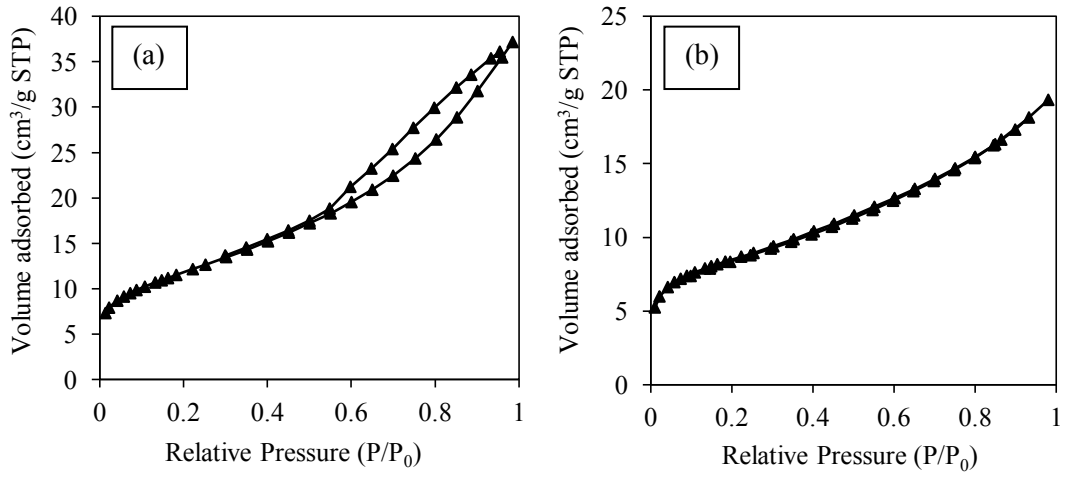

Figure 4.3 N_2 adsorption-desorption analysis of the synthesized tin dioxide with (a) and without RF gel (b).

4.2 Interaction between tin sol and RF gel template

Due to tin tetrachloride pentahydrate ($SnCl_4.5H_2O$) or tin precursor reacts violently with RF gel, tin precursor was firstly dissolved in formaldehyde in order to prevent rapid solidification by forming preformed tin sol. FTIR was used to confirm the formation of tin sol as shown in Figure 4.4.

Identification of IR bands corresponding with formaldehyde and $SnCl_4.5H_2O$ are listed in Table 4.1. Considering FTIR spectrum of the preformed tin sol, there are five interesting peaks that indicate the formation of tin sol. First, the absorption peak at 1159 cm^{-1} is decreased and the intensity of absorption band at 1174 cm^{-1} is increased while increasing the aging time for tin sol from 0 to 24 hour. While increasing the aging time of tin sol more than 24 hours, the spectrums are similar. This result means that the tin sol occurs during the aging time between 0 and 24 hour. Moreover, it seems that the intensity of C-OH bond at 1051 cm^{-1} is increased when $SnCl_4.5H_2O$ was added into formaldehyde. In addition, the absorption peak at 862 and 546 cm^{-1} which are referred to functional group in tin tetrachloride pentahydrate appear in tin sol. This result means that tin sol has some functional groups as same as tin tetrachloride pentahydrate but still can not specify these functional group.

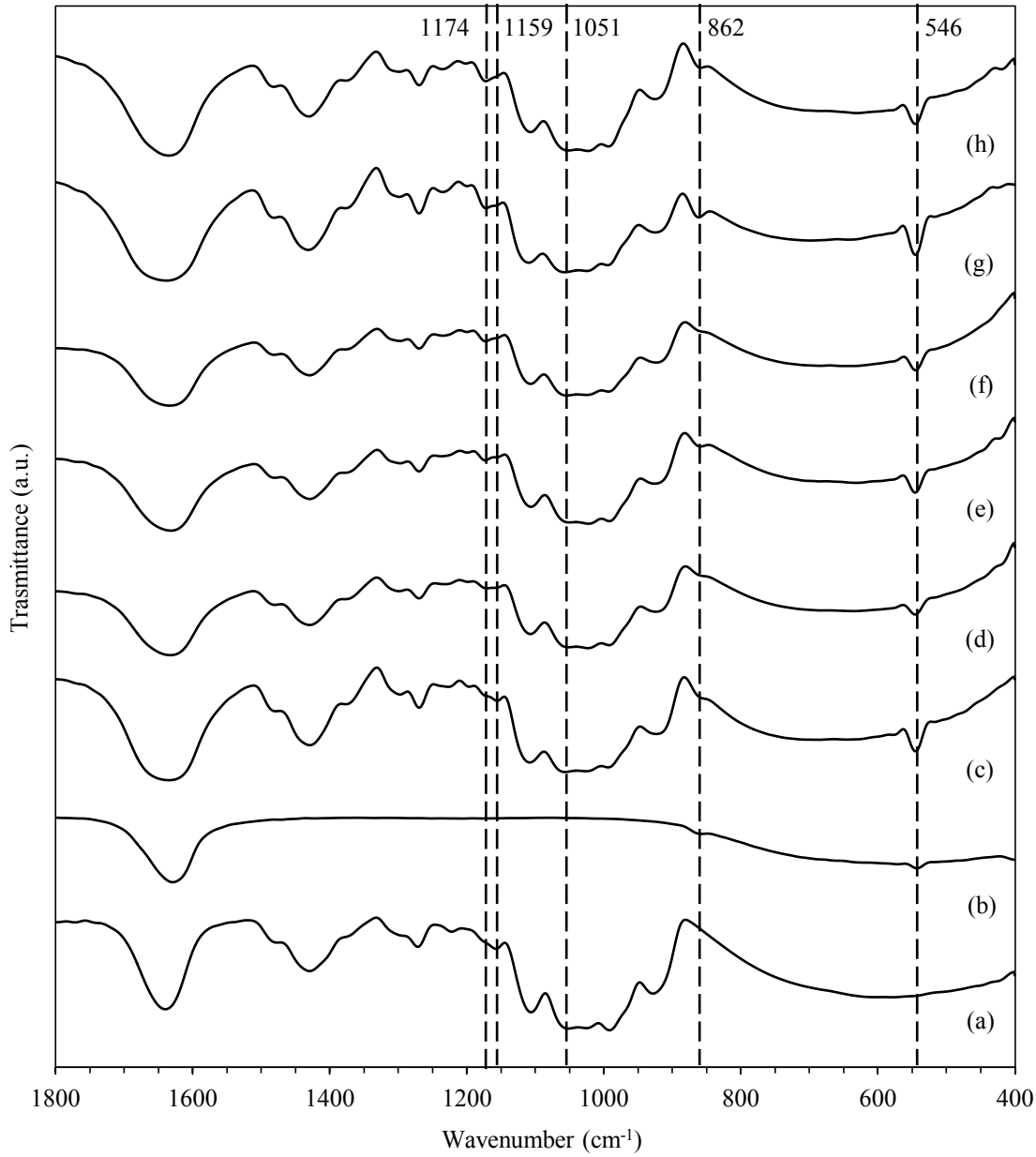

Figure 4.4 FTIR spectrum of formaldehyde (a), $SnCl_4.5H_2O$ (b), preformed tin sol aged for 0 (c), 1 (d), 2 (e), 24 (f), 48 (g) and 72 hour (h).

Table 4.1 FTIR peak assignment for formaldehyde and tin tetrachloride pentahydrate.

Wavenumber (cm^{-1})	Peak assignment	References
	Formaldehyde	
1642	C=O stretch	[85]
1433	C-H bend	[85]
1271		
1103	-C-OH	[85]
1051	-C-OH	[85]
992	C-H	[85]
934		
615		
	Tin tetrachloride pentahydrate ($SnCl_4.5H_2O$)	
1232-900	Sn-OH vibration	[86]
769	Sn-Cl	[87]
505		
406		
660-600	O-Sn-O bridge	[86]
560	Terminal oxygen vibration of Sn-OH	[86]

When the preformed tin sol was added into RF gel, the color of mixture was immediately changed from dark brown to light yellow. After a few minutes, the liquid mixture transformed into pink solid. While the neat RF gel transformed into dark brown solid. This observation implies that the interaction between the tin sol and RF gel is spontaneously occurred. Thermal decomposition result can be used to witness this interaction.

Figure 4.5 shows TG and DSC graph of precalcined tin sol, neat RF gel and Sn/RF composite in oxygen flow (45 ml/min) at heating rate of 10^{o}C/min. DSC method measures the energy required to keep the reference and the sample at the same temperature. It can be seen that all samples has endothermic peak around 90^{o}C due to evaporation of residue solvent and adsorbed water, which corresponds to the weight loss appeared at this temperature as shown in Figure 4.5(a). For tin sol, it was noticed that DSC graph shows endothermic peak around 100^{o}C and significant weight loss (>75%) appeared at this temperature. This could be resulted from oxidation of tin compound to tin dioxide. However, type of tin compound can not be

clearly indicated at this moment. At temperature above 600^{o}C, there was no further weight loss, indicating completion of the reaction involving a weight change.

For neat RF gel, the major mass loss occurred at temperature of 350^{o}C and 470^{o}C, which attributes to the breaking bond of C-O and C-H in the RF networks, respectively [58]. Considerating TG and DSC graph of Sn/RF composite, first weight loss (>55%) and second weight loss (>20%) with exothermic peak occurred around 240 and 400^{o}C, respectively. If tin sol does not interact with RF gel, TG result should show two weight losses at 100 and 400^{o}C, which corresponds to the temperature of major weight loss of precalcined tin sol and RF gel occurred, respectively. Therefore, the decomposition of Sn/RF composite that appeared at 240^{o}C can be the evidence for interaction between tin sol and RF gel. Moreover, the TG result of Sn/RF composite shows the second weight loss at 400^{o}C and characteristic of decomposition at this temperature is similar to decomposition of neat RF gel that occurred at the same temperature. From these results, it can be concluded that there are two compounds in Sn/RF composite. One is the composite like RF gel and the other is new compound resulted from the interaction between tin sol and RF gel.

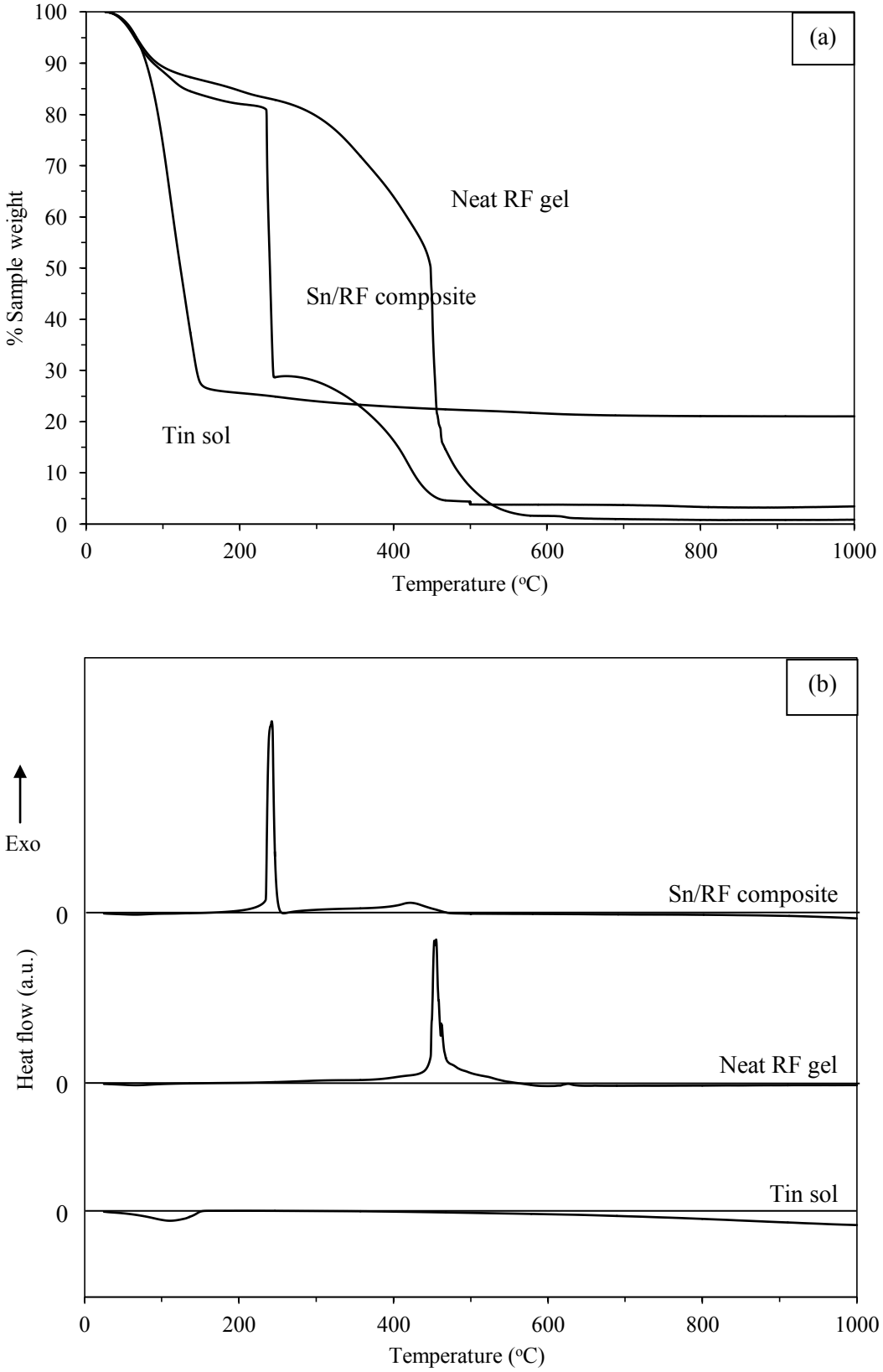

Figure 4.5 TG (a) and DSC (b) analysis of tin sol, RF gel and Sn/RF composite.

Another result to confirm the interaction between tin sol and RF gel is a result from FTIR technique. Table 4.2 shows assignments of FTIR absorption bands of RF gel. In Figure 4.6, the spectrum of neat RF gel and Sn/RF composite composed of the absorption band, which refers to -CH_2- scissor vibration at 1477 cm^{-1}, C=C in aromatic rings at 1612 cm^{-1} and CH_2-O-CH_2 bridges at 1220 and 1092 cm^{-1}. The interesting peaks are -CH_2- bonding and CH_2-O-CH_2 bridges, which resulted from condensation of hydroxylmethyl derivatives and polycondensation of resorcinol by formaldehyde. Comparing FTIR spectrum of neat RF gel with Sn/RF composite (See in Figure 4.6), the intensity of CH_2-O-CH_2 bridges is dramatically increased by adding the preformed tin sol. It suggested that tin sol can accelerate condensation reaction between resorcinol and formaldehyde. The tin sol does not only accelerate the reaction but also interacts with RF gel. It can be confirmed by the absorption band at 1612 cm^{-1} assigned to C=C aromatic ring stretching vibration that is quite shifted. These results attribute to the interaction between tin sol and RF gel. The absorption band of Sn-O-Sn bonding at 600-660 cm^{-1} appears in both of tin sol sample and Sn/RF composite. However, altering of Sn-O-Sn bonding is not clearly noticed, so this result can not indicate that the formation of Sn-O bonding is carried on or not.

Table 4.2 FTIR peak assignment for resorcinol-formaldehyde gel.

Wavenumber (cm^{-1})	Peak assignment	References
	Resorcinol-formaldehyde gel (RF gel)	
1612	C=C aromatic ring	[85]
1477	CH_2- methylene bridges	[36]
1298	C-O stretching	[85]
1220	C-O-C stretching vibrations of methylene ether bridges	[36]
1175	CH aromatic	[85]
1092	C-O-C stretching vibrations of methylene ether bridges	[36]

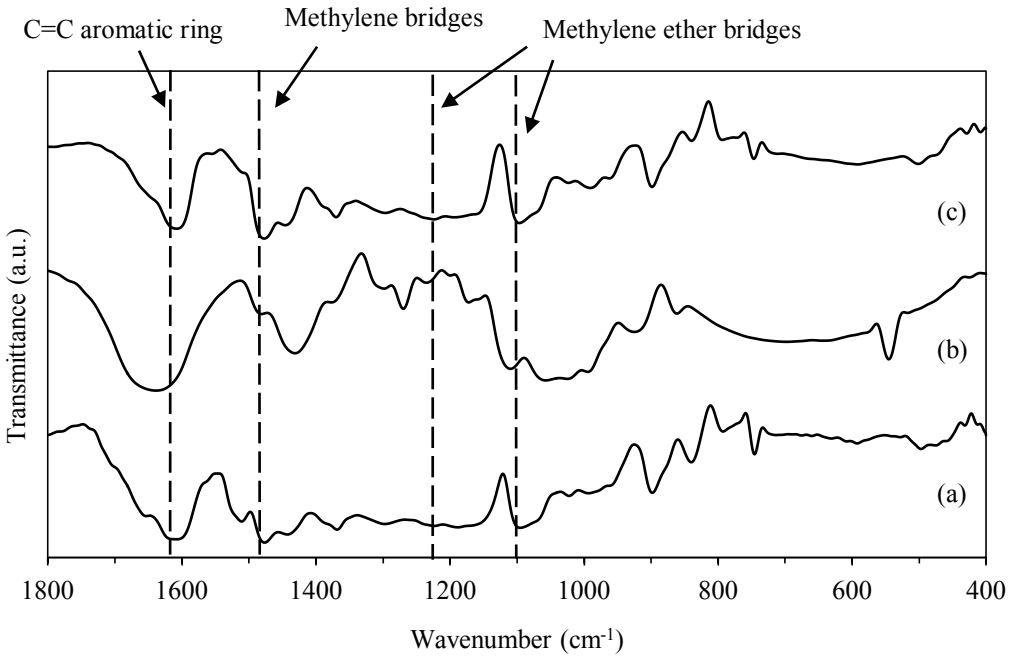

Figure 4.6 FTIR spectrums of neat RF gel (a), preformed tin sol (b) and Sn/RF composite (c).

Figure 4.7 shows FTIR spectrum of Sn/RF composites that was aged for 2, 4, 24, 48 and 72 hours. The C=C in aromatic rings peak at 1612 cm^{-1} is used as the reference peak to study the formation of $-CH_2-$ bonding and CH_2-O-CH_2 bridges by calculate signal ratio (intensity of interesting peak/ intensity of reference peak) versus time. The signal ratio of $-CH_2-$ bonding is increased when increasing aging time of mixed gel as shown in Figure 4.8. The signal ratio of CH_2-O-CH_2 bridges and Sn-O-C bonding at 880-900 cm^{-1} [88] are also increased. This result means that even after the RF gel was mixed with tin sol, the condensation is still continued.

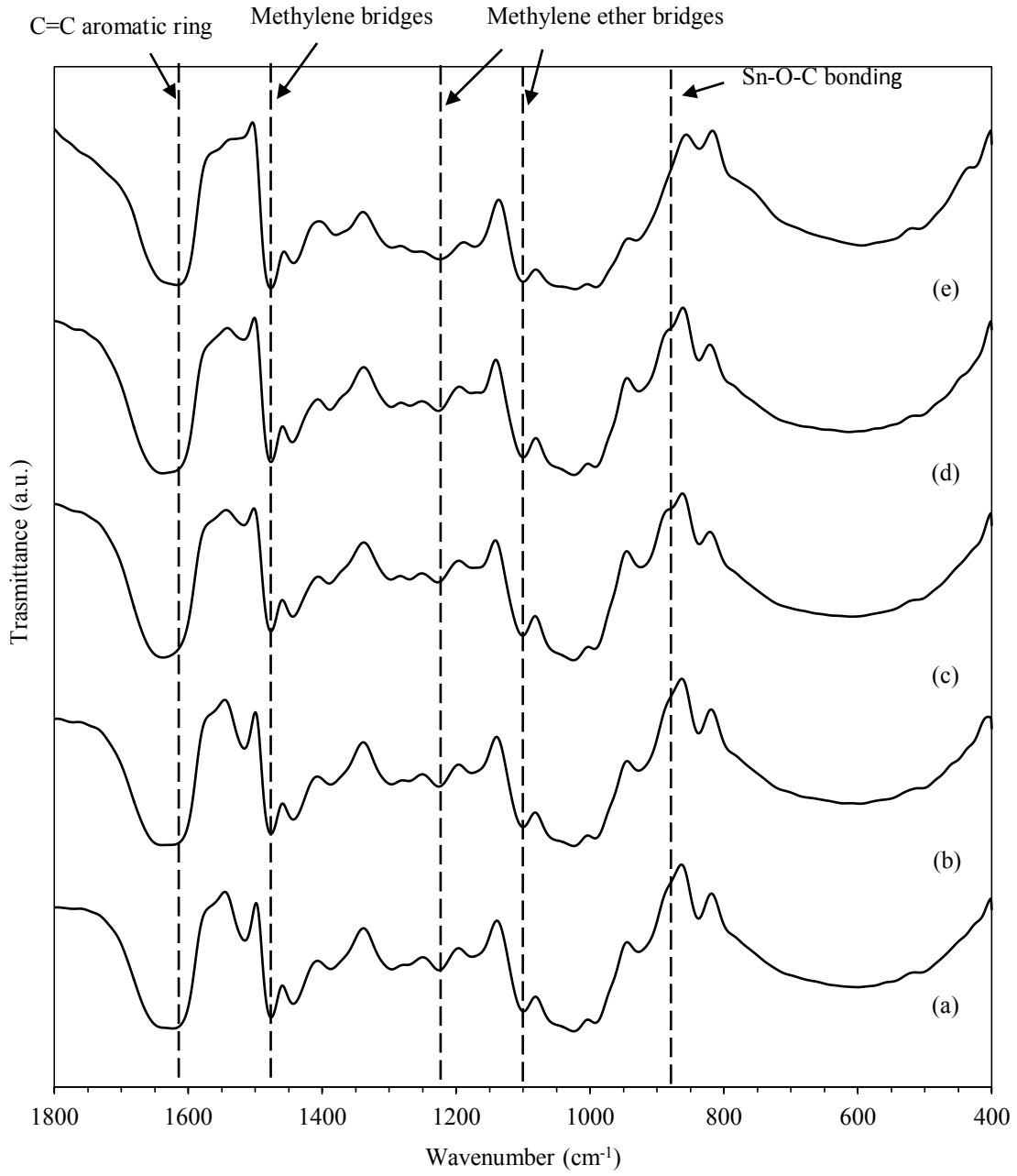

Figure 4.7 FTIR spectrum of Sn/RF composites with aged for 2 (a), 4 (b), 24 (c), 48 (d) and 72 hours (e).

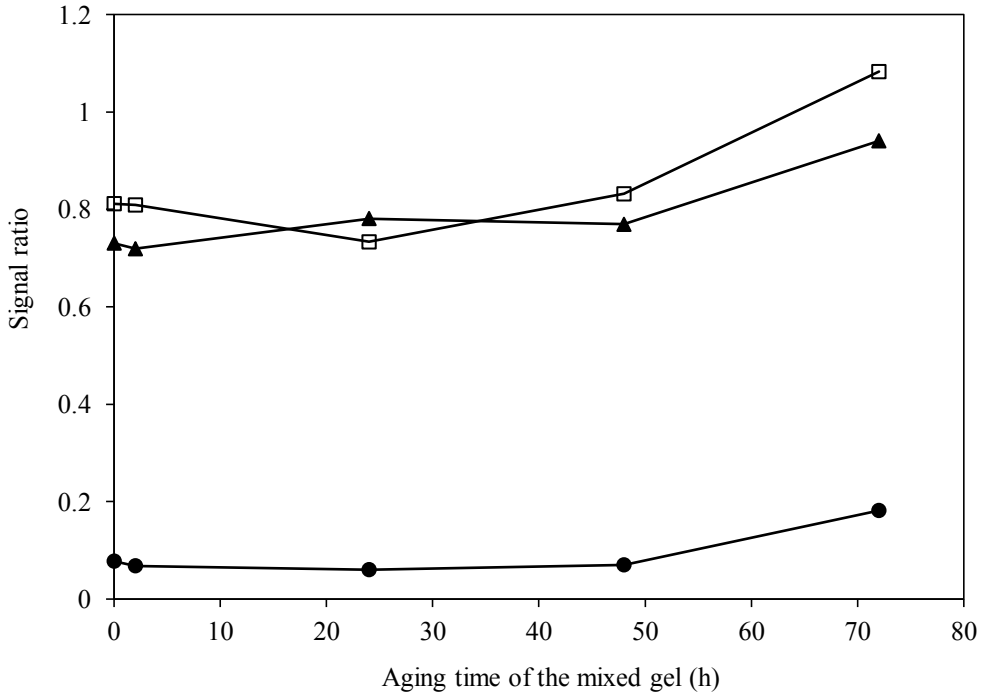

Figure 4.8 FTIR signals ratio of (□) methylene, (▲) methylene ether bridges and (●) Sn-O-C bonding of the mixed gel aged for various aging time with respect to aromatic rings in the gel.

4.3 Effect of various factors

Effects of process parameters, i.e., Sn/F molar ratio, R/C molar ratio, Sn/R molar ratio, type of diluting solvent, tin sol aging time, RF gel aging time, mixed gel aging time, drying process and calcination temperature, were studied and presented in this section.

4.3.1 Sn/F molar ratio

Tin dioxide product was prepared by using various Sn/F molar ratios, fixed R/C molar ratio of 50 and fixed Sn/R molar ratio of 0.08. The Sn/F molar ratios in the preformed tin sol that used to study the effect of Sn/F molar ratio on the final product are 0.003, 0.005, 0.007, 0.010, 0.020 and 0.060. In this investigation, the amount of formaldehyde used in preparation of tin sol was varied, while that used in RF gel preparation was fixed. The other chemicals, which are tin tetrachloride pentahydrate, resorcinol, water, sodium carbonate and ethanol, were fixed at the certain amount. RF gel was aged for 4 hours and tin sol was aged for 3 days. After adding the tin sol into RF gel, the mixture was aged for 3 days and dried by freeze drying and then calcined at 500^{o}C (Atmospheric pressure). After removing RF gel

template, the products were obtained and characterized by FTIR, SEM and N_2 adsorption-desorption analysis.

Figure 4.9 shows FTIR spectrum of the precalcined Sn/RF composite prepared with varying Sn/F molar ratio. There are three interesting peaks, namely, methylene bridge (-CH_2-) at 1477 cm^{-1}, methylene ether bridge (-CH_2-O-CH_2-) at 1092 cm^{-1} and Sn-O-C bond at 880-900 cm^{-1} [36, 85, 88]. It is noticed that the intensity of methylene ether bridge peak at 1092 cm^{-1} was increased when increasing concentration of formaldehyde (lower Sn/F molar ratio) as shown in FTIR signal ratio (See in Figure 4.10). On the other hand, the intensity of absorption band at 1477 cm^{-1} corresponding to methylene bridge was slightly increased. This result means the excess amount of formaldehyde in the preformed tin sol reacts with RF gel. Therefore, it results in greater extent of crosslinked network (increased CH_2-O-CH_2 bridge). The increased network caused RF gel is less reactive with tin precursor. However, it is essentially beneficial in preventing the rapid solidification of the mixture when adding the tin sol into RF gel. Consequently, homogeneous mixture are obtained, which results in more uniform interaction between tin sol and RF gel throughout the composite. This interaction is witnessed from the increase in Sn-O-C bond when increasing concentration of formaldehyde. If the interaction between tin sol and RF gel is increased, it will prevent pore collapsing during calcination. Thus, the surface area of the tin dioxide is enhanced by increasing concentration of formaldehyde (lower Sn/F molar ratio) in the range of 0.007-0.060 as shown in Table 4.3.

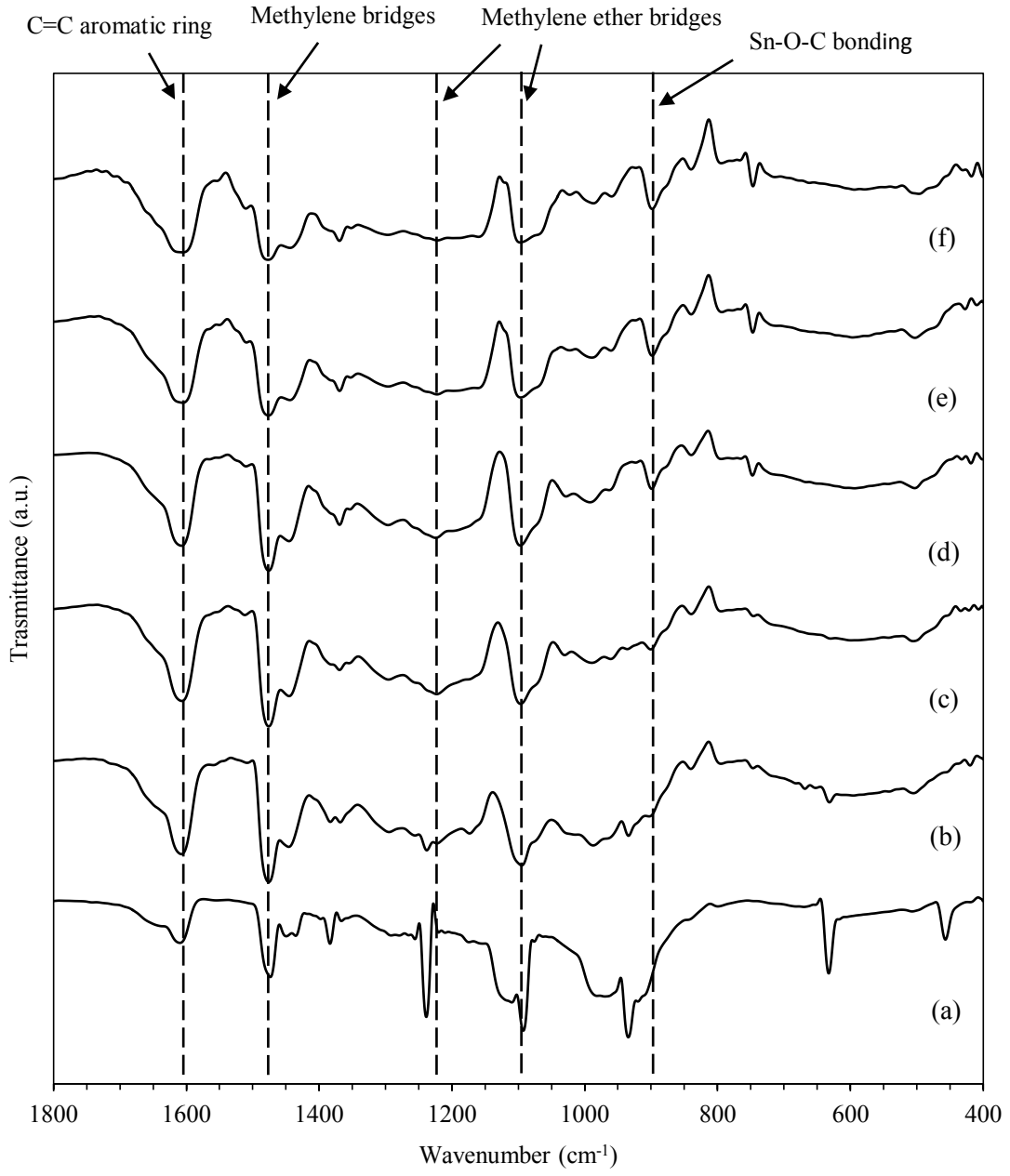

Figure 4.9 FTIR spectrum of the product prepared with Sn/F molar ratio at 0.003 (a), 0.005 (b), 0.007 (c), 0.010 (d), 0.020 (e) and 0.060 (f).

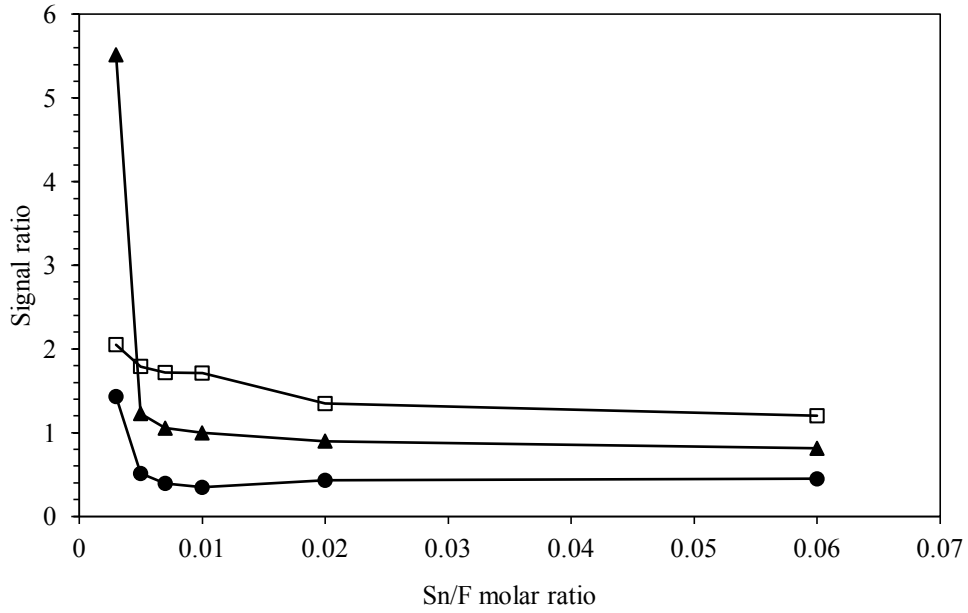

Figure 4.10 FTIR signal ratio of (□) methylene, (▲) methylene ether bridges and (●) Sn-O-C bonding of the mixed gel with various Sn/F molar ratios with respect to aromatic rings in the gel.

Table 4.3 Properties of the synthesized products with various Sn/F molar ratios.

Sn/F molar ratio	Surface area (m^2/g)	V_p (cm^3/g)	Mean pore diameter (nm)
0.003	32.98	0.0277	-
0.005	37.20	0.0320	-
0.007	44.04	0.0549	4.82
0.010	41.16	0.0575	4.82
0.020	38.10	0.0511	4.82
0.060	29.53	0.0521	24.47

Nevertheless, too excessive amount of formaldehyde results in non-porous structure (See in Figure 4.11). The result from N_2 adsorption-desorption analysis show that N_2 adsorption-desorption isotherm in the low Sn/F molar ratio (i.e., 0.003 and 0.005) is type II isotherm which indicates the presence of non-porous structure in the sample. This result may be caused by dilution effect from the addition of formaldehyde, which results in larger size of the RF particles [85]. On the other hand, N_2 adsorption-desorption isotherm of the product from high Sn/F molar ratio (i.e., 0.007, 0.010, 0.020 and 0.060) is type IV isotherm, which indicate mesoporous structure as demonstrated in Figure 4.11. BJH method reveals that pore

size distribution is broader when increasing Sn/F molar ratio (See in Figure 4.12). Moreover, decrease in concentration of formaldehyde leads to high pore volume as indicated in Table 4.3.

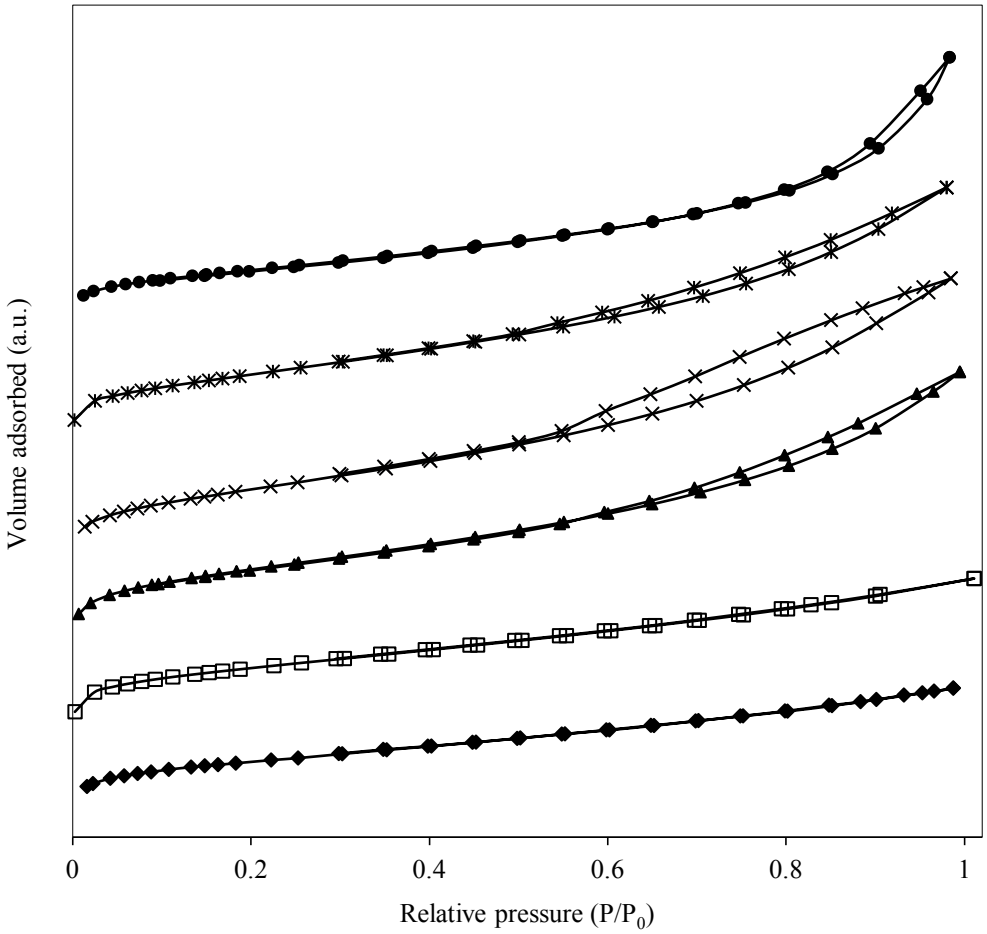

Figure 4.11 N_2 adsorption-desorption isotherm of the products with Sn/F molar ratio of (♦) 0.003, (□) 0.005, (▲) 0.007, (×) 0.010, (✳) 0.020 and (●) 0.060.

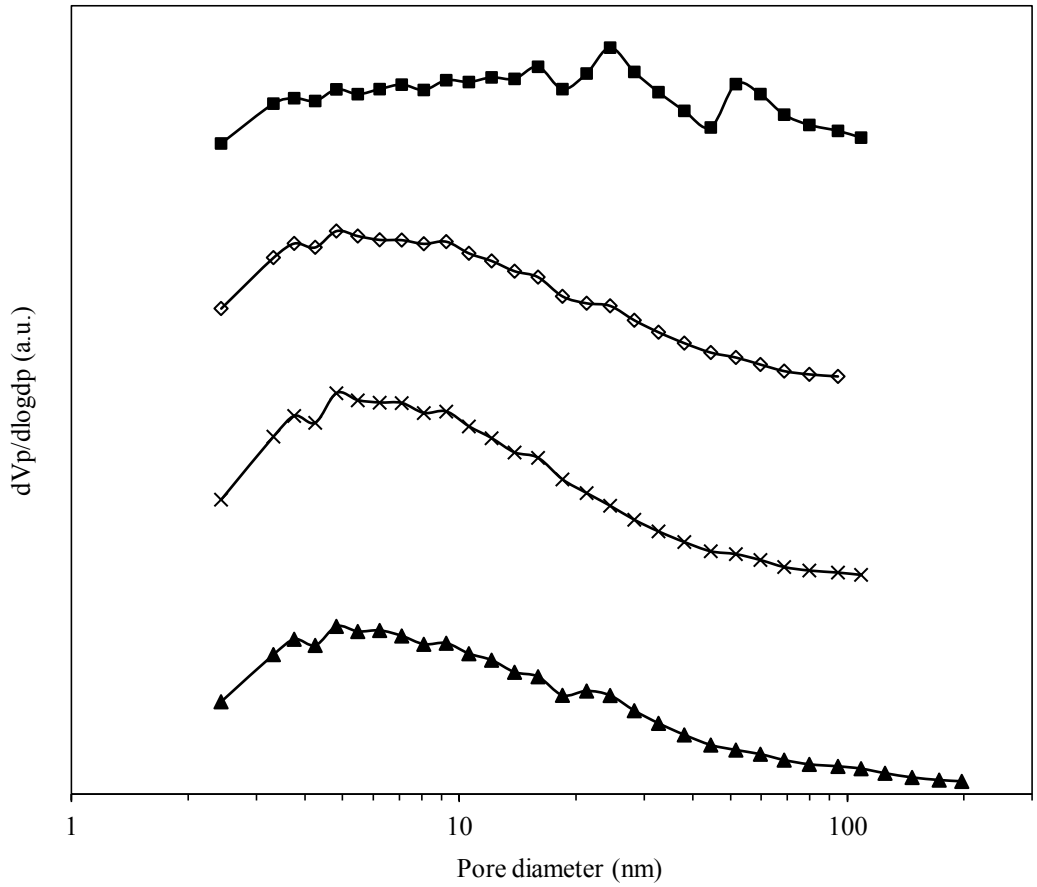

Figure 4.12 Pore size distribution of the products with Sn/F molar ratio of (▲) 0.007, (×) 0.010, (◇) 0.020 and (■) 0.060.

Figure 4.13 shows SEM images of the obtained product with various Sn/F molar ratios. It was found that increase in Sn/F molar ratio results in smaller tin dioxide particles. This result indicates that excess amount of formaldehyde causes dilution effect, thus decrease in Sn/F molar ratio results in larger tin dioxide particles.

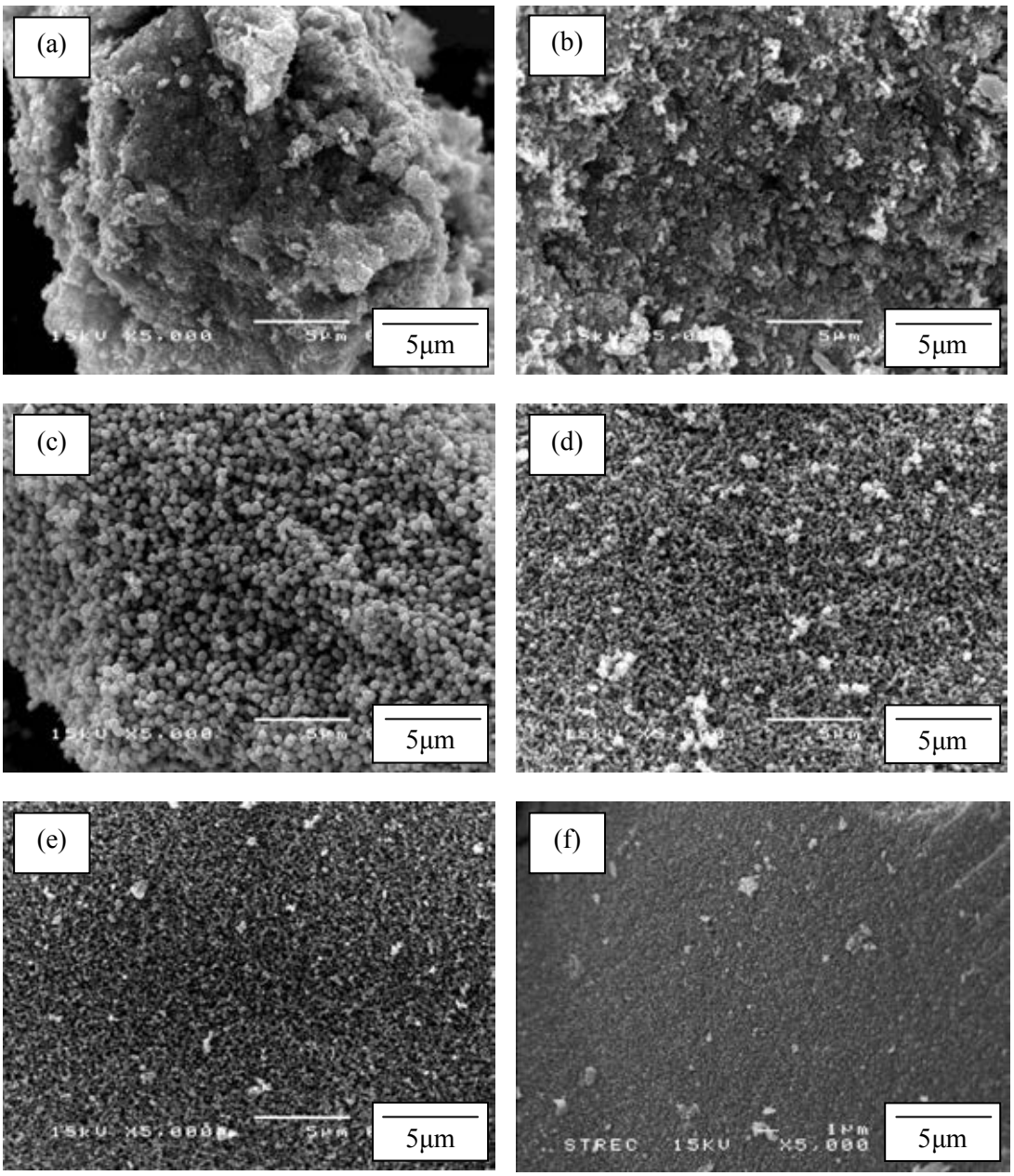

Figure 4.13 SEM image of synthesized product with Sn/F molar ratio at 0.003 (a), 0.005 (b), 0.007 (c), 0.010 (d), 0.020 (e) and 0.060 (f).

4.3.2 R/C molar ratio

In this study, the R/C molar ratio was varied from 50 to 300 in order to study effect of R/C molar ratio on the final properties of the product. These R/C molar ratios are mostly used for fabrication of carbon gel. The mixed gels were aged for 3 days and then removed the template and residue carbon by calcination at 500^{o}C. It should be noted that an amount of

chemicals, i.e., resorcinol, formaldehyde, water and tin tetrachloride, were fixed. The effect of catalyst ratio was investigated using FTIR, N_2 adsorption-desorption analysis and SEM.

Figure 4.14 shows FTIR spectrum of precalcined Sn/RF composites that were prepared with R/C ratio of 50, 100, 200 and 300. It was found that all spectrums are similar. It is clearly seen in FTIR signal ratio as shown in Figure 4.15. The results indicate that the functional groups within the product are not affected by R/C molar ratio.

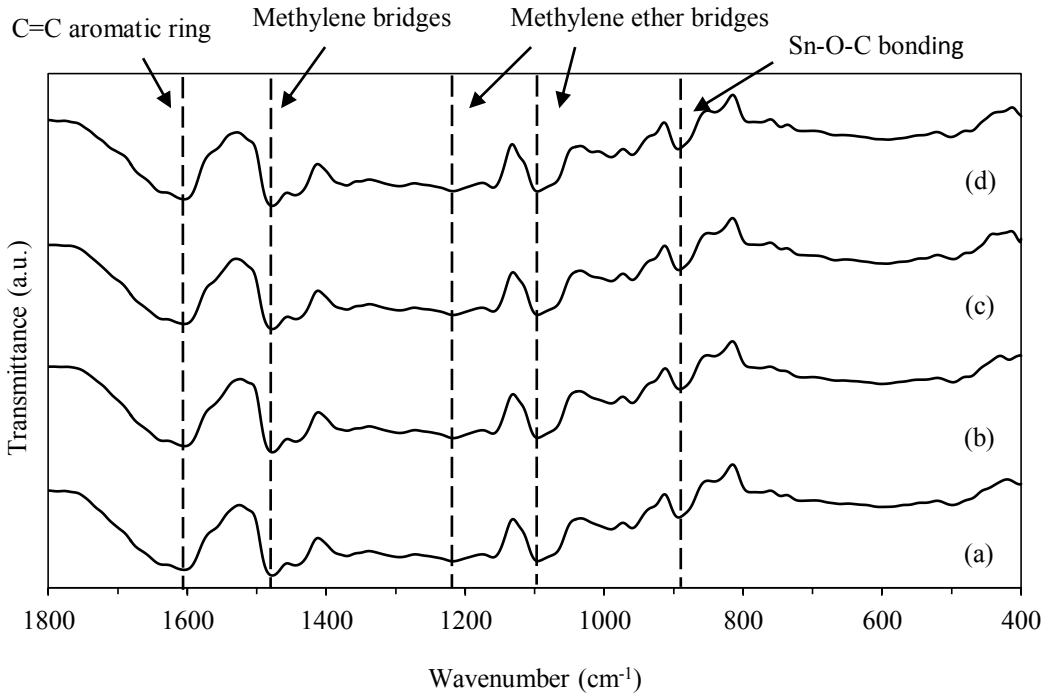

Figure 4.14 FTIR spectrum of the precalcined composites with R/C molar ratio at 50 (a), 100 (b), 200 (c) and 300 (d).

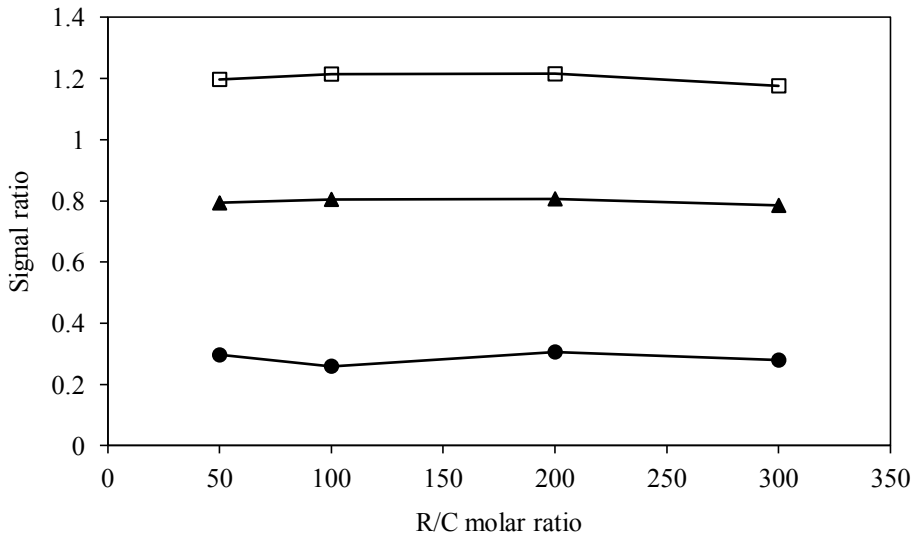

Figure 4.15 FTIR signal ratio of (□) methylene, (▲) methylene ether bridges and (●) Sn-O-C bonding of the mixed gel with various R/C molar ratios with respect to aromatic rings in the gel.

In the previous study, the carbon which is produced from RF gel with R/C molar ratio of 50 has the maximum surface area [68]. In the fabrication of mesoporous tin dioxide, the product with R/C molar ratio of 50 was found to have the highest surface area as well (See in Table 4.4). As the amount of catalyst is decreased, i.e., increasing R/C molar ratio, size of the RF particle becomes larger [89].Owing to RF gel is used as the template for synthesis mesoporous tin dioxide, the properties of the template has an impact on the properties of the obtained product. Therefore, surface area of the synthesized tin dioxide is decreased by increasing R/C molar ratio as illustrated in Table 4.4. In Figure 4.16, N_2 adsorption-desorption analysis reveals that all the products has the mesoporous structure (Type IV isotherm). Nevertheless, the mean pore diameter of the products remains the same. This means that increased R/C molar ratio enhances the number of pores in the product. BJH plot shows pore size distribution of the products (See in Figure 4.17). It was noticed that pore size distribution of synthesized product, which prepared with low R/C molar ratio, is narrower distribution.

Table 4.4 Properties of the products with various R/C molar ratios.

R/C molar ratio	Surface area (m^2/g)	V_p (cm^3/g)	Mean pore diameter (nm)
50	38.15	0.0511	4.82
100	35.51	0.0519	4.82
200	34.15	0.0402	4.82
300	31.28	0.0379	4.82

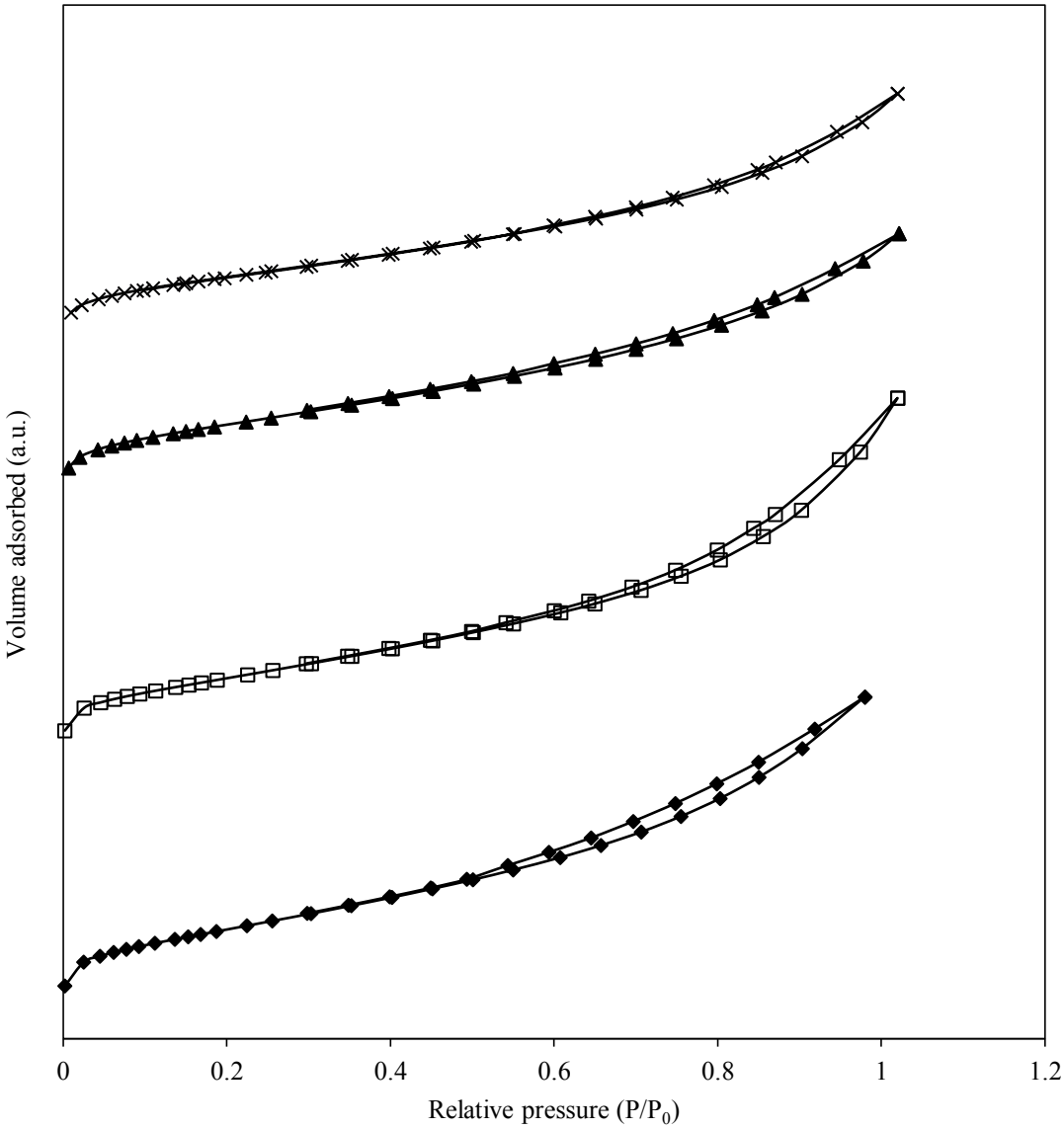

Figure 4.16 N_2 adsorption-desorption isotherm of the products with R/C molar ratio of (♦) 50, (□) 100, (▲) 200 and (×) 300.

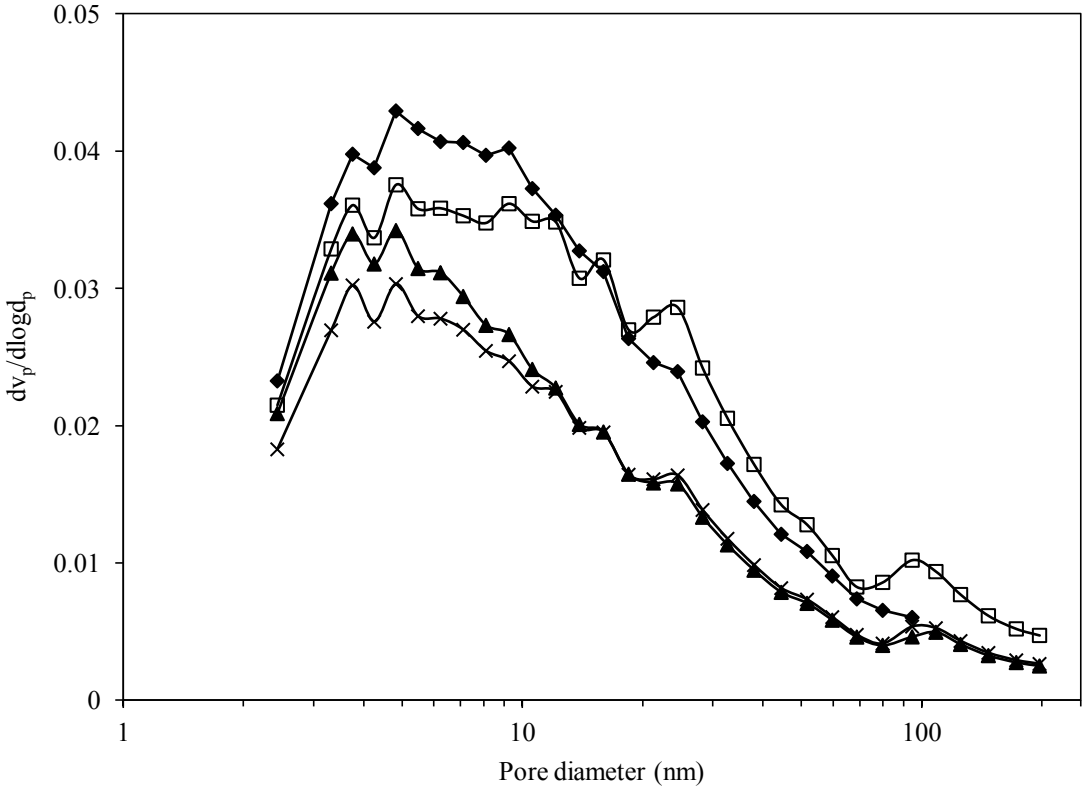

Figure 4.17 Pore size distribution of the products with R/C molar ratio of (♦) 50, (□) 100, (▲) 200 and (×) 300.

In Figure 4.18, SEM images of the obtained products with varying R/C molar ratio confirm that varying R/C molar ratio does not affect morphology of the particle.

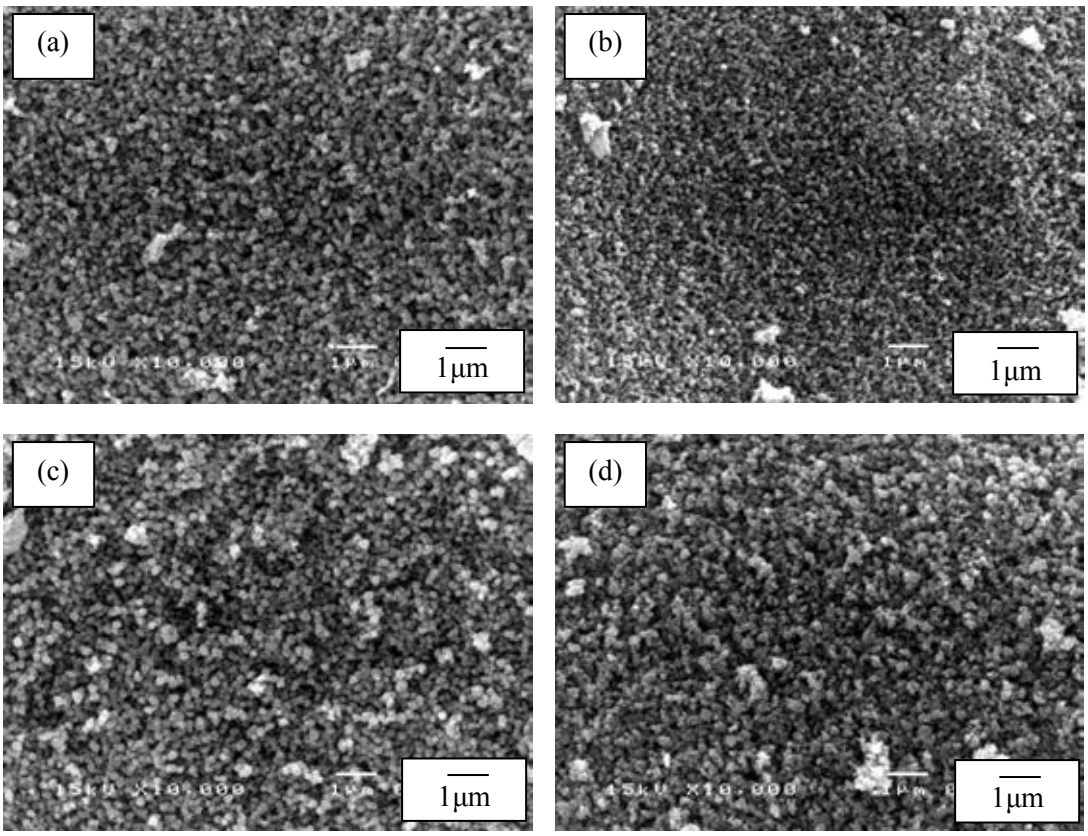

Figure 4.18 SEM image of tin dioxide products with R/C molar ratio of 50 (a), 100 (b), 200 (c) and 300 (d).

4.3.3 Sn/R molar ratio

In order to study the effect of Sn/R molar ratio, the RF gel was prepared by fixing all concentrations of reactants and aged for 4 hours. Then, the preformed tin sol with various concentrations of tin tetrachloride pentahydrate was added into the RF gel after aging for 3 days. The amount of formaldehyde was fixed, but the amount of tin tetrachloride pentahydrate was changed at different Sn/R molar ratio, namely, 0.03, 0.05, 0.08 and 0.10. The mixed gel was aged, dried by freeze drying and calcined at 500^{o}C. The tin dioxide products and the mixed gels were investigated using SEM, FTIR and N_2 adsorption-desorption analysis.

Figure 4.19 and Figure 4.20 show FTIR spectrum of the mixed gel aged for 1 and 3 days, respectively. It was found that the intensity of methylene (at 1477 cm^{-1}), methylene ether bridge (at 1092 cm^{-1}) and Sn-O-C bonding (at 880-900 cm^{-1}) [36, 85, 88] are obviously increased by increasing Sn/R molar ratio in the beginning of the aging period (the mixed gels aged for 1 day) as shown in FTIR signal ratio in Figure 4.21. However, the intensity of

interesting peaks, i.e., methylene, methylene ether bridge and Sn-O-C bonding, of the mixed gel aged for 3 days are not different in range of Sn/R molar ratio from 0.05 to 0.10 (See in Figure 4.22). At Sn/R molar ratio of 0.03, the intensity of these interesting peaks is significantly different from the other Sn/R molar ratio but still can not explain this occurrence. From above results, this can be concluded that the tin sol only catalyzes the formation of RF-networks and Sn-O-C bonding in the beginning of aging. For high Sn/R molar ratio, the small tin sol particles are formed due to high concentration of the precursor. Thus, the surface area of the synthesized product is enhanced by increasing Sn/R molar ratio in the range of 0.05-0.10 as shown in Table 4.5. Although their effect enhanced the surface area, the rapid solidification could occur by too large of the Sn/R molar ratio. N_2 adsorption-desorption analysis reveals that all samples has mesoporous structure (Type IV isotherm) as presented in Figure 4.23. From BJH plot (Figure 4.24), pore size distribution of the product is narrowed by increasing Sn/R molar ratio in the range of 0.05-0.10.

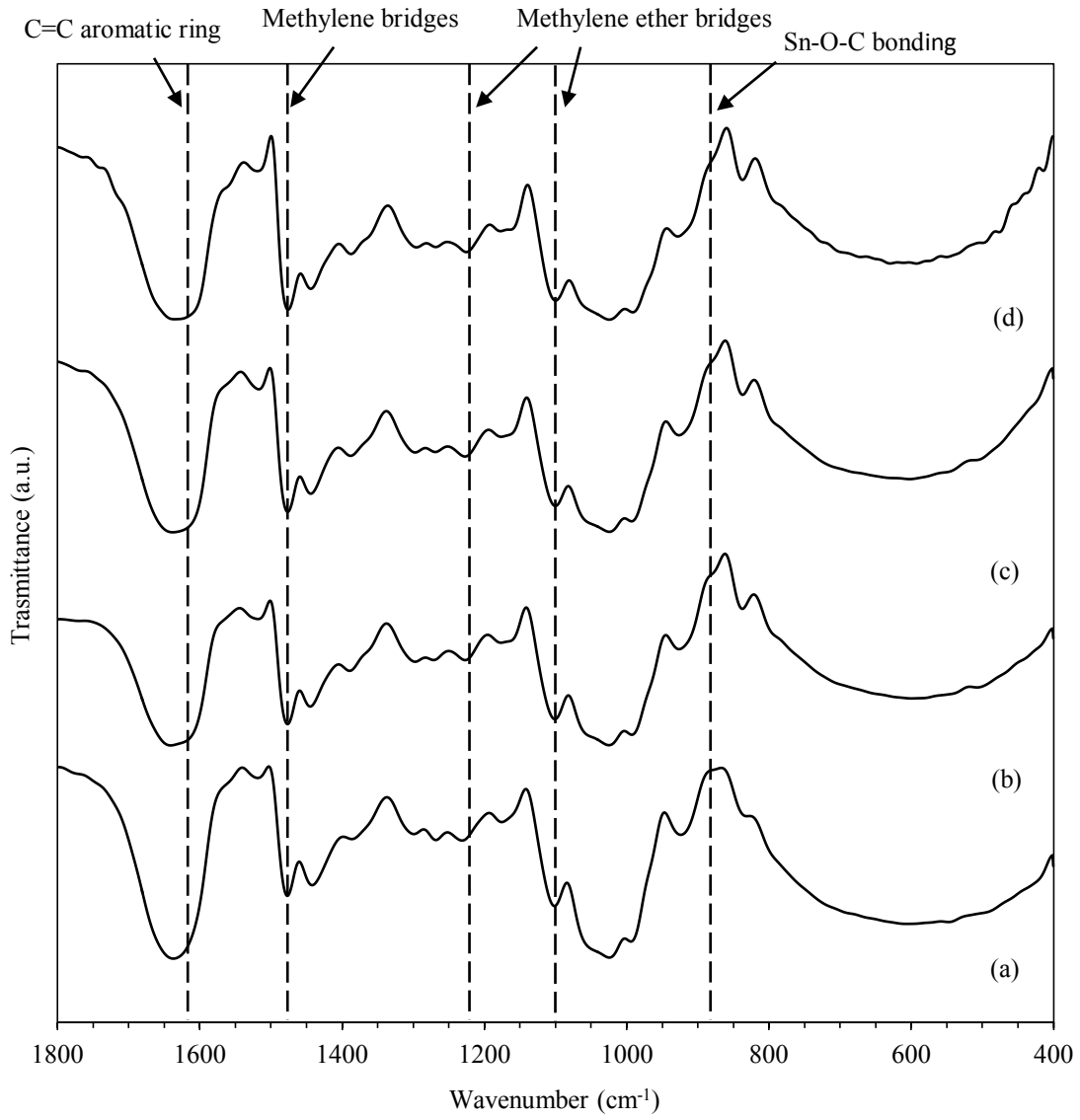

Figure 4.19 FTIR spectrum of the mixed gel aged for 1 day with Sn/R molar ratio at 0.03 (a), 0.05 (b), 0.08 (c) and 0.10 (d).

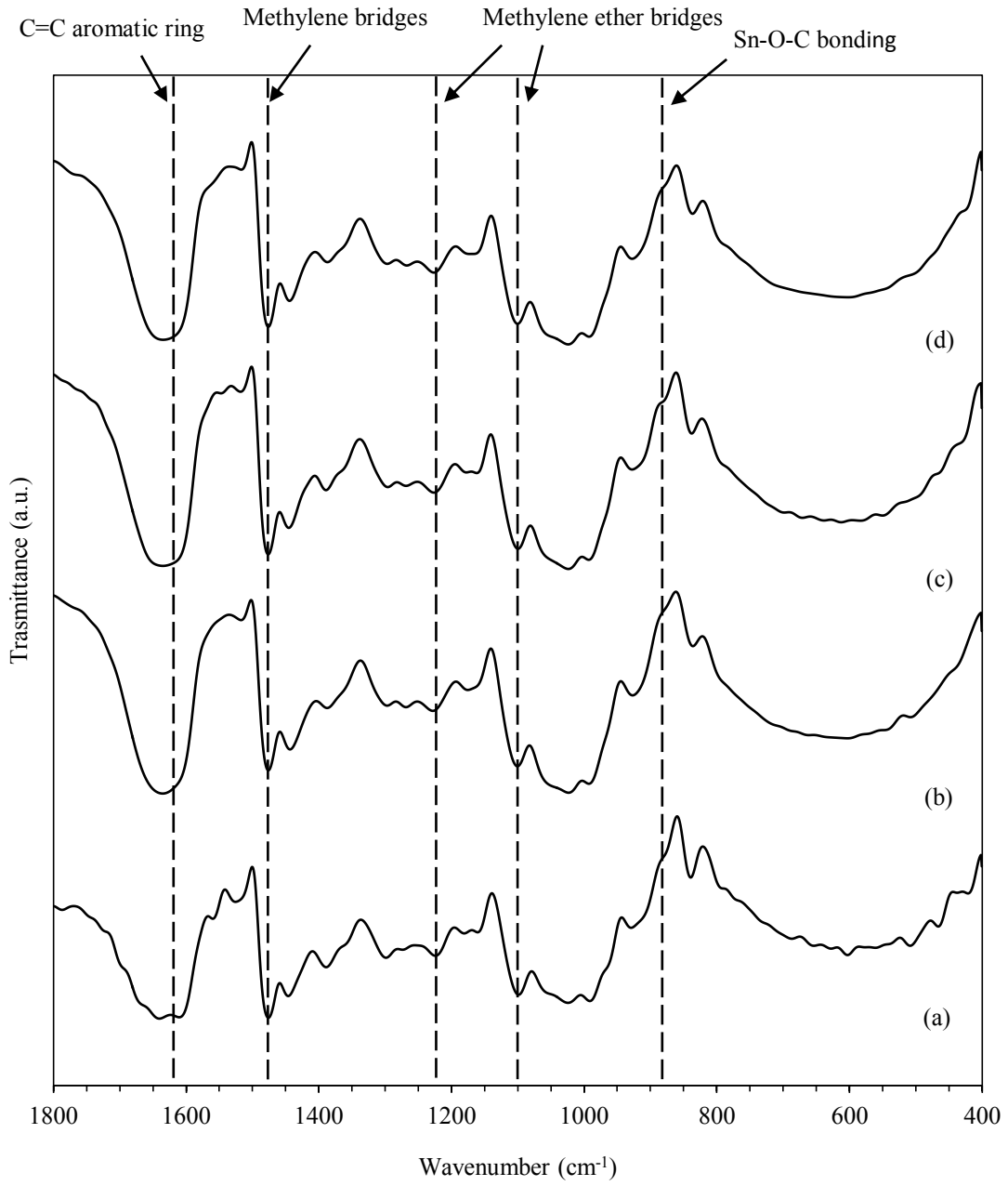

Figure 4.20 FTIR spectrum of the mixed gel aged for 3 days with Sn/R molar ratio at 0.03 (a), 0.05 (b), 0.08 (c) and 0.10 (d).

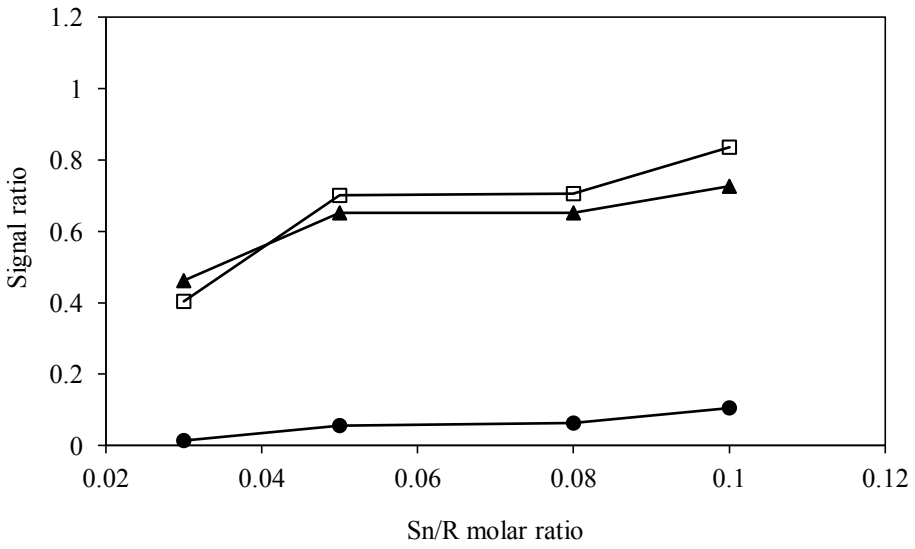

Figure 4.21 FTIR signal ratio of (□) methylene, (▲) methylene ether bridges and (●) Sn-O-C bonding of the mixed gel aged for 1 day with various Sn/R molar ratios with respect to aromatic rings in the gel.

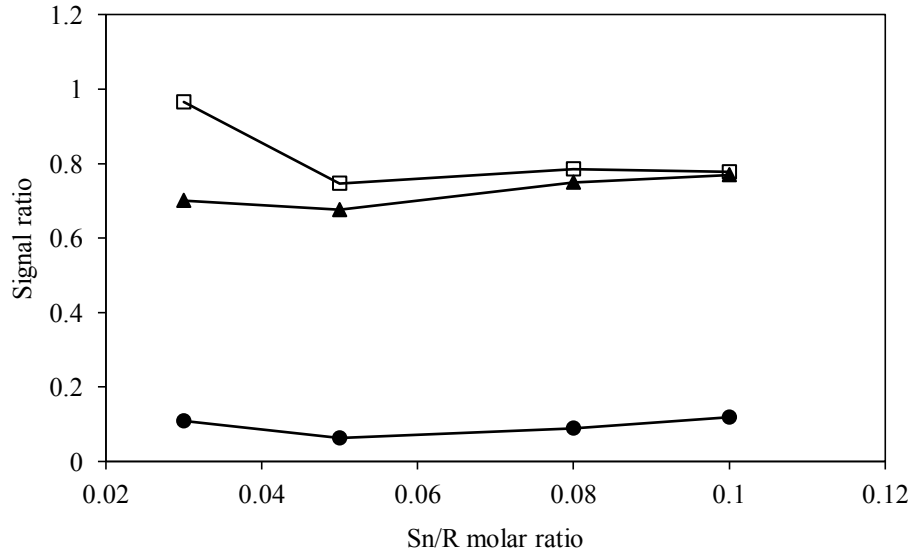

Figure 4.22 FTIR signal ratio of (□) methylene, (▲) methylene ether bridges and (●) Sn-O-C bonding of the mixed gel aged for 3 days with various Sn/R molar ratios with respect to aromatic rings in the gel.

Table 4.5 Properties of the products with various Sn/R molar ratios.

Sn/R molar ratio	Surface area (m^2/g)	V_p (cm^3/g)	Mean pore diameter (nm)
0.03	42.59	0.0473	4.82
0.05	30.04	0.0331	3.75
0.08	31.40	0.0397	4.82
0.10	34.17	0.0426	4.82

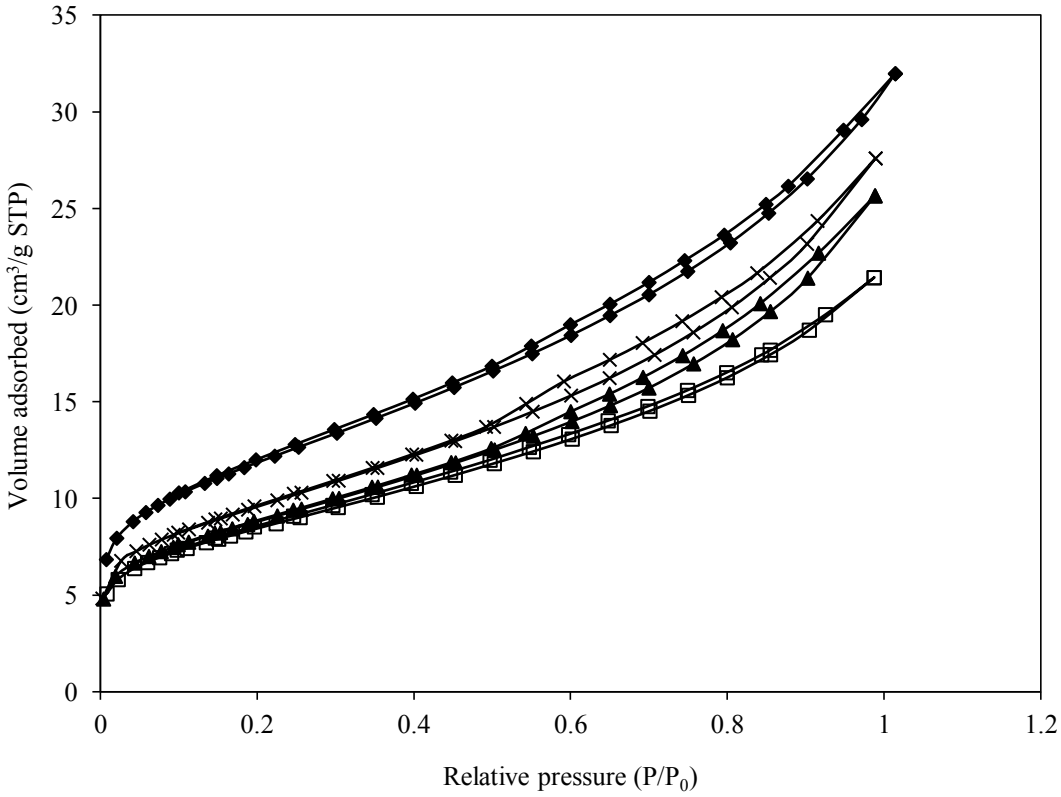

Figure 4.23 N_2 adsorption-desorption isotherm of the products with Sn/R molar ratio of (♦) 0.03, (□) 0.05, (▲) 0.08 and (×) 0.10.

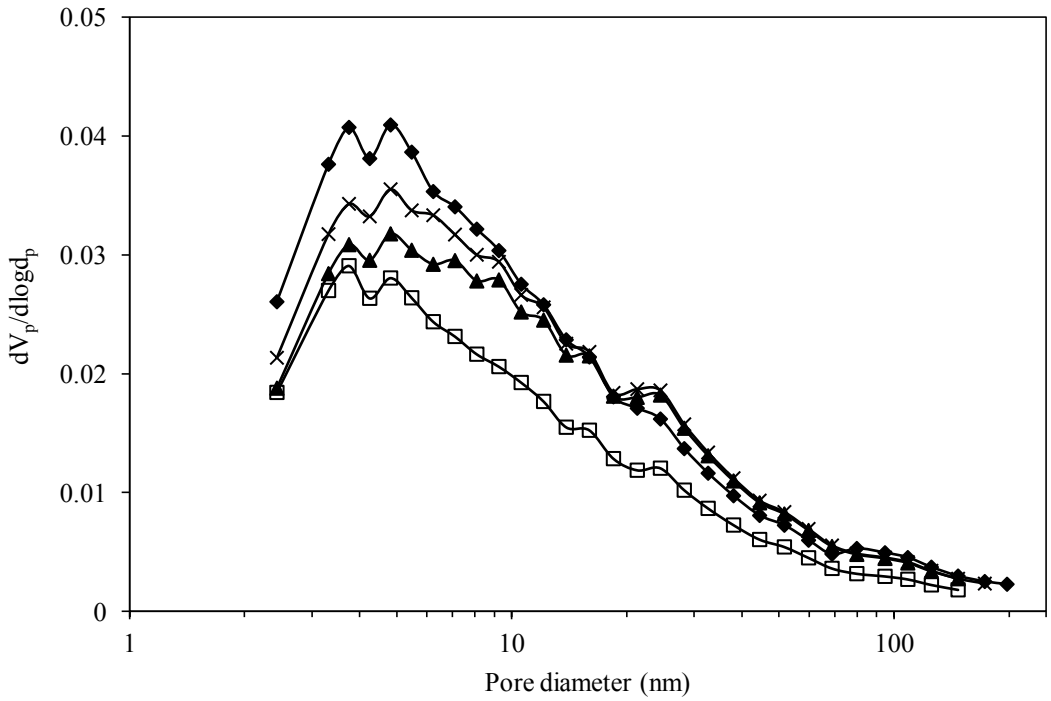

Figure 4.24 Pore size distribution of the products with Sn/R molar ratio of (♦) 0.03, (□) 0.05, (▲) 0.08 and (×) 0.10.

Although, the small tin sol particles are formed, the particles aggregated as shown in Figure 4.24. SEM image shows that the tin dioxide particles seems to aggregate when Sn/R molar ratio is increased. This means that the reaction rate during aging also has an effect on morphology and properties of the products (according to FTIR and SEM results). Nevertheless, the aggregation of particles does not affect the surface area of the product.

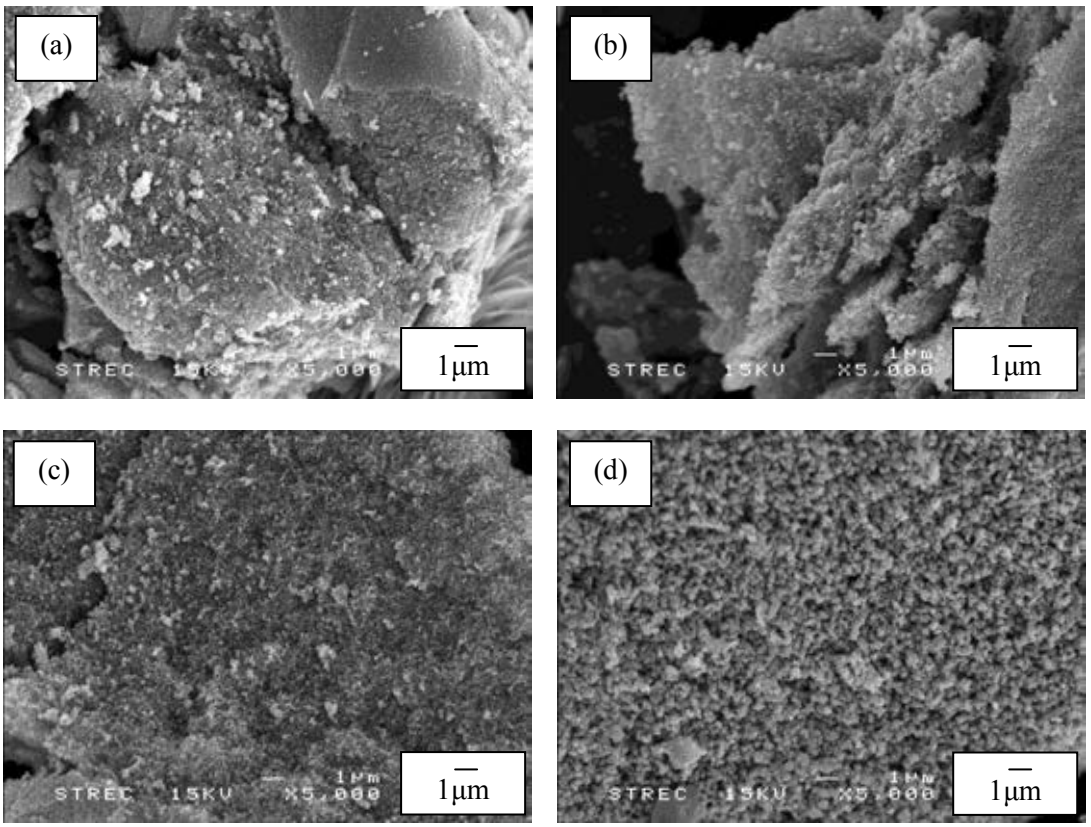

Figure 4.25 SEM image of tin dioxide products with Sn/R molar ratio of 0.03 (a), 0.05 (b), 0.08 (c) and 0.10 (d).

4.3.4 Type of diluting solvent

The solvent were added into RF gel before mixing the tin sol and the RF gel in order to prevent rapid solidification. Water and ethanol are used as the diluting solvent to study the effect of type of the diluting solvent. Composition of chemicals in tin sol and RF gel, aging time of tin sol and aging time of RF gel were fixed. The effect of adding the solvent and type of diluting solvent were studied using FTIR, SEM and N_2 adsorption-desorption analysis.

FTIR spectrum of the dried samples, namely, neat RF gel, RF gel with addition of water and RF gel with addition of ethanol are similar as shown in Figure 4.26. The results demonstrate that water and ethanol only act as the solvent. In the preparation step of RF gel, after the gel was aged, the viscosity of the RF gel is increased. When the gel nearly transformed into solid (high viscosity), ethanol was added and the mixture was stirred violently. It was found that the viscosity of the RF gel can be decreased by adding ethanol. This confirmed that ethanol is good solvent for RF gel. However, the intensity of absorption

band of those gels at 1477 cm^{-1} (-CH_2- scissor vibration) and at 1220 and 1092 cm^{-1} (CH_2-O-CH_2 bridges) [36, 90] are not different as illustrated in Table 4.6. It suggests that the addition of solvent does not affect the formation of RF gel.

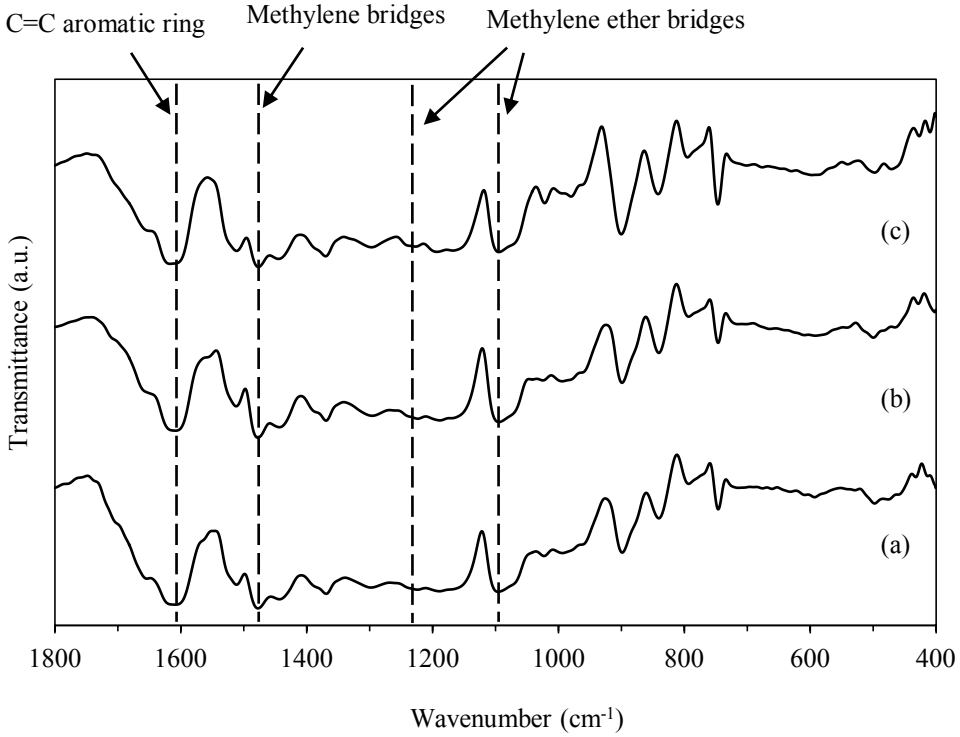

Figure 4.26 FTIR spectrum of neat RF gel (a), RF gel with water (b) and RF gel with ethanol (c).

Table 4.6 FTIR signal ratio of neat RF gel (a), RF gel with water (b) and RF gel with ethanol (c).

Sample	Signal ratio	
	Methylene ether bridge	Methylene bridge
Neat RF gel	1.095	0.772
RF gel with water	1.176	0.843
RF gel with ethanol	1.083	0.786

Figure 4.27 shows FTIR spectra of the precalcined samples, i.e., Sn/RF gel, Sn/RF gel added with water and Sn/RF gel added with ethanol. The intensity of the absorption band at 1220 and 1092 cm^{-1}, which assigned to CH_2-O-CH_2 bridges [36, 90], are not different but intensity of Sn-O-C bonding at 880-900 cm^{-1} [88] is increased by addition of either ethanol or

water as shown in Table 4.7. This result indicates that the addition of solvent into the RF gel enhances the interaction between tin sol and RF gel.

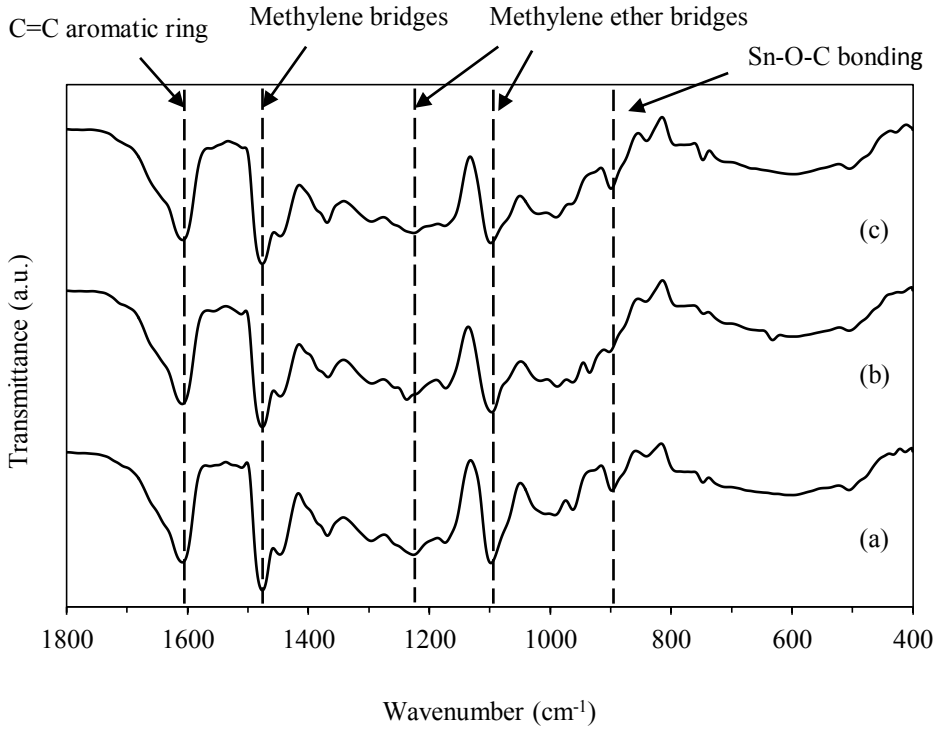

Figure 4.27 FTIR spectrum of Sn/RF gel (a), Sn/RF gel added with water (b) and Sn/RF gel added with ethanol (c).

Table 4.7 FTIR signal ratio of Sn/RF gel (a), Sn/RF gel added with water (b) and Sn/RF gel added with ethanol (c).

Sample	Signal ratio		
	Methylene ether bridge	Methylene bridge	Sn-O-C bonding
Sn/Neat RF gel	1.742	0.997	0.261
Sn/RF gel with water	1.618	1.167	0.409
Sn/RF gel with ethanol	1.639	1.056	0.415

Because RF gel is used as the template, the interaction between tin sol and RF gel is important to preserve mesoporous structure. If the Sn-O-C bonding is increased, the structure will be strong enough to prevent the pore collapse during calcination. However, dilution effect from addition of solvent also occurred, this effect resulted in larger RF particle [85].

The RF particle size could affect the properties of the obtained product such that surface area is decreased by increased particle size. Nevertheless, the specific surface area of product prepared by adding ethanol or water is higher than the product without solvent as shown in Table 4.8, while the mean pore diameter of the product with solvent is lower than the synthesized product without solvent. This result suggests that the dilution effect has less effect on the final product properties than the interaction between tin sol and RF-gel. In Figure 4.28, the result from N_2 adsorption-desorption analysis reveals that these products have mesoporous structure (Type IV isotherm). This result indicates that the addition of solvent does not affect pore structure, but pore distribution of the obtained product with solvent is narrower than the product without solvent as shown in Figure 4.29.

Table 4.8 Surface area and mean pore diameter of the obtained product with different type of diluting solvent.

Type of diluting solvent	Surface area (m^2/g)	V_p (cm^3/g)	Mean pore diameter (nm)
None	31.38	0.0535	15.96
Water	40.29	0.0579	9.25
Ethanol	40.55	0.0641	9.25

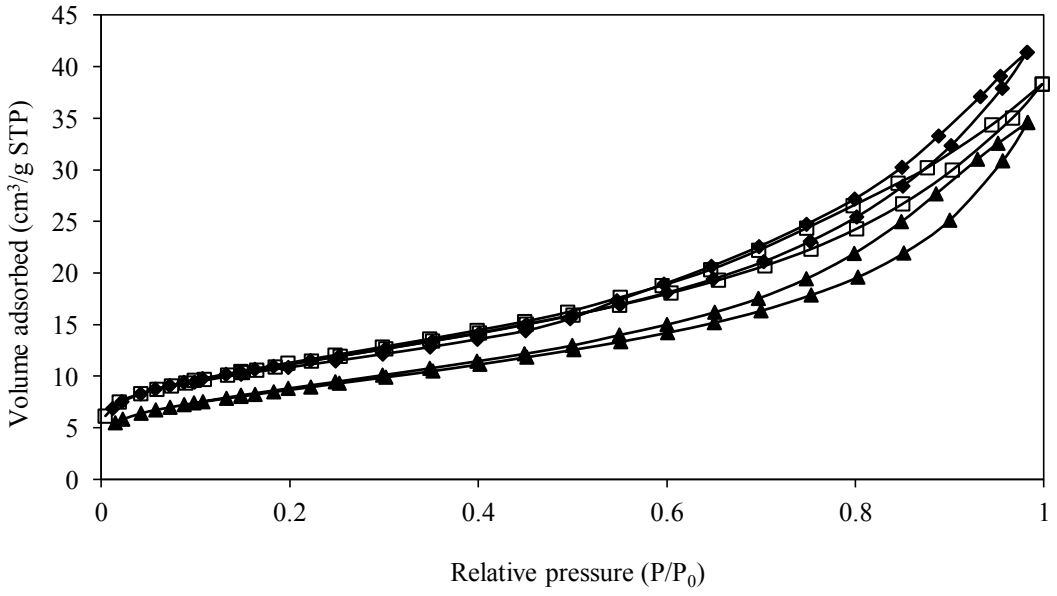

Figure 4.28 N_2 adsorption-desorption isotherm of the products prepared (▲) without addition of solvent, (♦) with ethanol and (□) with water.

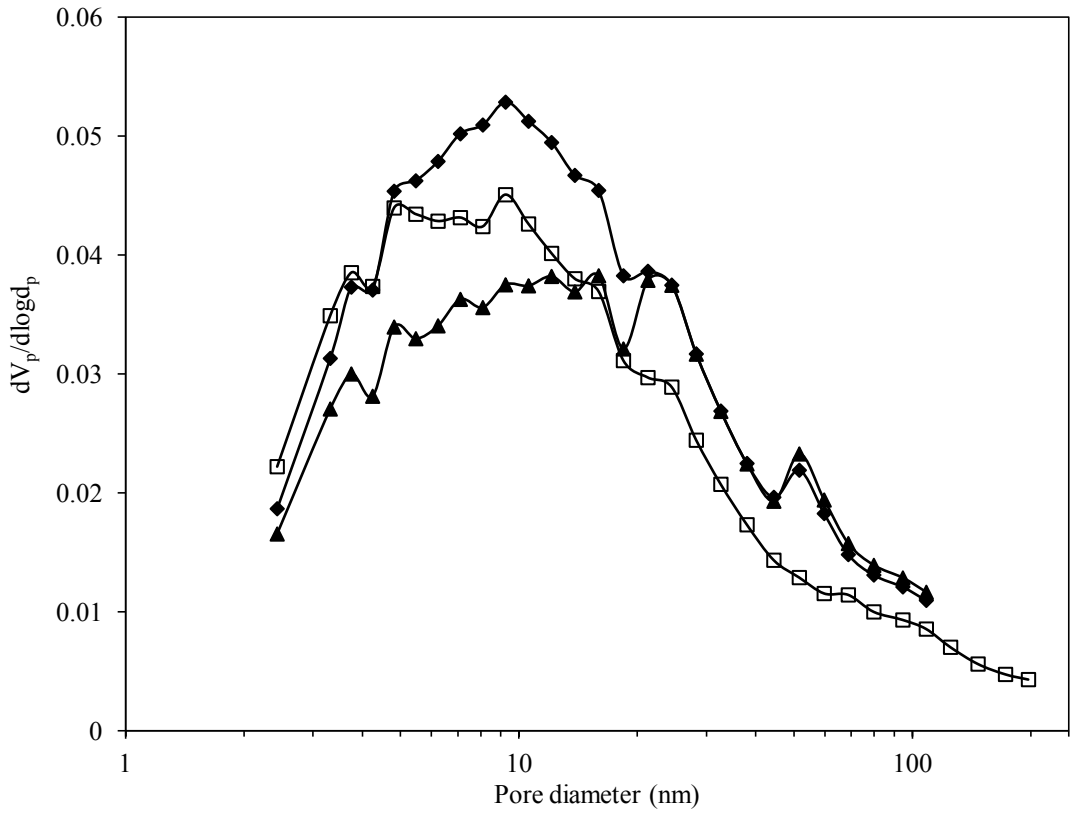

Figure 4.29 Pore size distribution of the products prepared (▲) without addition of solvent, (♦) with ethanol and (□) with water.

In Figure 4.30, SEM image shows the synthesized products prepared with neat RF gel, RF gel with water and RF gel with ethanol. It can be seen that morphology of the product without diluting solvent seems to aggregate.

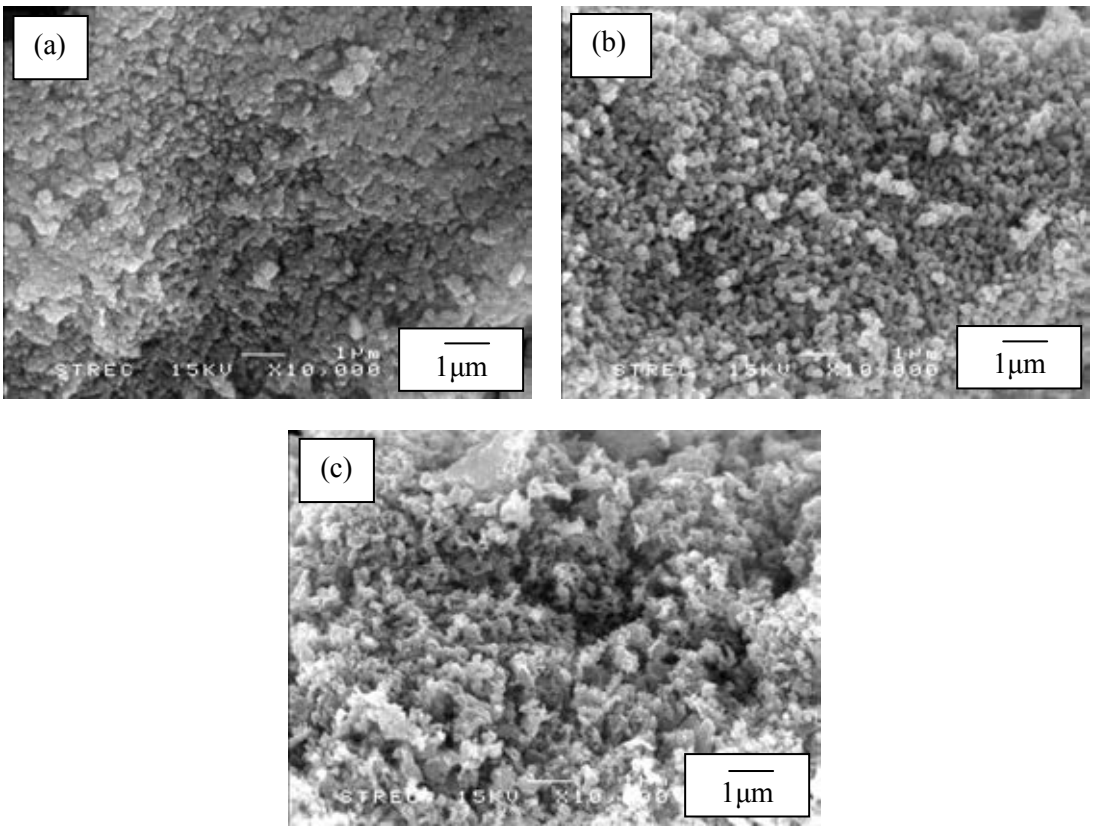

Figure 4.30 SEM image of the products prepared without addition of solvent (a), with ethanol (b) and with water (c).

4.3.5 Tin sol aging time

In this study, the tin dioxide products were prepared from various aging time of tin sol, i.e., 0, 24, 48, 72 and 120 hours. The mixed gels were aged for three days and dried by freeze drying. The dried gels were calcined at 500^{o}C. The obtained white products were characterized by FTIR, SEM and N_2 adsorption-desorption analysis.

Figure 4.31 shows FTIR spectrum of precalcined Sn/RF composites with varying aging time of the tin sol. It was noticed that all spectrums are similar. The intensity ratio of the methylene, methylene ether bridge and Sn-O-C bonding (at 1477, 1092 and 880-900 cm^{-1} [36, 85, 88], respectively) are not changed by varying aging time of tin sol as shown in Figure 4.32. It means the aging time of the tin sol does not affect either the interaction between tin precursor and the RF gel or the other functional groups. Moreover, it has no significantly effect on the morphology of the products (See in Figure 4.33).

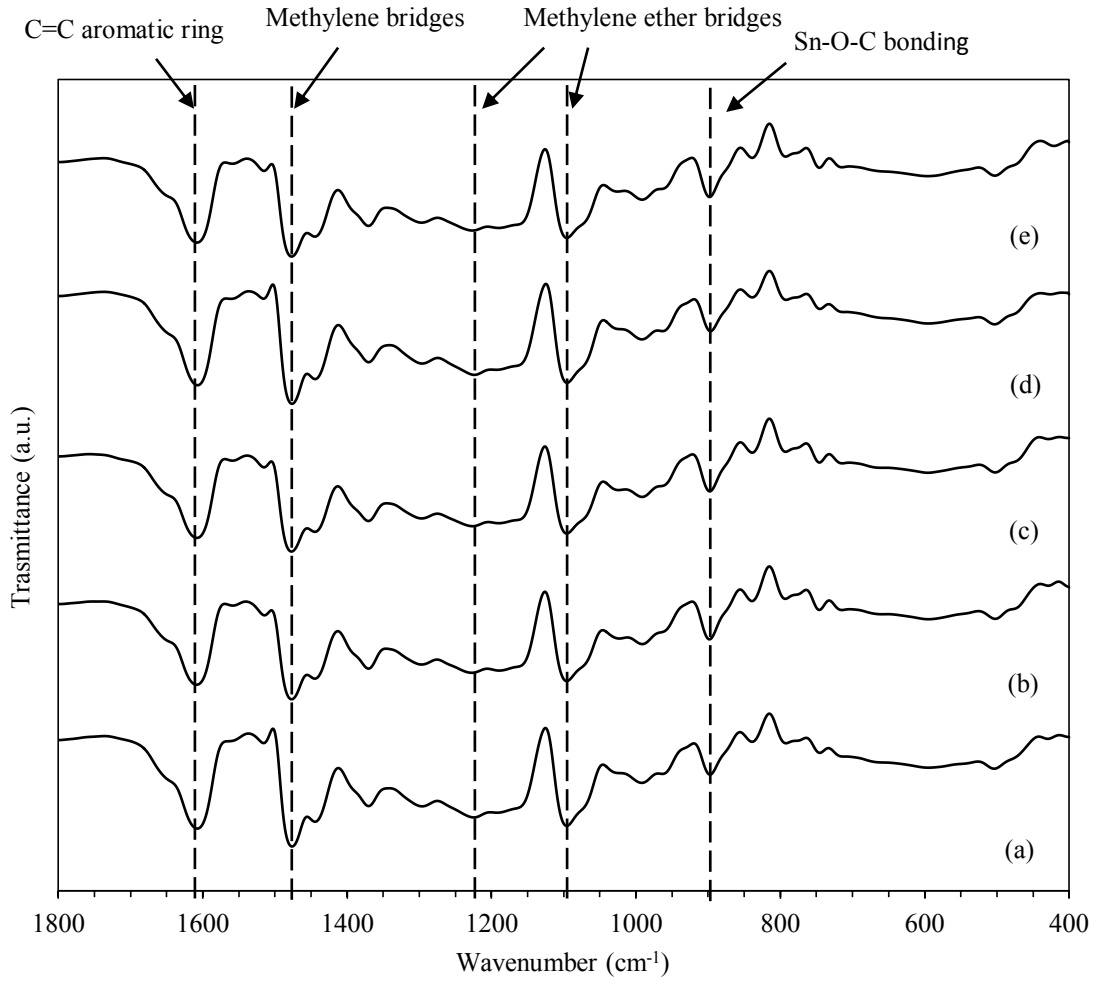

Figure 4.31 FTIR spectrum of the synthesized product prepared from the preformed tin sol aged for 0 (a), 24 (b), 48 (c), 72 (d) and 120 hours (e).

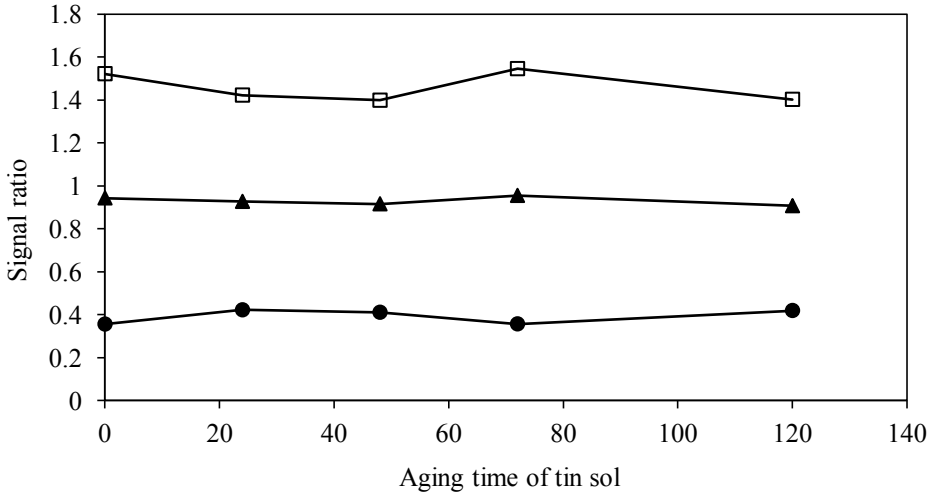

Figure 4.32 FTIR signal ratio of (□) methylene, (▲) methylene ether bridges and (●) Sn-O-C bonding of the mixed gel with various aging time of tin sol with respect to aromatic rings in the gel.

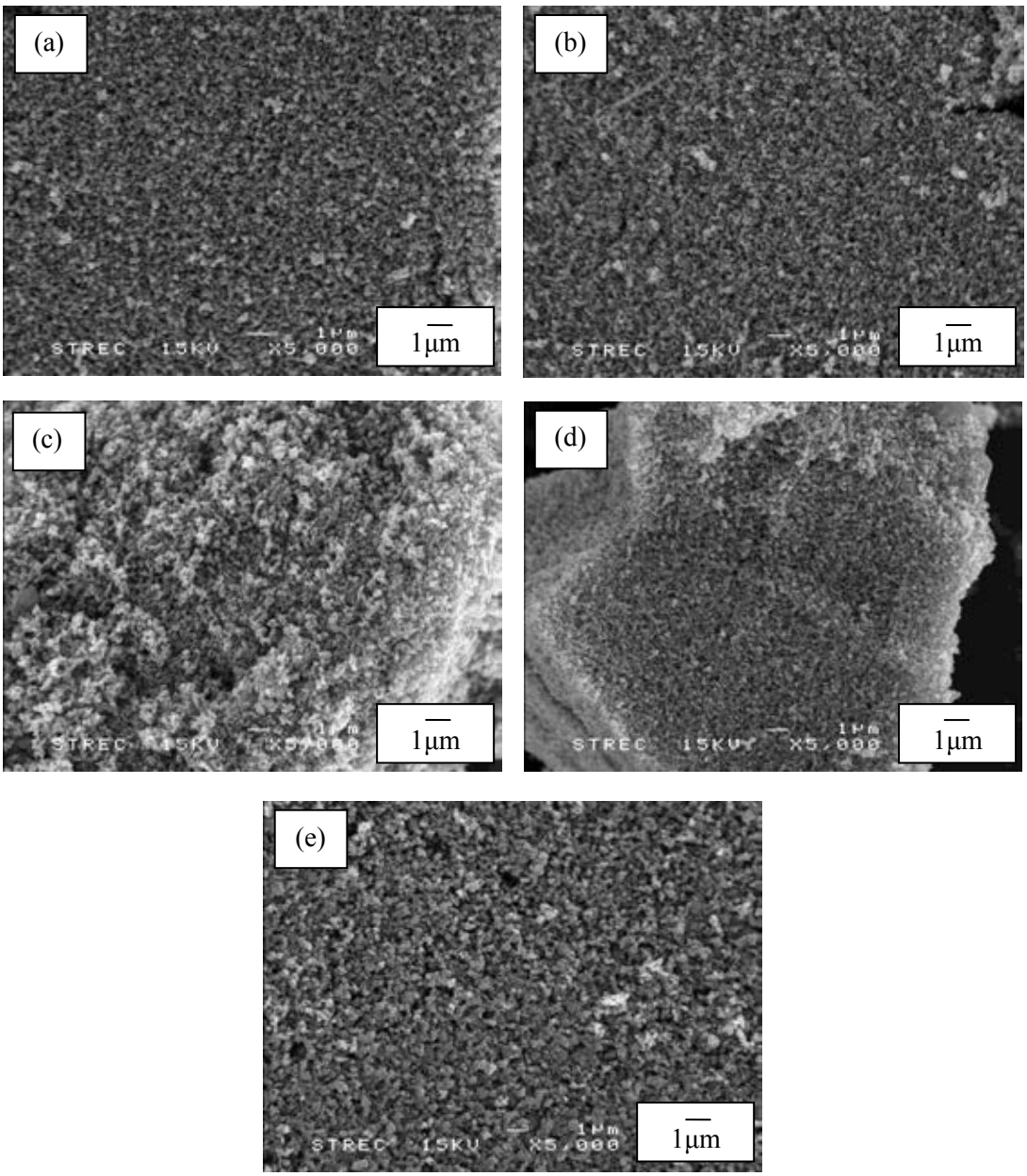

Figure 4.33 SEM image of the synthesized product prepared from the preformed tin sol aged for 0 (a), 24 (b), 48 (c), 72 (d) and 120 hours (e).

Nevertheless, the specific surface area of these products was increased by increasing aging time of the tin sol as demonstrated in Table 4.9. Although the mean pore diameter remains the same, the pore size distribution is narrowed by increasing the aging time (See in Figure 4.34). This could be resulted from mechanism in the mixing step. The size of tin sol particles are larger when increasing aging time of tin sol. In the beginning of tin sol aging, the small tin sol particles are formed and these particles accelerate RF gel more than the big tin sol particles. Thus, size of RF gel that was used as the template was changed by varying aging

time of tin sol. Prolonged aging time of tin sol resulted in smaller RF particles. This reason agrees with the results from varying R/C molar ratio as discussed earlier. For above reason, the obtained product formed from tin sol that was aged for 120 hours has the highest surface area as shown in Table below. From N_2 adsorption-desorption analysis, the result shows that structure of particles is mesoporous structure (Type IV isotherm) as presented in Figure 4.35.

Table 4.9 Properties of the synthesized products with varying aging time of tin sol.

Aging time of tin sol (h)	Surface area (m^2/g)	V_p (cm^3/g)	Mean pore diameter (nm)
0	35.13	0.0537	5.47
24	33.54	0.0583	4.82
48	34.79	0.0548	5.47
72	38.56	0.0628	4.82
120	51.04	0.0693	3.75

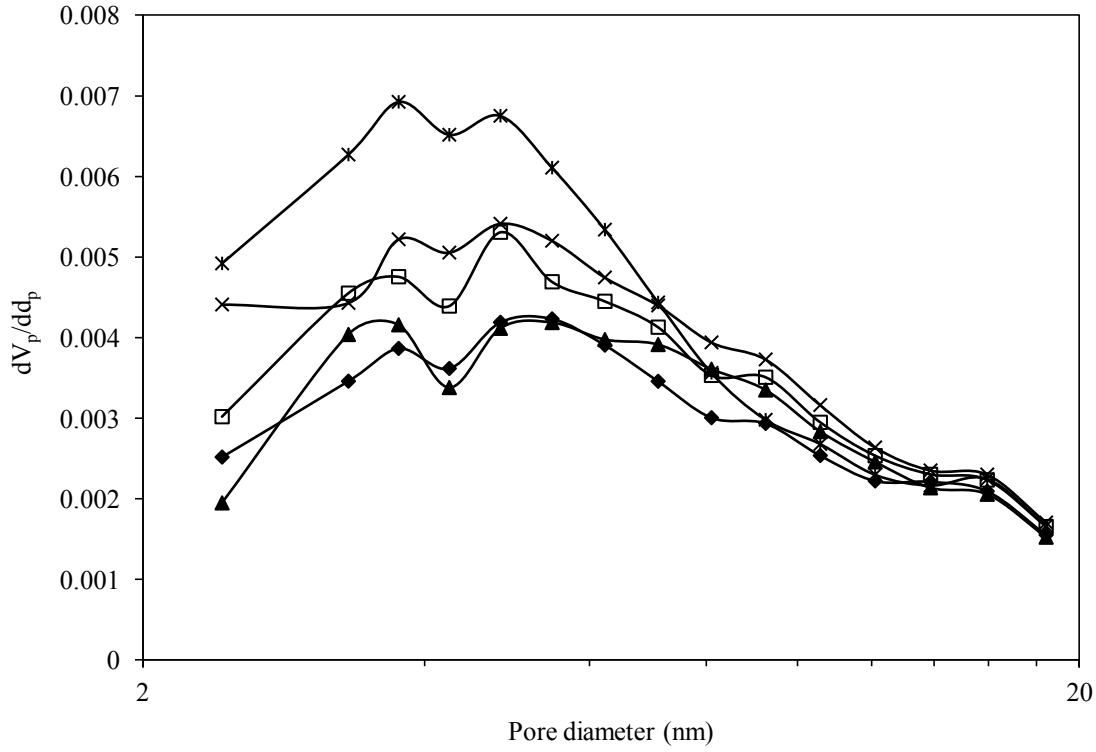

Figure 4.34 Pore size distribution of the products prepared from the preformed tin sol aged for (♦) 0, (□) 24, (▲) 48, (×)72 and (✳)120 hours.

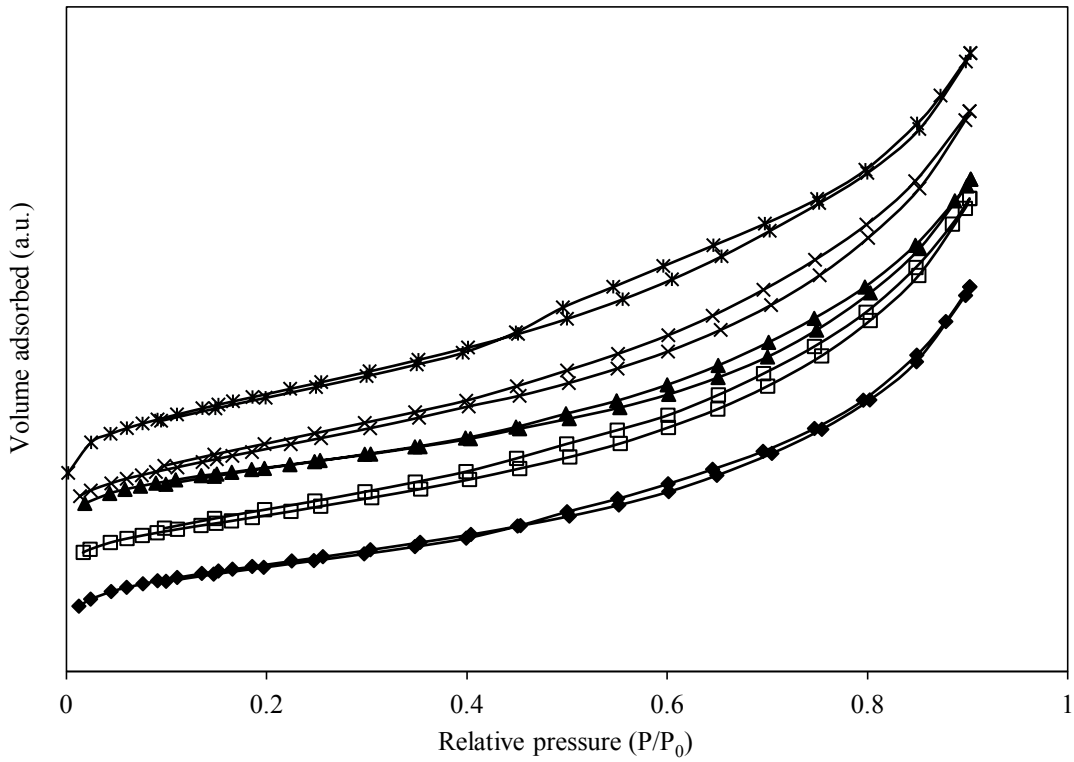

Figure 4.35 N_2 adsorption-desorption isotherm the products prepared from the preformed tin sol aged for (♦) 0, (□) 24, (▲) 48, (×)72 and (✳)120 hours.

4.3.6 RF gel aging time

In this section, tin dioxide products were prepared by fixed amount of all chemicals. The aging time of the preformed tin sol was fixed at 72 hours. After aging the mixed gel for three days and freeze drying for 24 hours, the template was removed by calcination at 500°C. The white products are obtained and investigated by FTIR, SEM and N_2 adsorption-desorption analysis. The aging time for RF gel was varied in the range of 1 to 4 hours since it had been observed that neat RF gel became solid after about 4.25 hours.

Figure 4.36 shows FTIR spectrum of the precalcined Sn/RF composite prepared using various aging time for RF gel. The adsorption bands corresponding with RF gel in all products are quite similar, indicating the same functional groups. Nevertheless, the aging time of RF gel has an effect on interaction between tin sol and RF gel as shown in Figure 4.37. As the aging time was increased, the signal associated with Sn-O-C bond locating at wavenumber of 880-900 cm^{-1} [88] was intensified. Prolonged aging time of the RF gel results in greater extent of RF networking within the condensed gel. As previously discussed, the increased RF network results in less reactivity with the preformed tin sol. From above reason,

it allows tin sol to interact with RF gel more uniformly. Thus, the intensity of the signal for Sn-O-C bonding became the highest in the product prepared with RF gel that had been aged for 4 hours.

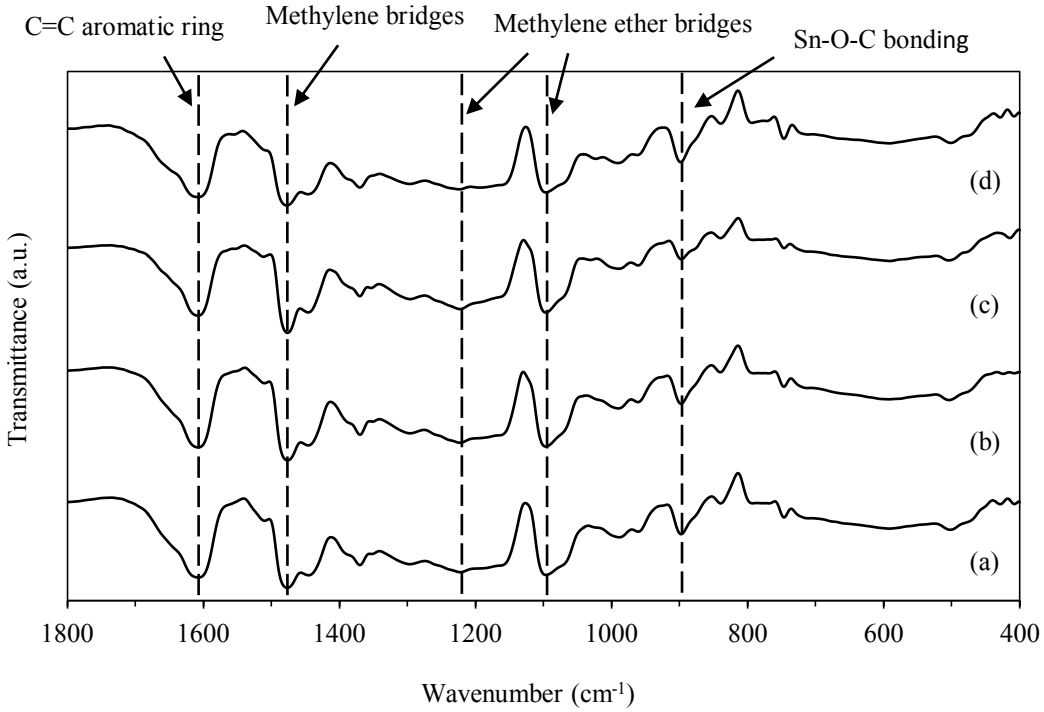

Figure 4.36 FTIR spectrum of precalcined Sn/RF composites that were prepared by using RF gel aged for 1 (a), 2 (b), 3 (c) and 4 hours (d).

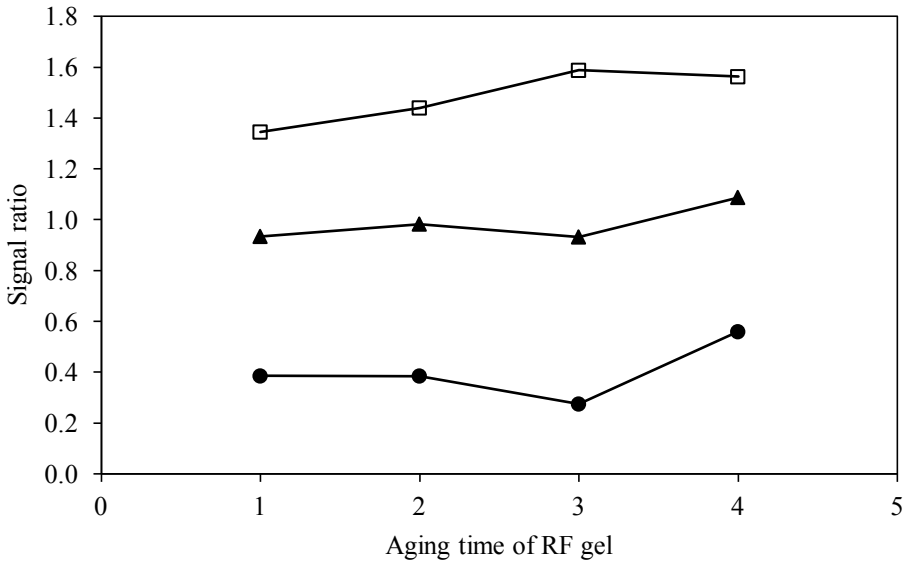

Figure 4.37 FTIR signal ratio of (□) methylene, (▲) methylene ether bridges and (●) Sn-O-C bonding of the mixed gel with varying aging tine of RF gel with respect to aromatic rings in the gel.

The interaction between tin sol and RF gel is necessary for fabrication of mesoporous tin dioxide. If Sn-O-C bonding is increased, the gel structure will be strong enough to preserve mesoporous structure during calcinations process. According to the BET analysis, the surface area of tin dioxide is increased by increasing aging time of RF gel, while the mean pore diameter is decreased. The results are shown in Table 4.10.

Table 4.10 Properties of the products with various aging time for RF gel.

RF aging time (h)	Surface area (m^2/g)	V_p (cm^3/g)	Mean pore diameter (nm)
1	28.55	0.0468	24.47
2	36.77	0.0474	5.47
3	38.10	0.5114	4.82
4	40.77	0.0562	4.82

In Figure 4.38, SEM image demonstrates that the aging time has significant effect on the morphology of the products. It was noticed that prolonged aging time of RF gel prevent aggregation of the particles.

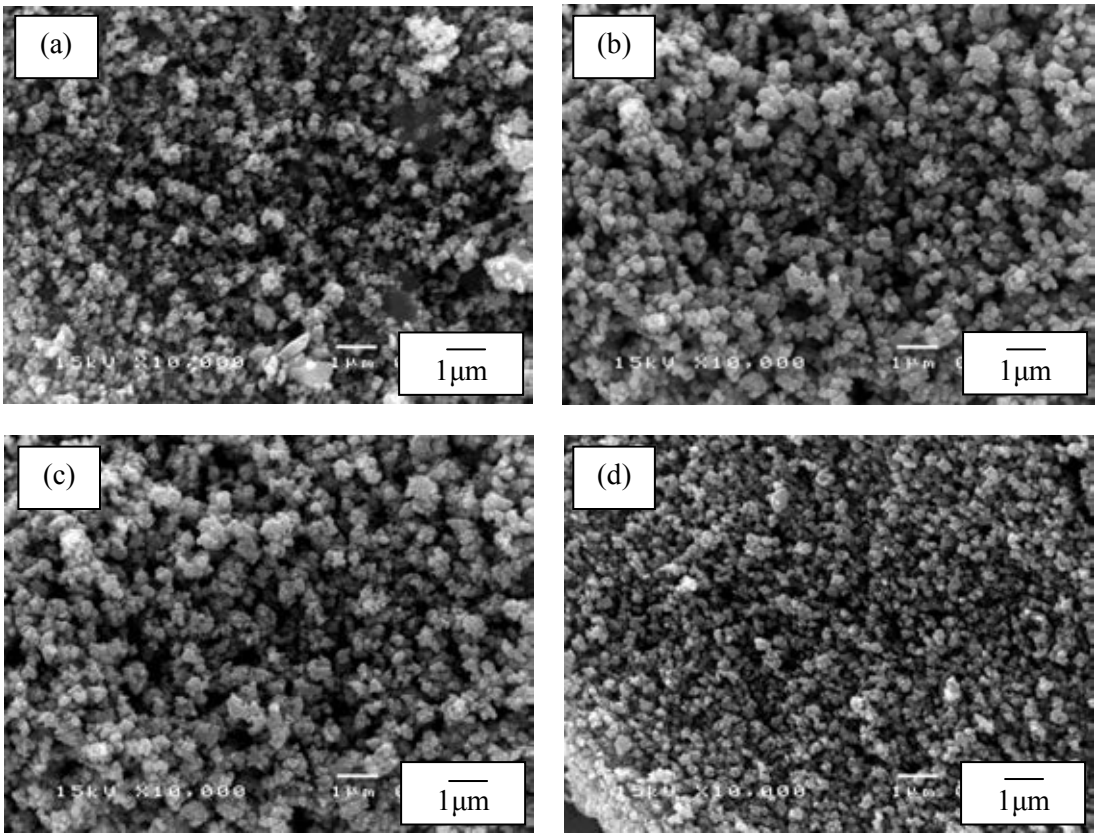

Figure 4.38 SEM image of the synthesized product prepared from RF gel aged for 1 (a), 2 (b), 3 (c) and 4 hours (d).

However, pore structure of the products is mesopore as indicated in N_2 adsorption-desorption isotherm in type IV isotherm (See in Figure 4.39). From BJH plot, pore size distribution of the aging time for 4 hours is the narrowest as shown in Figure 4.40.

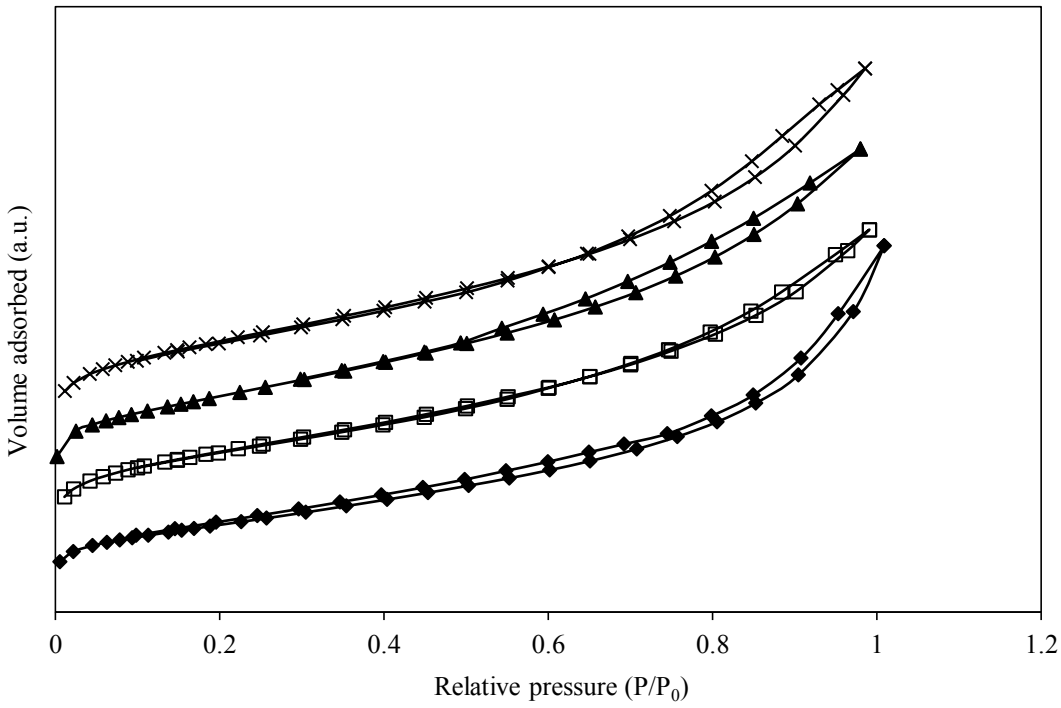

Figure 4.39 N_2 adsorption-desorption isotherm of the products with aging time for RF gel (♦) 1, (■) 2, (▲) 3 and (⊗) 4 hours.

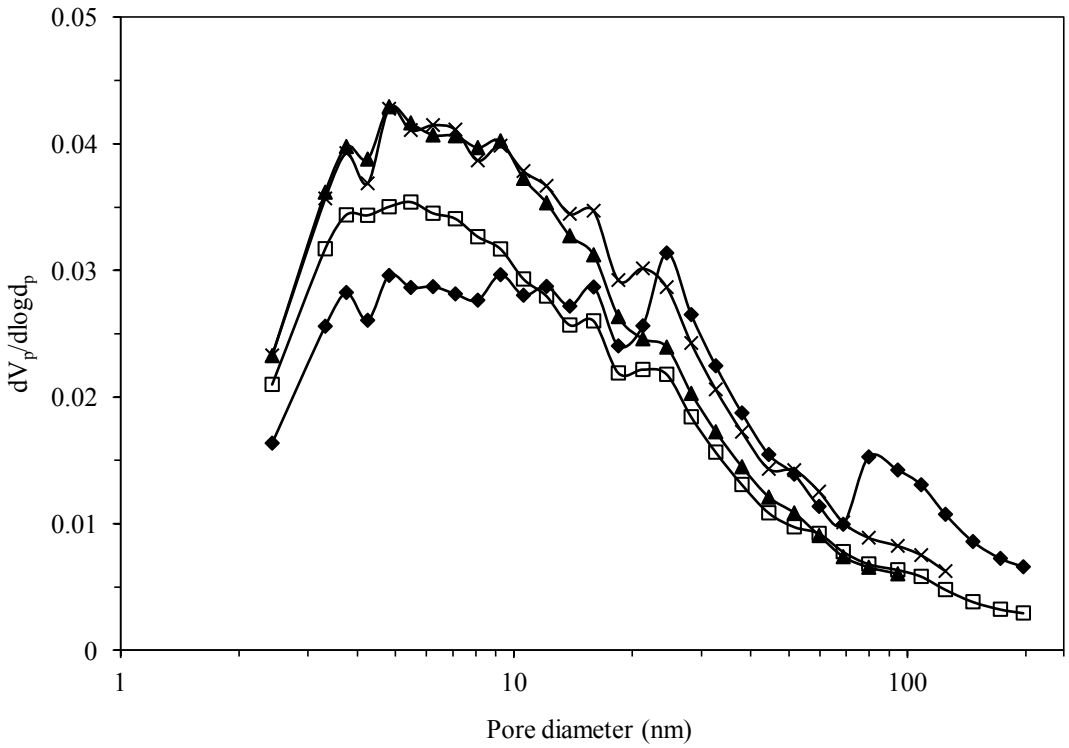

Figure 4.40 Pore size distribution of the products with aging time for RF gel (♦) 1, (■) 2, (▲) 3 and (⊗) 4 hours.

4.3.7 Mixed gel aging time

In the previous section, it was found that prolonged aging time of the mixed gel results in greater extent of RF network and enhanced Sn-O-C bonding as previously discussed in section 4.2. To investigate the effect of the mixed gel aging time, tin dioxide was synthesized by the mixed gel aged for 2, 3, 4 and 5 days.

FTIR spectrum reveals that all precalcined samples has the same functional group as presented in Figure 4.41. Interestingly, the intensity of methylene, methylene ether bridge and Sn-O-C bonding (at 1477, 1092 and 880-900 cm^{-1} [36, 85, 88], respectively) are not changed by increasing the aging time of the mixed gel as shown in Figure 4.42. This result suggests that polycondensation of resorsinol and formaldehyde still occurs during washing process with tert-butanol. Moreover, the interaction between tin sol and RF gel also arises.

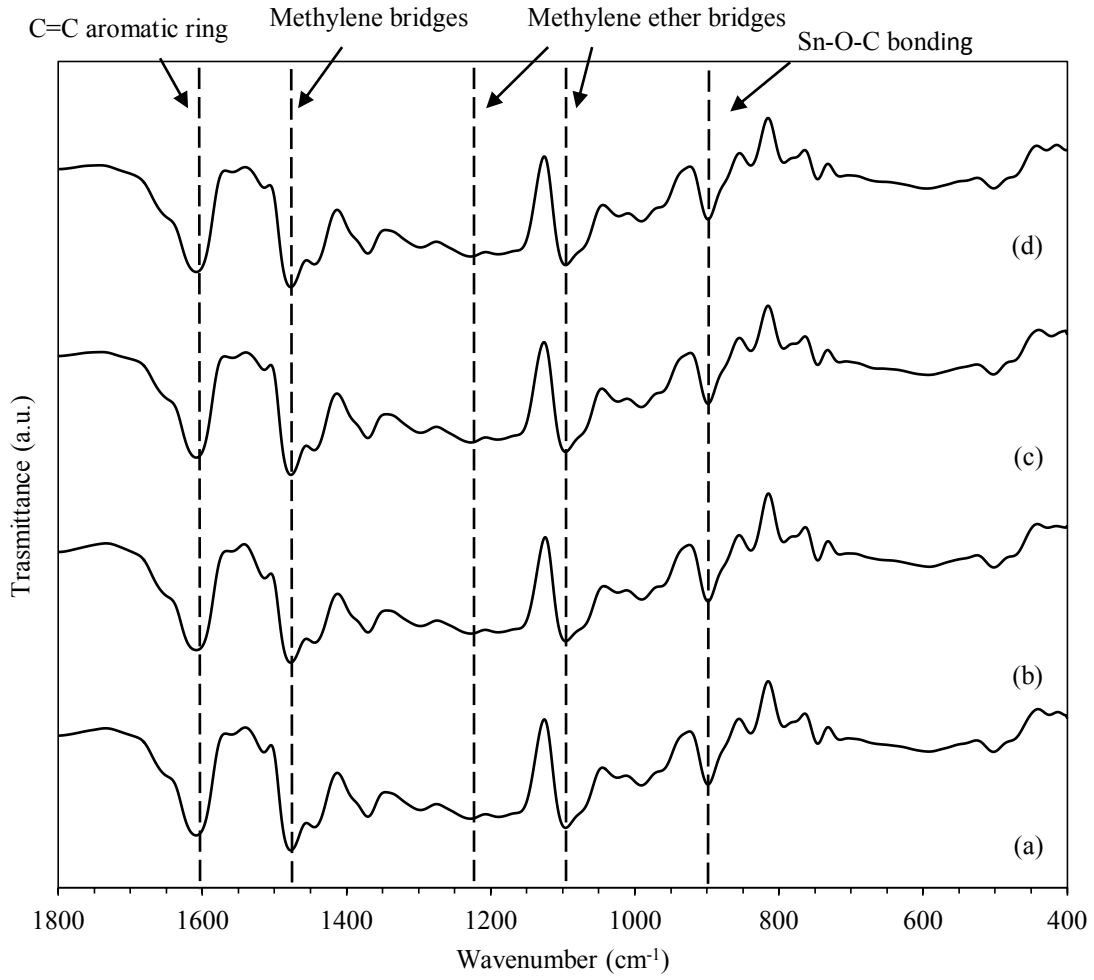

Figure 4.41 FTIR spectrum of precalcined Sn/RF composites prepared by aged mixed gel for 2 (a), 3 (b), 4 (c) and 5 days (d).

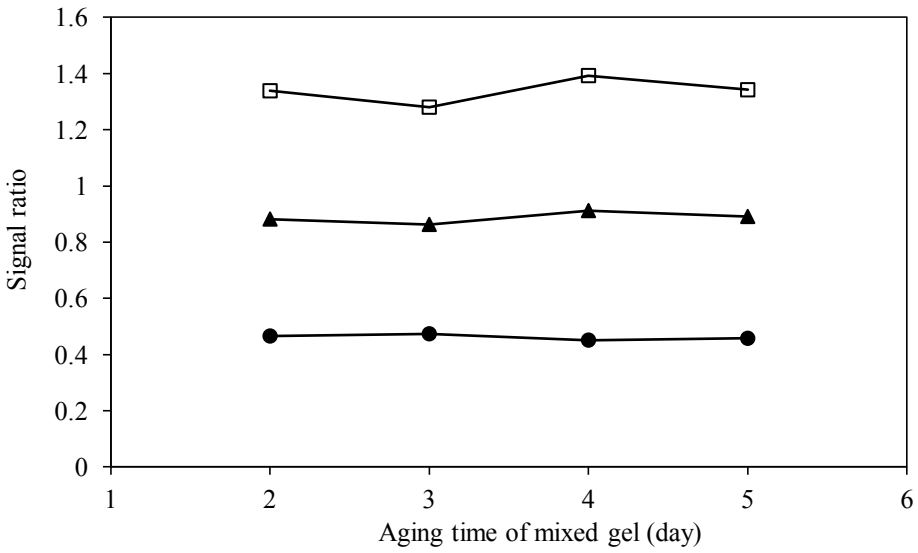

Figure 4.42 FTIR signals ratio of (□) methylene, (▲) methylene ether bridges and (●) Sn-O-C bonding of the mixed gel with varying aging time of mixed gel with respect to aromatic rings in the gel.

However, polycondensation in different environment results in the mixed gel with different properties. Therefore, the properties of synthesized product are different as shown in Table 4.11. The surface area of the final product is increased by increasing aging time of the mixed gel. From N_2 adsorption-desorption analysis, the result indicates that these samples has mesopores in structure (Type IV isotherm) as shown in Figure 4.43. BJH plot shows pore size distribution of the products. It can be seen that the product which be prepared by the mixed gel aged for 5 days has the narrowest pore size distribution (See in Figure 4.44).

Table 4.11 Properties of the products with varying aging time of mixed gel.

Aging time of mixed gel (day)	Surface area (m^2/g)	V_p (cm^3/g)	Mean pore diameter (nm)
2	34.76	0.0561	24.47
3	39.43	0.0602	5.47
4	41.98	0.0728	4.82
5	56.95	0.0783	4.82

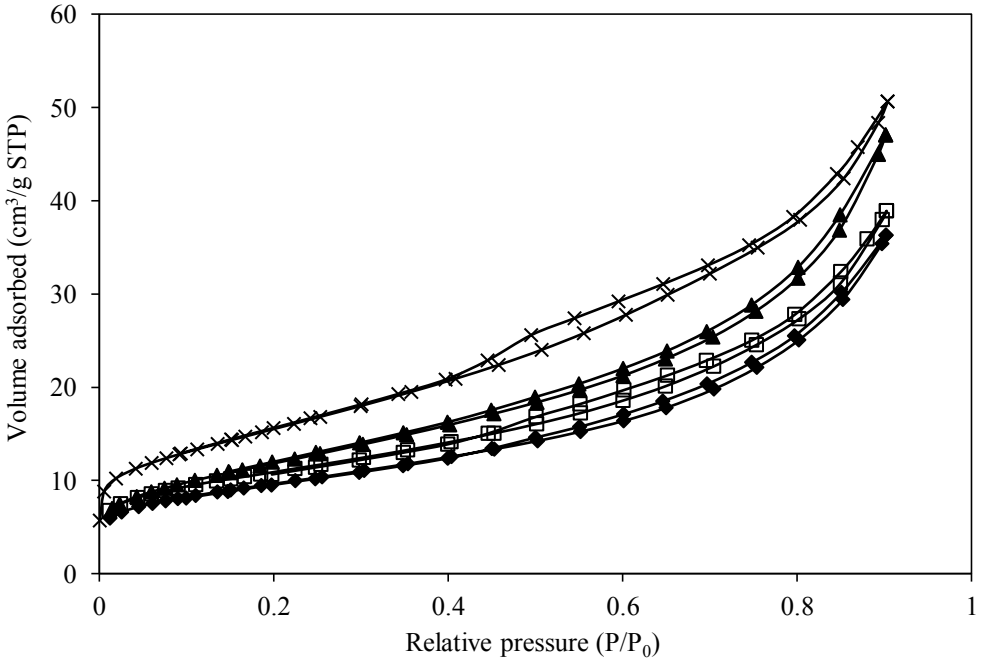

Figure 4.43 N_2 adsorption-desorption isotherm of the products with aging time for mixed gel (♦) 2, (□) 3, (▲) 4 and (×) 5 days.

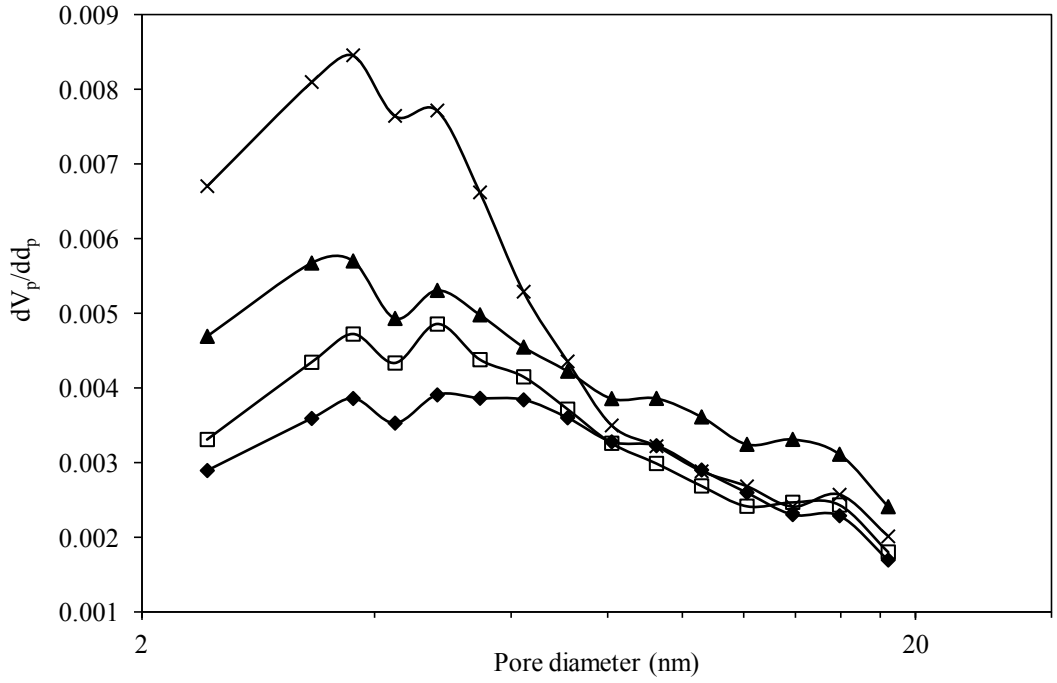

Figure 4.44 Pore size distribution of the products with aging time for mixed gel (♦) 2, (□) 3, (▲) 4 and (×) 5 days.

Figure 4.45 shows SEM image of the products prepared from the mixed gel aged for 2, 3, 4 and 5 days. It can be concluded that the aging time for mixed gel has no impact on morphology of the product.

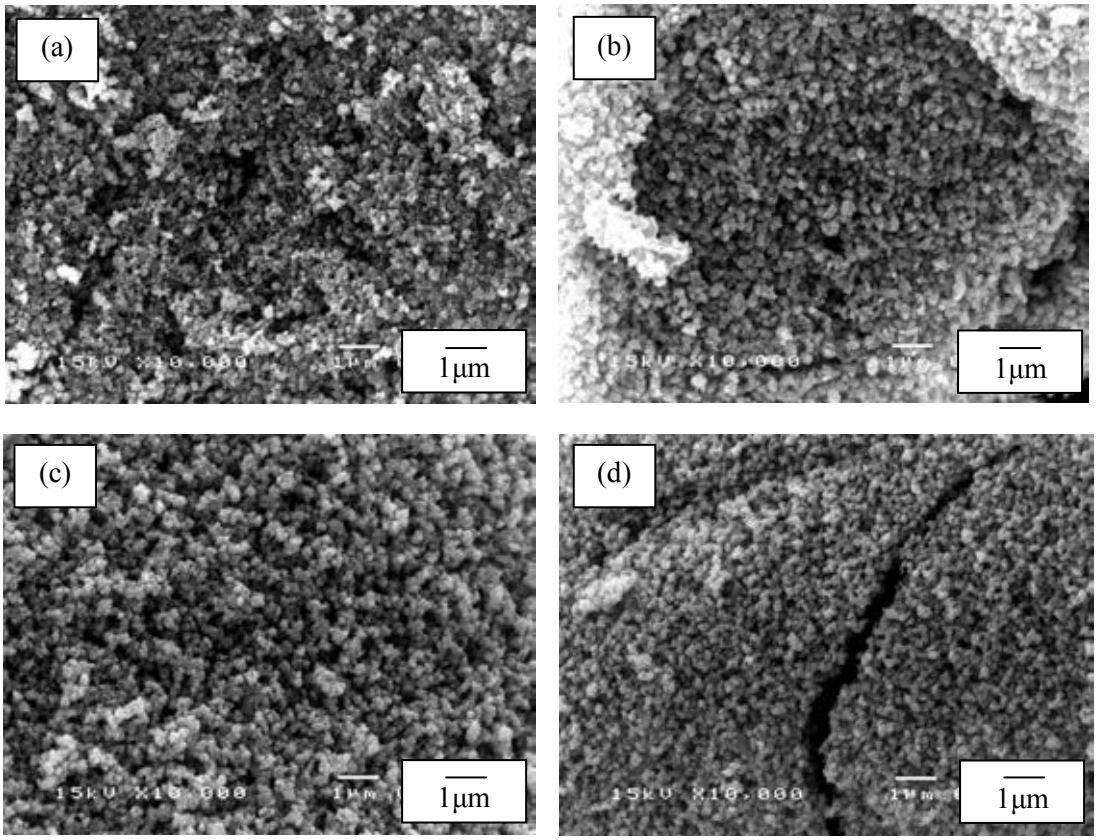

Figure 4.45 SEM image of the products prepared from the mixed gel aged for 2 (a), 3 (b), 4 (c) and 5 days (d).

4.3.8 Drying process

In this study, the products were synthesized using fixed composition and amount of both of the preformed tin sol and RF gel. The other process conditions were also fixed except drying process. After washing the Sn/RF composites with tert-butanol for three days, the gels were dried by freeze drying and conventional drying at 110^{o}C to compare the effect of drying process. The white products were investigated by SEM, FTIR, Thermal analysis and N_2 adsorption-desorption analysis.

SEM image shows the similar morphology of the product, when the products were obtained from different drying process as shown in Figure 4.46. However, surface area of the product dried from freeze drying is obviously higher than the obtained product from

conventional drying as illustrated in Table 4.12**.** This result means that freeze drying could maintain small pore inside the product. This phenomenon could be described by considering drying step. Freeze drying is drying process that removes solvent by sublimation, so there are no drastic changes in the surface tension of vapor and liquid during drying process that result in collapse of the pores [88]. On the other hand, conventional drying process is drying process that involves evaporation. Therefore, the pore could collapse because of drastic changes in the surface tension of vapor and liquid. From above reason, the BET result shows the product with freeze drying has surface area more than the obtained product from conventional drying, while mean pore diameter is less than tin dioxide synthesized from conventional dry process. This result means freeze drying could maintain small pores inside the product. It could be confirmed by pore size distribution as shown in Figure 4.47. In Figure 4.48, N_2 adsoption-desorption analysis reveals that all the products has mesoporous structure (Type IV isotherm).

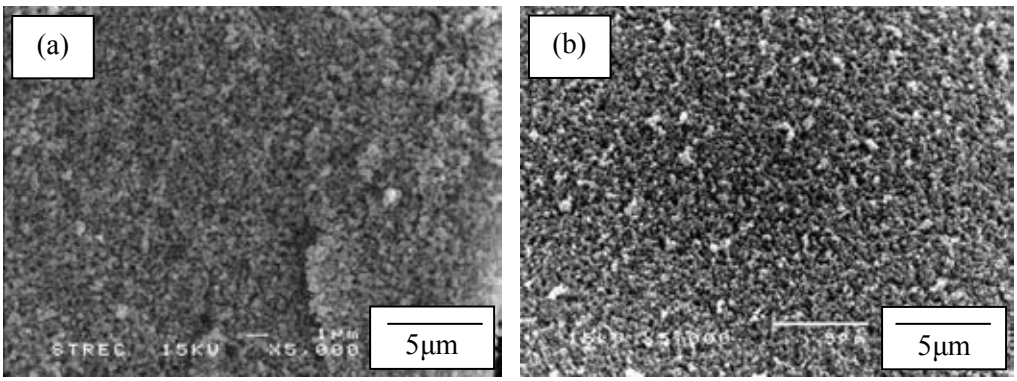

Figure 4.46 SEM images of tin dioxide synthesized by freeze drying (a) and conventional drying (b).

Table 4.12 Surface area and mean pore diameter of the obtained product prepared from different drying process.

Drying process	Surface area (m^2/g)	V_p (cm^3/g)	Mean pore diameter (nm.)
Freeze drying	42.99	0.0575	4.82
Conventional drying	37.00	0.2254	24.47

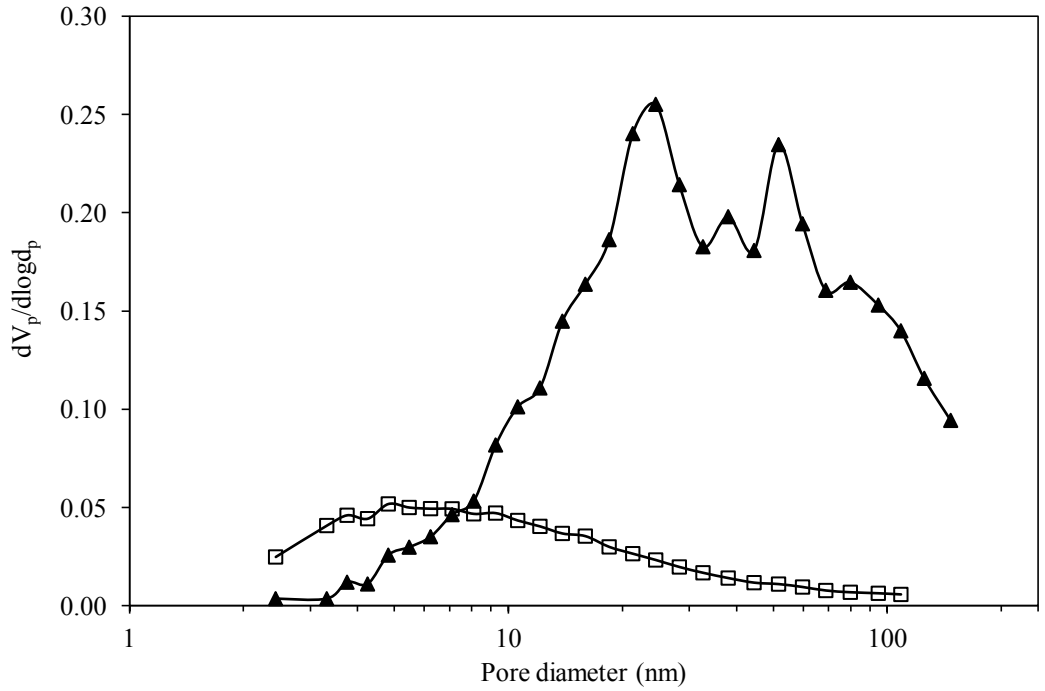

Figure 4.47 Pore size distribution of tin dioxide synthesized by (□) freeze drying and (▲) conventional drying.

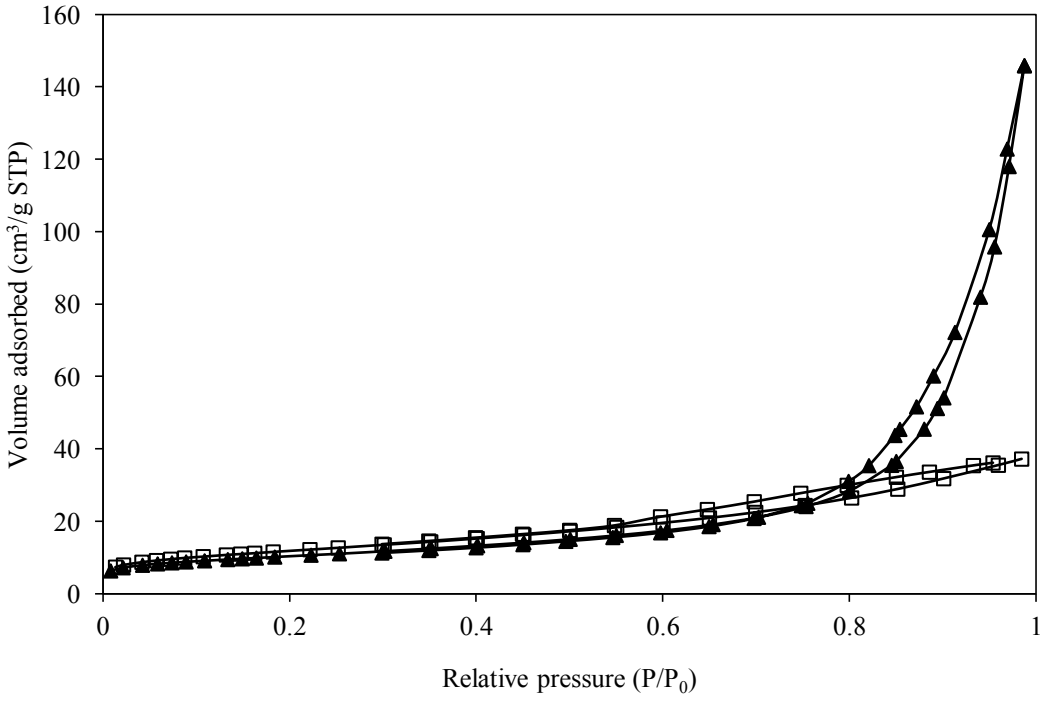

Figure 4.48 N_2 adsorption-desorption isotherm of tin dioxide synthesized by (□) freeze drying and (▲) conventional drying.

Although conventional drying cannot prevent the collapse of small pores, the heat treatment in this drying process accerelates the aging of the mixed gel. Comparing FTIR spectrum of precalcined Sn/RF composites via freeze drying and conventional drying, it was found that the interesting peaks at 1477, 1092 and 880-900 cm^{-1}, ascribed to methylene bridge, methylene ether bridge and Sn-O-C bond [36, 85, 88], are increased by using conventional drying step as indicated in Figure 4.49 and Table 4.13. This means freeze drying stop the aging of the mixed gel, therefore FTIR spectrum of composites from freeze drying is not similar to the dry gel from conventional drying.

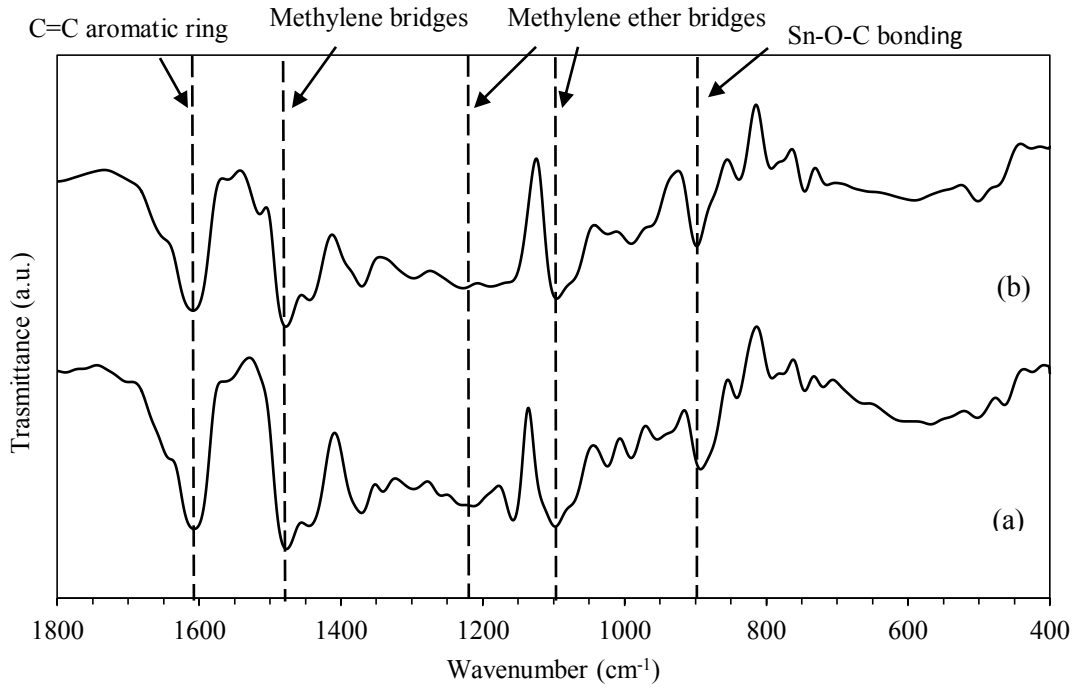

Figure 4.49 FTIR spectrum of Sn/RF composites dried by freeze drying (a) and conventional drying (b).

Table 4.13 FTIR signal ratio of methylene, methylene ether bridges and Sn-O-C bonding of the mixed gel with different drying process with respect to aromatic rings in the gel.

Drying process	Signal ratio		
	Methylene ether bridge	Methylene bridge	Sn-O-C bonding
Conventional dry	1.35	0.97	0.51
Freeze dry	1.28	0.86	0.47

4.3.9 Calcination temperature

Tin dioxide products were synthesized by calcination at various temperatures to study their effect. The tin sol and RF gel were prepared and aged for 72 and 4 hours, respectively. After mixing the preformed tin sol and RF gel, the mixed gel was aged for 3 days, washed with tert-butanol for 3 days, dried by freeze drying and calcined at 400, 500, 600 and 700^{o}C. The white products were investigated by SEM, XRD and N_2 adsorption-desorption analysis.

It was found that calcination temperature does not affect the morphology of the product (See in Figure 4.50). Nevertheless, it has an effect on properties of the tin dioxide. From Table 4.14, the surface area of the product is decreased due to pores collapse during calcination at high temperature but tin dioxide still has mesoporous structure as presented in Figure 4.51. It was observed that the surface area is dramatically decreased in range of 400-500^{o}C because of removing residue carbon in the product. Moreover, growth of particles occur in range of 600-700^{o}C. This occurrence results in decreased surface area of the obtained products. BJH plot shows pore size distribution of the product is broaden by increasing calcination temperature (See in Figure 4.52). These results confirm using RF gel assist fabrication of mesoporous tin dioxide at temperature below 600^{o}C. At higher than 700^{o}C, the mesoporous structure of tin dioxide product is destroyed.

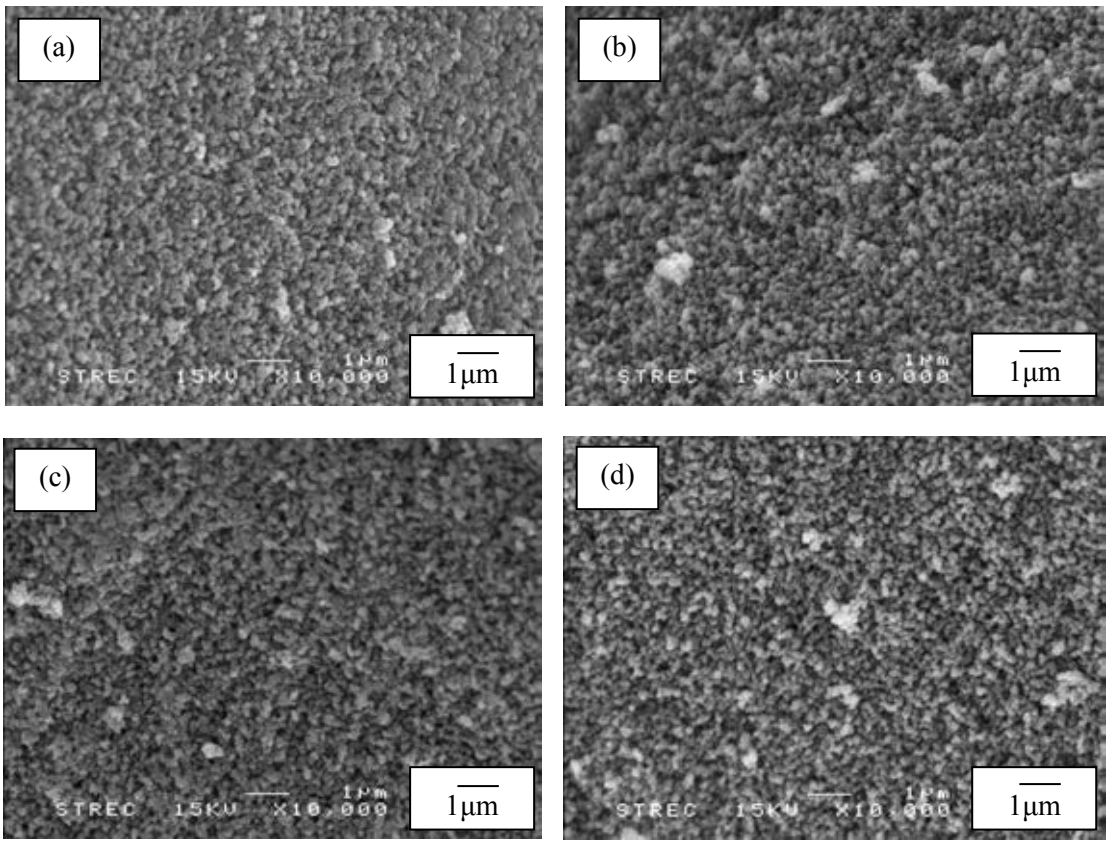

Figure 4.50 SEM images of the obtained tin dioxide calcined at 400°C (a), 500°C (b), 600°C (c) and 700°C (d).

Table 4.14 Properties of the products calcined at various calcination temperatures.

Calcination temperature (°C)	Surface area (m^2/g)	V_p (cm^3/g)	Mean pore diameter (nm.)
400	46.05	0.0322	3.75
500	31.20	0.0237	3.75
600	32.65	0.0293	4.82
700	22.17	0.0215	4.82

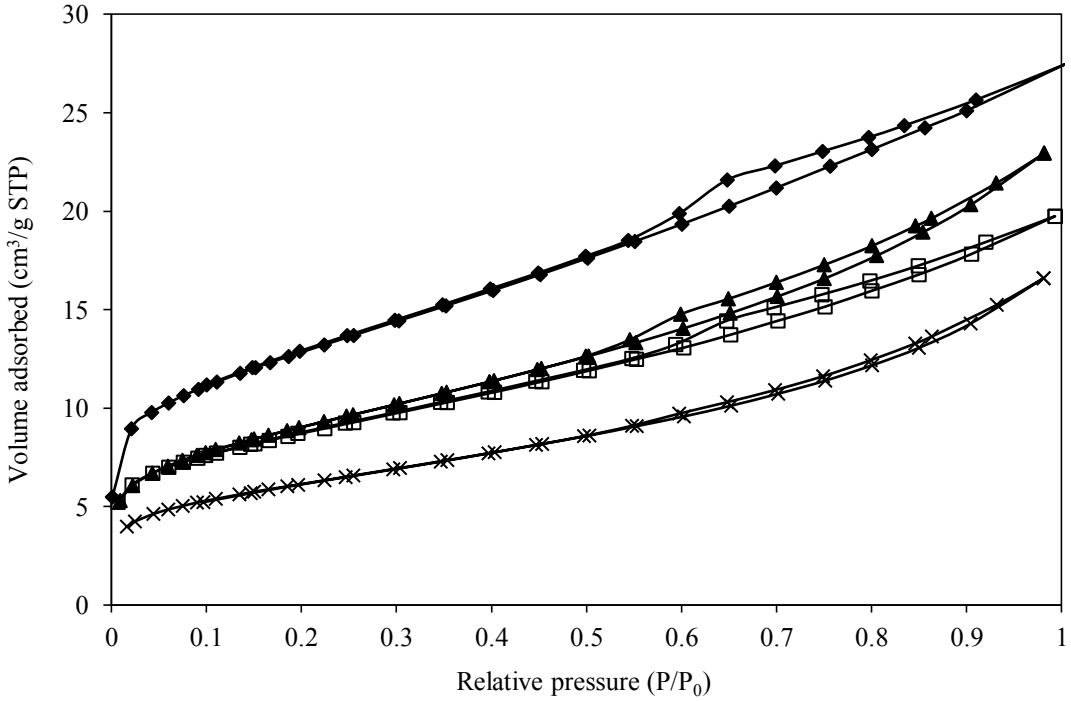

Figure 4.51 N_2 adsorption-desorption isotherm of tin dioxide calcined at (♦) 400°C, (□) 500°C, (▲) 600°C and (×) 700°C.

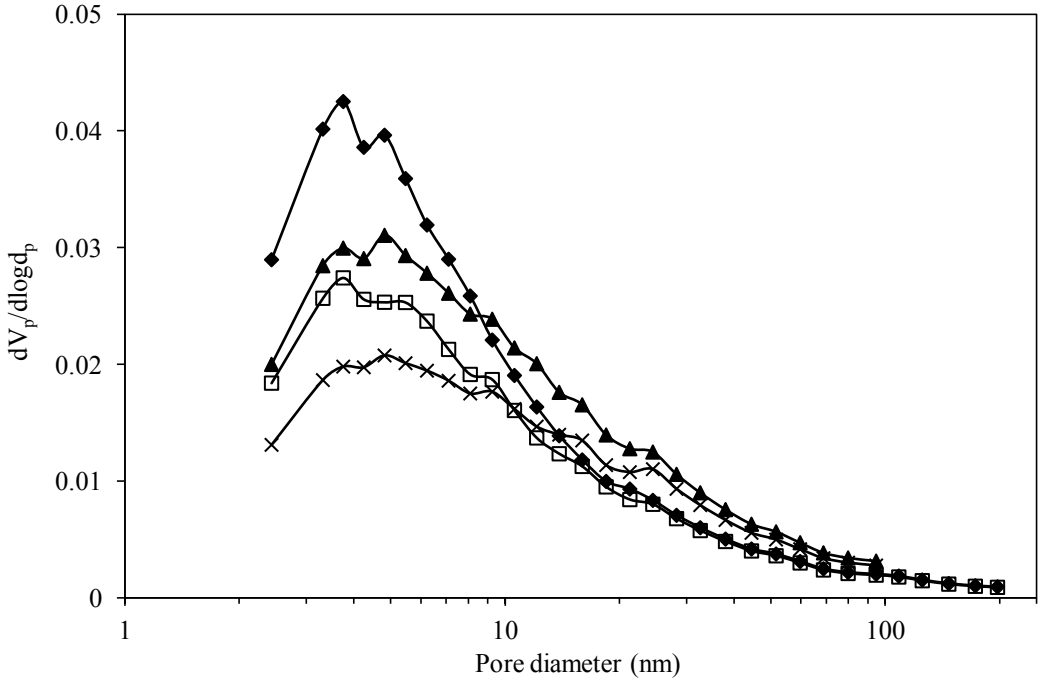

Figure 4.52 Pore size distribution of the tin dioxide calcined at (♦) 400°C, (□) 500°C, (▲) 600°C and (×) 700°C.

Figure 4.53 shows XRD pattern of the synthesized products calcined at different temperature. It was found that, for the product calcined at 400-600°C, there are two appeared phase, namely, metallic tin and tin dioxide as shown in the pattern. At 500°C, tin dioxide phase seems to be the predominant phase. Then, Increase in calcination temperature to 700°C results in pure tin dioxide phase, which has tetragonal rutile structure. This results means at low temperature some amount of metallic tin transforms to tin dioxide and then fully changes to tin dioxide phase at 700°C. According to previous study, metallic tin transforms to tin oxide phase around 300-400°C and at 500°C there are only metallic tin and tin dioxide phase appeared in XRD pattern [89]. However, in this study, tin oxide phase was not observed. This could be resulted from fast transformation from tin oxide phase to tin dioxide phase, which is more stable than tin oxide phase. Calcination temperature affects not only the phase transformation but also crystallite size of the product as shown in Table 4.15. Increase in calcination temperature caused growth of the particle. Thus, the crystallite size was increased at high calcination temperature.

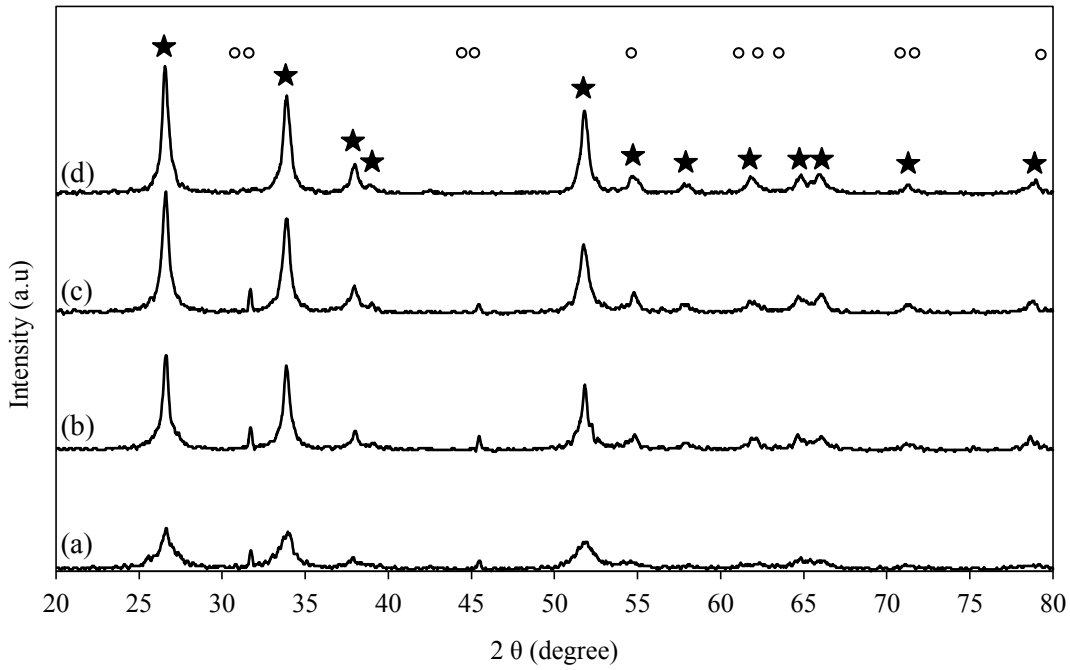

Figure 4.53 XRD patterns of the synthesized tin dioxide calcined at 400°C (a), 500°C (b), 600°C (c) and 700°C (d). ○ and ★ denotes Sn phase and SnO_2, respectively.

Table 4.15 Crystallite size of the products at various calcination temperatures.

Calcination temperature (°C)	Crystallite size (nm)
400	9.36
500	22.69
600	24.86
700	27.53

Considering the synthesized tin dioxide without RF gel, the phase product calcined at 500°C is totally tin dioxide phase, which also has tetragonal rutile structure. This means that RF gel retards phase transition of tin dioxide. XRD result is an evidence for this conclusion. It was noticed that metallic tin phase is remained in both the product prepared with RF gel and the product which was pyrolyzed before removing carbon by calcination as shown in Figure 4.54. Although using RF gel as a template assists tin dioxide having mesoporous structure, it can not prevent growth of particles during calcination as shown in Table 4.16. However, crystallite size of the synthesized tin dioxide without RF gel is smaller than the product with

RF gel. This means the difference in mechanism formation of tin dioxide could affect crystallite size of product.

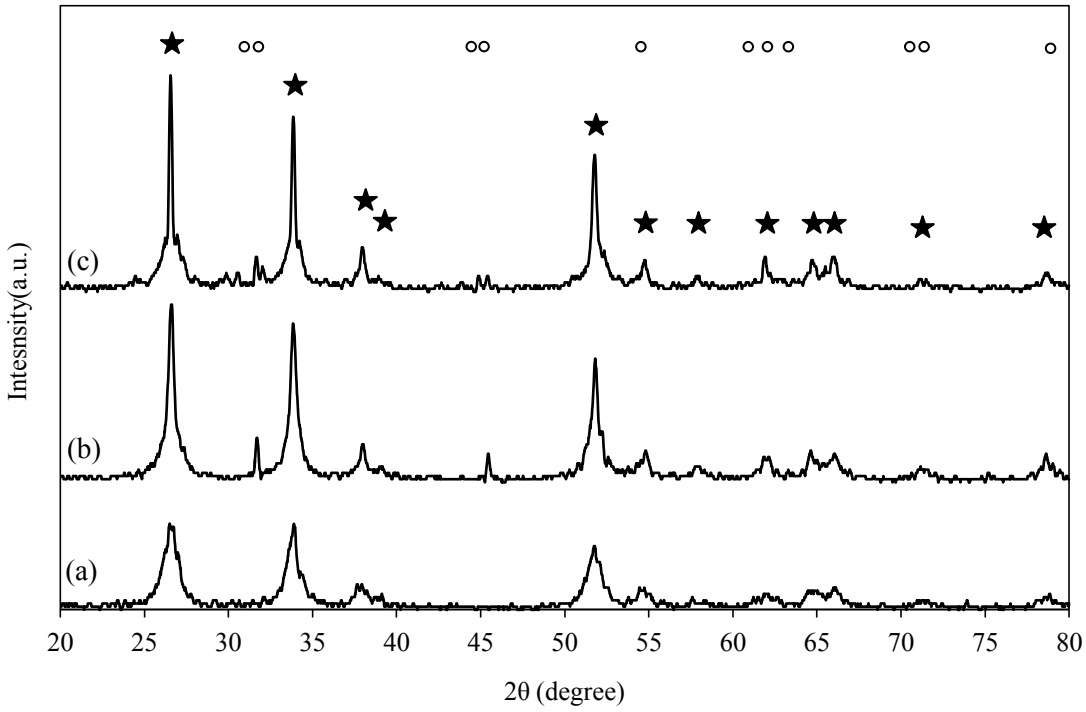

Figure 4.54 XRD patterns of the synthesized tin dioxide prepared without RF gel (a), with RF gel (b) and tin dioxide pyrolyzed before calcination. ○ and ★ denotes Sn phase and SnO_2, respectively.

Table 4.16 Crystallite size of tin dioxide without RF gel, with RF gel template and with carbon template

Sample	Crystallite size (nm)
Without RF gel	6.98
With RF gel template	22.69
With Carbon template	35.33

Pyrolysis is the process that decomposes organic material at elevated temperature in the absence of oxygen. In this study, pyrolysis of the dried gel is used to convert RF gel to carbon template before removing the template by calcination in order to assure that RF gel is not decomposed before tin dioxide occurred. The dried gel was pyrolyzed in N_2 atmosphere at 500^{o}C for 6 hours with heating rate 5^{o}C/min. After pyrolysis, the Sn/carbon composite is

obtained. Then, Sn/carbon composite was calcined at 500^{o}C for 6 hours. The result from surface measurement indicates that surface area is decreased after calcination due to removing carbon template as illustrated in Table 4.17. Comparing the tin dioxide product with and without pyrolysis, it was found that pyrolysis does not affect an amount of surface area as shown in BET result (See in Table 4.17). Moreover, N_2 adsorption-desorption analysis reveals that both products have mesoporous structure (Type IV isotherm) as presented in Figure 4.55. Nevertheless, pore volume of the product using carbon template is higher than the synthesized product using RF gel template as shown in Table 4.17. This means pore size of the product using carbon template is bigger than pore size of the product using RF template. Moreover, pyrolysis of the dried gel before calcination results in larger crystallite size (See in Table 4.16). It may be resulted from heat treatment time, affecting growth of particles due to total heat treatment time of the product prepared from pyrolyzed gel is higher than the product synthesized without pyrolysis. It can be concluded that not only calcination temperature has an effect on crystallite size but also a period of time that spends in calcination process.

Table 4.17 properties of Sn/Carbon composite and the tin dioxide synthesized using RF gel template and carbon template.

Sample	Surface area (m^2/g)	V_p (cm^3/g)
Sn/Carbon composite	791.27	0.3961
Tin dioxide using RF gel template	31.19	0.0304
Tin dioxide using carbon template	30.62	0.0736

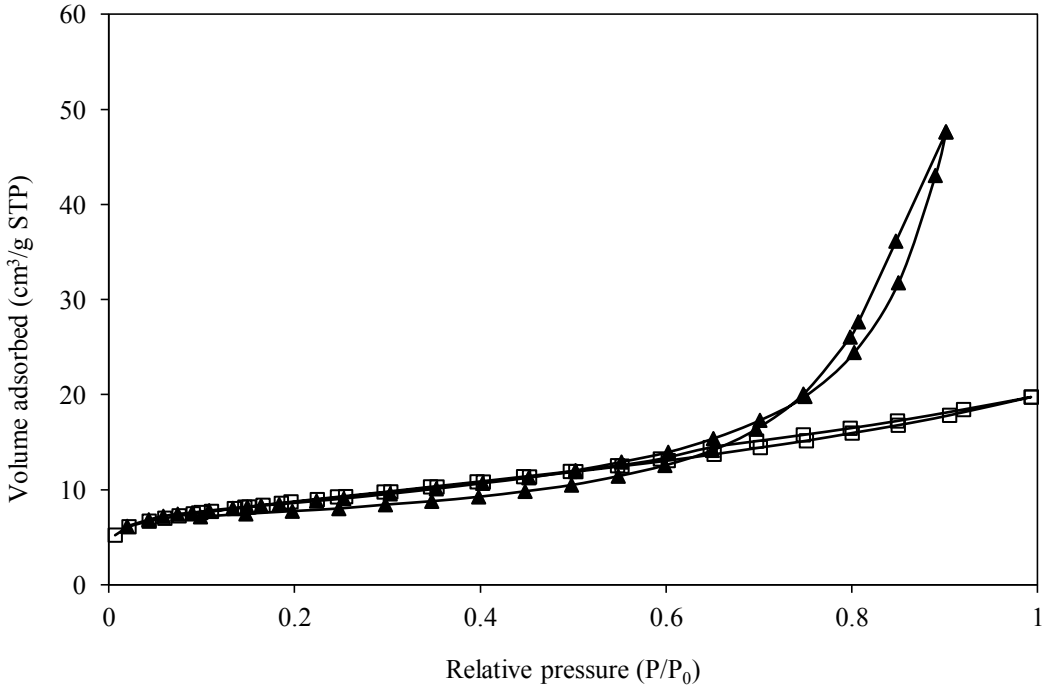

Figure 4.55 N_2 adsorption-desorption isotherm of tin dioxide synthesized using (□) RF gel template and (▲) carbon template.

These results confirm that using RF gel as a template has an efficiency as same as using carbon template. There are some advantages of RF gel template such obtained small pore product. However, it depends on the application that tin dioxide was used. For example, the product synthesized by using carbon template is suitable for gas sensor application owing to wide range of pore size that can accommodate complex chemicals.

4.4 Comparison of the tin dioxide using surfactant template and rf template

Although the specific surface area of the obtained product assisted by rf gel is less than tin dioxide prepared by surfactant template (previous research), synthesis of mesoporous tin dioxide using RF gel as template has outstanding advantages, namely, low cost and easy to handle. The lower specific surface area of tin dioxide can be explained by consideration at mechanism formation of the tin dioxide. Using surfactant template involves the arrangement of molecules to form porous structure, whereas using rf gel only relates to connection of the particles.

CHAPTER V

CONCLUSION AND RECOMMENDATIONS

5.1 Summary of results

The summary of the results are listed as follows:

1. The obtained tin dioxide with using RF-gel has mesoporous structure and higher surface area than the synthesized product prepared without RF gel.
2. There is an interaction between tin sol and RF gel involving in the synthesis of mesoporous tin dioxide. Moreover, tin sol accerelates formation of RF networks.
3. Process parameters, i.e., concentration of reactants, aging time of tin sol, aging time of RF gel and aging time of mixed gel, affect properties of final product. Surface area of product is increased by increasing Sn/R molar ratio, aging time of tin sol, aging time of RF gel and aging time of mixed gel, whereas decreasing Sn/F molar ratio and R/C molar ratio results in decreased surface area.
4. Addition of diluting solvent, i.e., ethanol and water enhances the interaction between tin sol and RF gel. This results in increased surface area of the product.
5. Different drying process results in different properties of the product. The surface area of tin dioxide prepared from freeze dried gel is higher than the product prepared by conventional drying.
6. The highest surface area of synthesized tin dioxide is 56.95 m^2/g. This product was prepared by aging for the mixed gel of 5 days.
7. At high calcination temperature (700^oC), the product is pure tin dioxide, which has tetragonal rutile structure. Metallic tin phase still appeared in the product calcined at temperature lower than 700^oC.
8. RF-gel template has an efficiency as same as carbon gel. The surface of synthesized product with RF gel template is nearly equal to the product prepared by using carbon template.

5.2 Conclusion

Mesoporous tin dioxide was successfully synthesized via sol-gel method using resorcinol-formaldehyde gel as a template. Strong interaction between tin sol and RF gel results in high surface area of the obtained product. Size of RF particles also has impact on its properties such as pore size distribution and surface area. These factors could be controlled by

altering process condition such as concentration of reactants, aging time of tin sol, aging time of RF gel and aging time of mixed gel. Freeze drying can retain porosity of the tin dioxide mesoporous during drying process.

5.3 Recommendations for future work

There are some recommendations for future work as shown in the following:

1. For product synthesized without RF-gel, its color is quite yellow. However, XRD pattern shows the product is cassiterite, which has tetragonal rutile structure. This result should be further investigated.
2. The applications of obtained tin dioxide should be studied such as kinetically efficient and long-term lithium storage and gas sensing performance.

REFERENCES

[1] Alothman, Z. A Review: Fundamental Aspects of Silicate Mesoporous Materials.Materials. 5 (2012): 2874-2902.

[2] Bouzerara, F., Harabi, A., Achour, S., and Larbot, A. Porous ceramic supports for membranes prepared from kaolin and doloma mixtures. Journal of the European Ceramic Society. 26 (2006): 1663-1671.

[3] Mao, X., Wang, S., and Shimai, S. Porous ceramics with tri-modal pores prepared by foaming and starch consolidation. Ceramics International. 34 (2008): 107-112.

[4] Zhang, W., Wang, H., and Jin, Z. Gel casting and properties of porous silicon carbide/silicon nitride composite ceramics. Materials Letters. 59 (2005): 250-256.

[5] Isobe, T., Shimizu, M., Matsushita, S., and Nakajima, A. Preparation and gas permeability of the surface-modified porous Al_2O_3 ceramic filter for CO_2 gas separation. Journal of Asian Ceramic Societies. 1 (2013): 65-70.

[6] Li, J., Lin, H., and Li, J. Factors that influence the flexural strength of SiC-based porous ceramics used for hot gas filter support. Journal of the European Ceramic Society. 31 (2011): 825-831.

[7] Johnson, B. R., Canfield, N. L., Tran, D. N., Dagle, R. A., Li, X. S., Holladay, J.D., and Wang, Y. Engineered SMR catalysts based on hydrothermally stable, porous, ceramic supports for microchannel reactors. Catalysis Today. 120 (2007): 54-62.

[8] Yokota, T., Takahata, Y., Katsuyama, T., and Matsuda, Y. A new technique for preparing ceramics for catalyst support exhibiting high porosity and high heat resistance. Catalysis Today. 69 (2001): 11-15.

[9] Basu, S., Saha, M., Chatterjee, S., Mistry, K. K., Bandyopadhay, S., and Sengupta, K. Porous ceramic sensor for measurement of gas moisture in the ppm range. Materials Letters. 49 (2001): 29-33.

[10] Guo, W., Liu, T., Wang, J., Yu, W., Sun, R., Chen, Y., Hussain, S., Peng, X., and Wang, Z. Hierarchical ZnO porous microspheres and their gas-sensing properties. Ceramics International. 39 (2013): 5919-5924.

[11] Bagheri-Mohagheghi, M. M., Shahtahmasebi, N., Alinejad, M. R., Youssefi, A., and Shokooh-Saremi, M. The effect of the post-annealing temperature on the nano-structure and energy band gap of SnO_2 semiconducting oxide nano-particles synthesized by polymerizing-complexing sol-gel method. Physica B. 403 (2008): 2431-2437.

[12] Shimizu, Y. and Egashira, M. Basic aspects and challenges of semiconductor gas sensors. Mrs Bulletin. 24 (1999): 18-24.

[13] Yamazoe, N. New approaches for improving semiconductor gas sensors. Sensors and Actuators B: Chemical. 5 (1991): 7-19.

[14] Zhang, P., Huang, S.-Y., and Popov, B. N. Mesoporous Tin Oxide as an Oxidation-Resistant Catalyst Support for Proton Exchange Membrane Fuel Cells. Journal of the Electrochemical Society. 157 (2010): B1163-B1172.

[15] Jin, Z., Zhou, H.-J., Jin, Z.-L., F Savinell, R., and Liu, C.-C. Application of nano-crystalline porous tin oxide thin film for CO sensing. Sensors and Actuators B: Chemical. 52 (1998): 188-194.

[16] Shimizu, Y., Jono, A., Hyodo, T., and Egashira, M. Preparation of large mesoporous SnO_2 powder for gas sensor application. Sensors and Actuators B: Chemical. 108 (2005): 56-61.

[17] Toupance, T., Babot, O., Jousseaume, B., and Vilaça, G. Nanocrystalline mesoporous tin dioxide prepared by the sol-gel route from a dialkoxydi (β-diketonato) tin complex. Chemistry of materials. 15 (2003): 4691-4697.

[18] Wen, Z., Wang, Q., Zhang, Q., and Li, J. In Situ Growth of Mesoporous SnO_2 on Multiwalled Carbon Nanotubes: A Novel Composite with Porous‐Tube Structure as Anode for Lithium Batteries. Advanced Functional Materials. 17 (2007): 2772-2778.

[19] Li, G. J. and Kawi, S. Synthesis, characterization and sensing application of novel semiconductor oxides. Talanta. 45 (1998): 759-766.

[20] Xu, C., Tamaki, J., Miura, N., and Yamazoe, N. Grain size effects on gas sensitivity of porous SnO_2-based elements. Sensors and Actuators B: Chemical. 3 (1991): 147-155.

[21] Yamazoe, N. and Miura, N. Some basic aspects of semiconductor gas sensors. Chemical Sensor Technology. 4 (1992): 19-42.

[22] Fujihara, S., Maeda, T., Ohgi, H., Hosono, E., Imai, H., and Kim, S.-H. Hydrothermal routes to prepare nanocrystalline mesoporous SnO_2 having high thermal stability. Langmuir. 20 (2004): 6476-6481.

[23] Hieda, K., Hyodo, T., Shimizu, Y., and Egashira, M. Preparation of porous tin dioxide powder by ultrasonic spray pyrolysis and their application to sensor materials. Sensors and Actuators B: Chemical. 133 (2008): 144-150.

[24] Bruno, L., Pijolat, C., and Lalauze, R. Tin dioxide thin-film gas sensor prepared by chemical vapour deposition: influence of grain size and thickness on the electrical properties. Sensors and Actuators B: Chemical. 18 (1994): 195-199.

[25] Song, K. C. and Kim, J. H. Synthesis of high surface area tin oxide powders via water-in-oil microemulsions. Powder Technology. 107 (2000): 268-272.

[26] Chen, F. and Liu, M. Preparation of mesoporous tin oxide for electrochemical applications. Chem. Commun. (1999): 1829-1830.

[27] Emons, T. T., Li, J., and Nazar, L. F. Synthesis and characterization of mesoporous indium tin oxide possessing an electronically conductive framework. Journal of the American Chemical Society. 124 (2002): 8516-8517.

[28] Siciliano, P. Preparation, characterisation and applications of thin films for gas sensors prepared by cheap chemical method. Sensors and Actuators B: Chemical. 70 (2000): 153-164.

[29] Tang, W. and Cameron, D. C. Aluminum-doped zinc oxide transparent conductors deposited by the sol-gel process. Thin Solid Films. 238 (1994): 83-87.

[30] Ahmed, J., Vaidya, S., Ahmad, T., Sujatha Devi, P., Das, D., and Ganguli, A. K. Tin dioxide nanoparticles: reverse micellar synthesis and gas sensing properties Materials Research Bulletin. 43 (2008): 264-271.

[31] Wang, Y.-D., Ma, C.-L., Sun, X.-D., and Li, H.-D. Synthesis of mesostructured SnO_2 with CTAB and hydrous tin chloride. Materials Letters. 51 (2001): 285-288.

[32] Zhou, S., Lu, S., Ke, Y., and Li, J. Synthesis of mesostructured tin oxide with neutral surfactant as a template in aqueous media. Materials Letters. 57 (2003): 2679-2681.

[33] G. Severin, K. and M. Abdel-Fattah, T. Supramolecular assembly of mesostructured tin oxide. Chemical Communications. 0 (1998): 1471-1472.

[34] Song, K. C. and Kang, Y. Preparation of high surface area tin oxide powders by a homogeneous precipitation method. Materials Letters. 42 (2000): 283-289.

[35] Yu, A. and Frech, R. Mesoporous tin oxides as lithium intercalation anode materials. Journal of Power Sources. 104 (2002): 97-100.

[36] Pekala, R. W. Organic aerogels from the polycondensation of resorcinol with formaldehyde. Journal of Materials Science. 24 (1989): 3221-3227.

[37] Babić, B., Kaluđerović, B., Vračar, L., and Krstajić, N. Characterization of carbon cryogel synthesized by sol–gel polycondensation and freeze-drying. Carbon. 42 (2004): 2617-2624.

[38] irglov , . and a ldonado- dar, F. J. Chemical Interactions of Surface-Active Agents with Growing Resorcinol-Formaldehyde Gels. Langmuir. 26 (2010): 16103-16109.

[39] Ihokura, K. and Watson, J. The stannic oxide gas sensor. CRC Press: Boca Raton, Florida, Chapters. 2 (1994): 4.

[40] Seiyama, T., Kato, A., Fujiishi, K., and Nagatani, M. A New Detector for Gaseous Components Using Semiconductive Thin Films. Analytical Chemistry. 34 (1962): 1502-1503.

[41] Dibbern, U., Kuersten, G., and Willich, P. Gas sensitivity, sputter conditions and stoichiometry of pure tin oxide layer. Chemical Sensors. (1986): 127-130.

[42] Mukhamedshina, D. M. and Beisenkhanov, N. B. Influence of Crystallization on the Properties of SnO_2 Thin Films. Advances in Crystallization Processes. (2012): 219-258.

[43] Pan, X. Q. and Fu, L. Oxidation and phase transitions of epitaxial tin oxide thin films on (1^{-} 012) sapphire. Journal of Applied Physics. 89 (2001): 6048-6055.

[44] Farrukh, M. A., Tan, P., and Adnan, R. Influence of reaction parameters on the synthesis of surfactant-assisted tin oxide nanoparticles. Turk J Chem. 1 (2012): 12.

[45] Haines, J. and Leger, J. M. X-ray diffraction study of the phase transitions and structural evolution of tin dioxide at high pressure: ffRelationships between structure types and implications for other rutile-type dioxides. Physical Review B. 55 (1997): 11144.

[46] Liu, C.-M., Chen, X.-R., and Ji, G.-F. First-principles investigations on structural, elastic and electronic properties of SnO_2 under pressure. Computational Materials Science. 50 (2011): 1571-1577.

[47] Geckeler, K. E. and Rosenberg, E. Functional nanomaterials: American Scientific Publishers Valencia, 2006.

[48] Pawar, B. G., Pinjari, D. V., Kolekar, S. S., Pandit, A. B., and Han, S. H. Effect of Sintering Temperatures on the Synthesis of SnO ISRN Chemical Engineering. 2012 (2012): 1-7.

[49] Sergent, N., Gélin, P., Périer-Camby, L., Praliaud, H., and Thomas, G. Preparation and characterisation of high surface area stannic oxides: structural, textural and semiconducting properties. Sensors and Actuators B: Chemical. 84 (2002): 176-188.

[50] Jensen, W. B. Holleman-Wiberg's Inorganic Chemistry (edited by Wiberg, Nils). Journal of Chemical Education. 79 (2002): 944.

[51] Salehi, H., Aryadoust, M., and Farbod, M. Electronic and structural properties of tin dioxide in cubic phase. Iranian Journal of Science & Technology. 34 (2010): 131-138.

[52] Velásquez, C., Rojas, F., Ojeda, M. L., Ortiz, A., and Campero, A. Structure and texture of self-assembled nanoporous SnO_2. Nanotechnology. 16 (2005): 1278.

[53] Göpel, W. and Schierbaum, K. D. SnO_2 sensors: current status and future prospects. Sensors and Actuators B: Chemical. 26 (1995): 1-12.

[54] Brinker, C. J. and Scherer, G. W. Sol-gel science: the physics and chemistry of sol-gel processing: Academic Pr, 1990.

[55] Kung, H. H. and Ko, E. I. Preparation of oxide catalysts and catalyst supports—a review of recent advances. The Chemical Engineering Journal and the Biochemical Engineering Journal. 64 (1996): 203-214.

[56] Mark, J. E., Allcock, H. R., and West, R. Inorganic Polymers: Oxford University Press, 1989.

[57] Van Boxtel, H. A., Kase, A., Iwasa, Y., and Toda, Y., Photographic colour material containing a resorcinol derivative as black coupler. Google Patents, 2008.

[58] Lin, C. and Ritter, J. A. Effect of synthesis pH on the structure of carbon xerogels. Carbon. 35 (1997): 1271-1278.

[59] Pekala, R. W., Alviso, C. T., Kong, F. M., and Hulsey, S. S. Aerogels derived from multifunctional organic monomers. Journal of non-crystalline solids. 145 (1992): 90-98.

[60] Lin, C. and Ritter, J. A. Carbonization and activation of sol–gel derived carbon xerogels. Carbon. 38 (2000): 849-861.

[61] Cook, R. C., Letts, S. A., Overturf Iii, G. E., Lambert, S. M., Wilemski, G., and Schroen-Carey, D. Low-density-foam shells. Inertial confinement. 1 (1996): 22-30.

[62] Pekala, R. W., Low density, resorcinol-formaldehyde aerogels. Google Patents, 1989.

[63] Berthon, S., Barbieri, O., Ehrburger-Dolle, F., Geissler, E., Achard, P., Bley, F., Hecht, A.-M., Livet, F., Pajonk, G. M., and Pinto, N. DLS and SAXS investigations of organic gels and aerogels. Journal of non-crystalline solids. 285 (2001): 154-161.

[64] Yamamoto, T., Nishimura, T., Suzuki, T., and Tamon, H. Control of mesoporosity of carbon gels prepared by sol–gel polycondensation and freeze drying. Journal of non-crystalline solids. 288 (2001): 46-55.

[65] Petričević, R., Glora, . , and Fricke, . Planar fibre reinforced carbon aerogels for application in PEM fuel cells. Carbon. 39 (2001): 857-867.

[66] Mendenhall, R. S., Andrews, G. R., Bruno, J. W., and Albert, D. F., Process for high temperature production of organic aerogels. Google Patents, 2000.

[67] Saliger, R., Bock, V., Petricevic, R., Tillotson, T., Geis, S., and Fricke, J. Carbon aerogels from dilute catalysis of resorcinol with formaldehyde. Journal of non-crystalline solids. 221 (1997): 144-150.

[68] Tamon, H., Ishizaka, H., Mikami, M., and Okazaki, M. Porous structure of organic and carbon aerogels synthesized by sol-gel polycondensation of resorcinol with formaldehyde. Carbon. 35 (1997): 791-796.

[69] Al-Muhtaseb, S. A. and Ritter, J. A. Preparation and properties of resorcinol–formaldehyde organic and carbon gels. Advanced materials. 15 (2003): 101-114.

[70] Zanto, E. J., Al-Muhtaseb, S. A., and Ritter, J. A. Sol-gel-derived carbon aerogels and xerogels: Design of experiments approach to materials synthesis. Industrial & engineering chemistry research. 41 (2002): 3151-3162.

[71] Pekala, R. W., Alviso, C. T., and LeMay, J. D., Organic aerogels: A new type of ultrastructured polymer. Lawrence Livermore National Lab., CA (USA), 1991.

[72] Pröbstle, H., Schmitt, C., and Fricke, J. Button cell supercapacitors with monolithic carbon aerogels. Journal of Power Sources. 105 (2002): 189-194.

[73] Liang, C., Sha, G., and Guo, S. Resorcinol–formaldehyde aerogels prepared by supercritical acetone drying. Journal of non-crystalline solids. 271 (2000): 167-170.

[74] Tamon, H., Ishizaka, H., Yamamoto, T., and Suzuki, T. Preparation of mesoporous carbon by freeze drying. Carbon. 37 (1999): 2049-2055.

[75] Yamamoto, T., Sugimoto, T., Suzuki, T., Mukai, S. R., and Tamon, H. Preparation and characterization of carbon cryogel microspheres. Carbon. 40 (2002): 1345-1351.

[76] Tamon, H., Ishizaka, H., Yamamoto, T., and Suzuki, T. Influence of freeze-drying conditions on the mesoporosity of organic gels as carbon precursors. Carbon. 38 (2000): 1099-1105.

[77] Kocklenberg, R., Mathieu, B., Blacher, S., Pirard, R., Pirard, J.-P., Sobry, R., and Van den Bossche, G. Texture control of freeze-dried resorcinol–formaldehyde gels. Journal of non-crystalline solids. 225 (1998): 8-13.

[78] Kaschmitter, J. L., Mayer, S. T., and Pekala, R. W., Process for producing carbon foams for energy storage devices. Google Patents, 1998.

[79] Feng, J., Feng, J., and Zhang, C. Shrinkage and pore structure in preparation of carbon aerogels. Journal of sol-gel science and technology. 59 (2011): 371-380.

[80] Inagaki, M. Pores in carbon materials-importance of their control. New Carbon Materials. 24 (2009): 193-232.

[81] Ariga, K., Vinu, A., Yamauchi, Y., Ji, Q., and Hill, J. P. Nanoarchitectonics for mesoporous materials. Bulletin of the Chemical Society of Japan. 85 (2012): 1-32.

[82] Rouquerol, J., Avnir, D., Fairbridge, C. W., Everett, D. H., Haynes, J. M., Pernicone, N., Ramsay, J. D. F., Sing, K. S. W., and Unger, K. K. Recommendations for the characterization of porous solids (Technical Report). Pure and Applied Chemistry. 66 (1994): 1739.

[83] Zhao, X. S., Lu, G. Q., and Millar, G. J. Advances in mesoporous molecular sieve MCM-41. Industrial & engineering chemistry research. 35 (1996): 2075-2090.

[84] Pierotti, R. A. and Rouquerol, J. Reporting physisorption data for gas/solid systems with special reference to the determination of surface area and porosity. (1985): 603-619.

[85] Poljanšek, I. and Krajnc, . Characterization of phenol-formaldehyde prepolymer resins by in line FT-IR spectroscopy. Acta Chimica Slovenica. 52 (2005): 238-244.

[86] Zhang, J. and Gao, L. Synthesis and characterization of nanocrystalline tin oxide by sol–gel method. Journal of Solid State Chemistry. 177 (2004): 1425-1430.

[87] Nlp, N. Characterization of poly (methyl methacrylate)-tin (IV) chloride blend by TG-DTG-DTA, IR and Pyrolysis-GC-MS techniques. Bull. Korean Chem. Soc. 32 (2011): 3295.

[88] Krissanasaeranee, M., Supaphol, P., and Wongkasemjit, S. Preparation of poly (vinyl alcohol)/tin glycolate composite fibers by combined sol–gel/electrospinning techniques and their conversion to ultrafine tin oxide fibers. Materials Chemistry and Physics. 119 (2010): 175-181.

[89] Han, S., Jang, B., Kim, T., Oh, S. M., and Hyeon, T. Simple Synthesis of Hollow Tin Dioxide Microspheres and Their Application to Lithium ‐ Ion Battery Anodes. Advanced Functional Materials. 15 (2005): 1845-1850.

[90] Ulagappan, N. and Rao, C. N. R. Mesoporous phases based on SnO_2 and TiO_2. Chem. Commun. (1996): 1685-1686.

APPENDICES

APPENDIX A

THERMAL ANALYSIS OF TIN DIOXIDE PARTICLES

Table A.1 shows carbon content in the product which has the highest surface area in each experiment in order to confirm the surface area of the product is not resulted from remaining carbon in the product.

Table A.1 Carbon content of the tin dioxide products.

Process condition	Condition	% Carbon content
Sn/F molar ratio	0.007	2.05
R/C molar ratio	50	2.92
	100	3.44
	200	5.01
	300	1.43
Sn/R molar ratio	0.03	8.44
Type of diluting solvent	None	7.18
	Water	9.11
	Ethanol	6.56
Aging time of tin sol	120 hours	5.01
Aging time of RF gel	4 hours	5.30
Aging time of mixed gel	5 days	5.33
Drying process	Freeze drying	5.99
	Conventional drying	4.88
Calcination temperature	400^{o}C	9.73
	500^{o}C	2.56
	600^{o}C	3.45
	700^{o}C	2.37

APPENDIX B

CALCULATION OF SPECIFIC AREA OF TIN DIOXIDE

In this part, the specific surface area of the product, which be calcined at 500^{o}C, was calculated from the following equation using given data.

Data: Size of tin dioxide particles (measured by Semafore program) 125.94 nm
Crystallite size 22.69 nm
Actual surface area

Equation: Specific surface area $= \frac{4\pi r^2}{(4/3)\pi r^3 \rho}$

where r is radius of tin dioxide particles and ρ is density of tin dioxide = 6.95 g/m^2.

The specific surface area of the products is 6.86 and 38.05 m^2/g calculated by using size of the particles from Semafore program and crystallite size, respectively. Comparing the specific surface area calculated by using size of the particles (measured by Semafore program) and measurement by BET analysis, the product has actual specific surface area more than calculation. This means each particle, called secondary particle, has pore inside the structure. However, the surface area which calculated from crystallite size is higher than the actual surface area. It indicates that primary particles connected together to form secondary particles. In addition, the size of tin dioxide particles which was measured by Semafore program is larger than crystallite size. This result suggests that the agglomeration occurs during the fabrication.

APPENDIX C

THERMAL EVENT OF SN/RF COMPOSITE

In order to study thermal event of Sn/RF composite at 240 ^{o}C, the functional group of composites which be calcined at 180 and 280 ^{o}C were identified by FTIR technique. It was found that some functional groups disappeared during calcinations as shown in Figure C.1. However, those functional groups can not be specified at this moment.

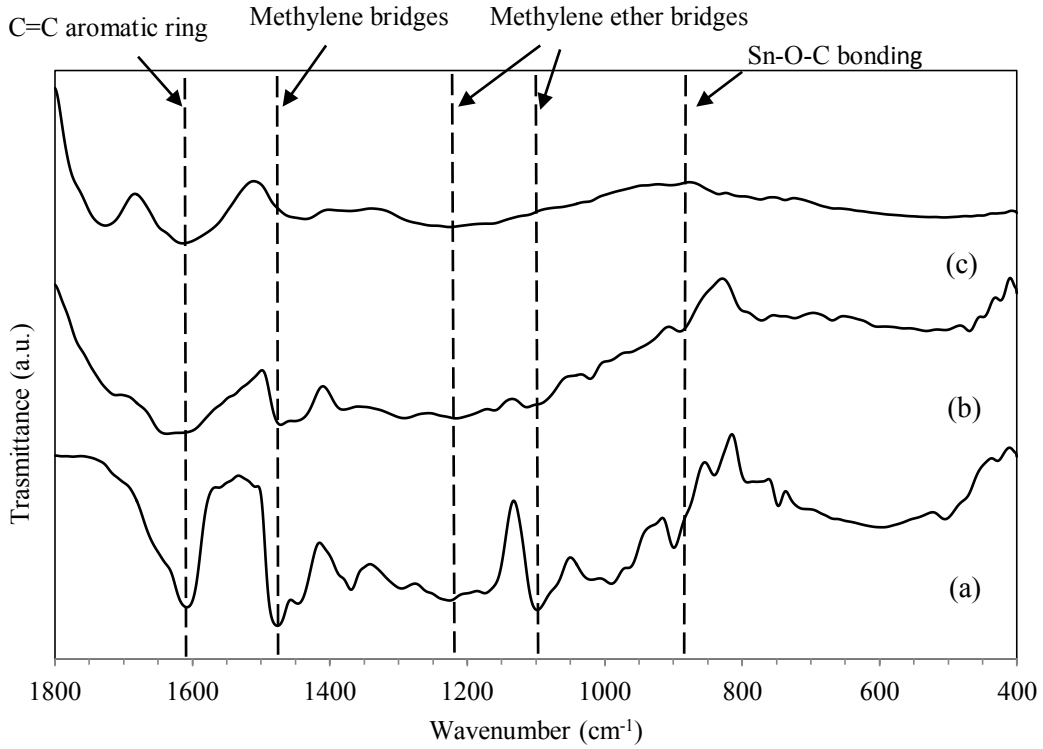

Figure C.1 FTIR spectrum of the precalcined composite (a), product calcined at 180^{o}C (b) and product calcined at 280^{o}C (c).

Table C.1 shows surface area and pore volume of the composites which be calcined at 180 and 280 ^{o}C. It can be seen that the composite calcined at 180^{o}C has high surface area due to carbon remains in the product. After calcination at 280^{o}C, residue carbon is removed out of the product. Thus, the surface area is dramatically decreased but still greatly higher than the product calcined at 500^{o}C.

Table C.1 Properties of the products calcined at various calcination temperatures.

Calcination temperature (^oC)	Surface area (m^2/g)	V_p $cm^3(STP)/g$
180	213.61	0.3365
280	152.31	0.2358
500	40.55	0.0640

Figure C.2 shows XRD pattern of the composites which be calcined at 180 and 280 ^oC. It reveals that at 180^oC the composite is amorphous material. After increasing calcination temperature to 280^oC, metallic tin phase, tin oxide phase and tin dioxide phase appeared. This means formation of tin dioxide phase occurs at lower 280^oC.

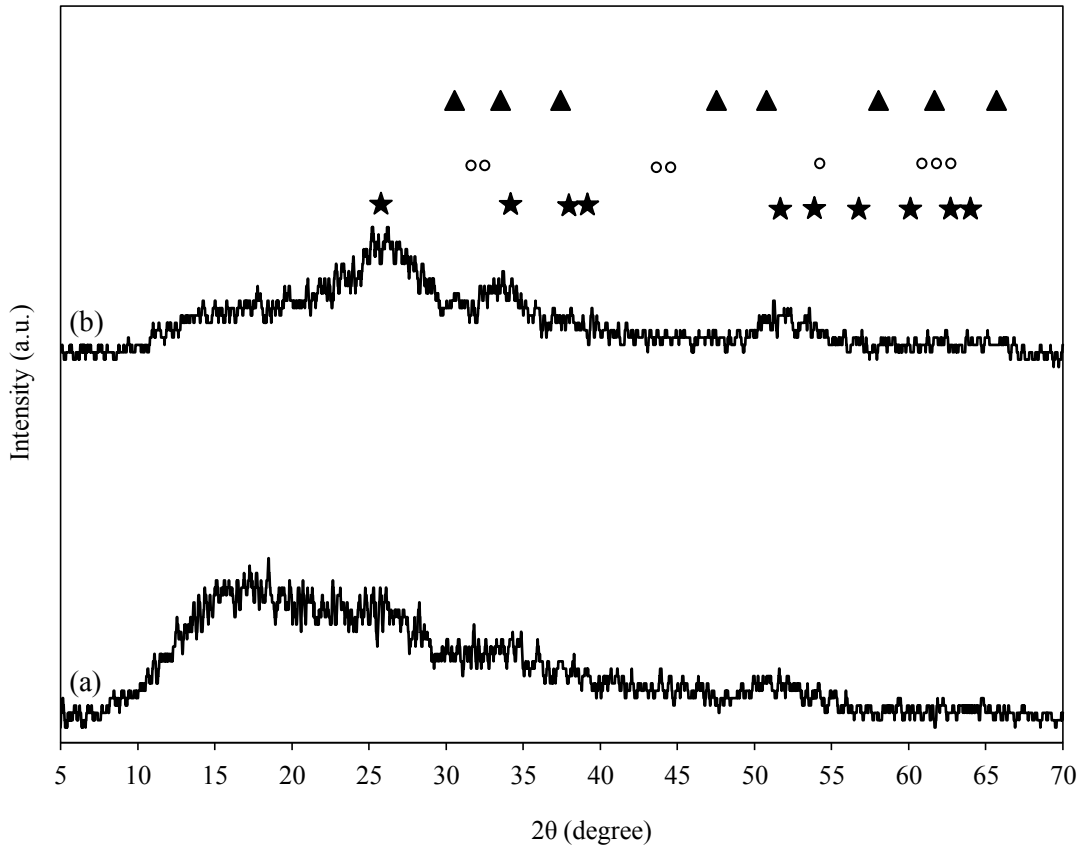

Figure C.2 XRD patterns of the synthesized tin dioxide product calcined at 180^oC (a) and 280^oC (b). ○, ▲ and ★ denotes Sn phase, SnO phase and SnO_2 phase, respectively.

APPENDIX D

THE MORPHOLOGY OF MATERIAL DURING SYNTHESIS

Figure D.1 shows SEM image of precalcined Sn/RF composite and tin dioxide product. It can be seen that the product obtained from drying process has the different morphology compared to tin dioxide product. The precalcined composite was composed of smaller interconnected particles.

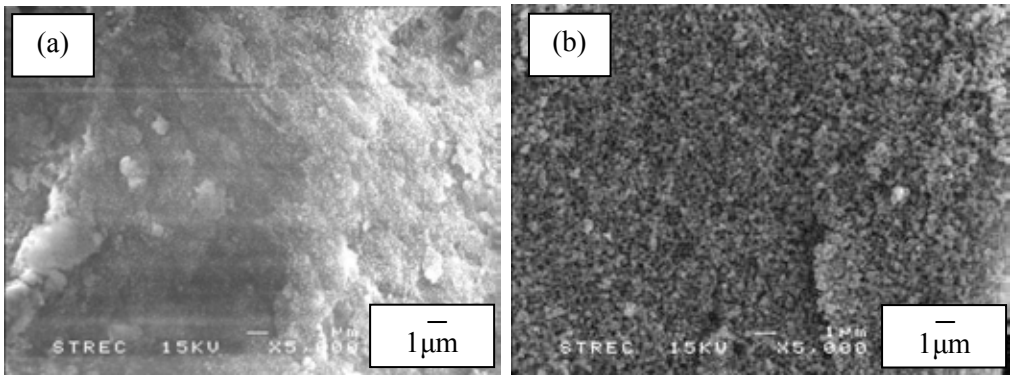

Figure D.1 SEM images of precalcined Sn/RF composite (a) and tin dioxide product (b).

APPENDIX E

EFFECT OF TYPE OF SOLVENT IN PREFORMED TIN SOL

In this study, tin dioxide was prepared with different type of solvent in preformed tin sol step. The amount of solvent, i.e., formaldehyde (F) and ethanol (E), is fixed. Concentration of chemicals is also fixed at certain amount. The mixed gel was aged for 3 days, dried by freeze drying process and then calcined at 500^{o}C.

Figure E.1 shows FTIR spectrum of the precalcined composite prepared with Sn/F sol and Sn/E sol. The spectrum of composite prepared with ethanol is quite similar to spectrum from composite prepared with formaldehyde. Moreover, FTIR signal ratio of methylene bridge, methylene ether bridge and Sn-O-C bonding is not changed by altering type of solvent in preformed tin sol as shown in Table E.1. This means type of solvent, which was used in the preformed tin sol step, does not affect interaction between tin sol and rf gel. Moreover, this result suggests that tin sol has greater effect on formation of RF gel and interaction between tin sol and rf gel than excess formaldehyde.

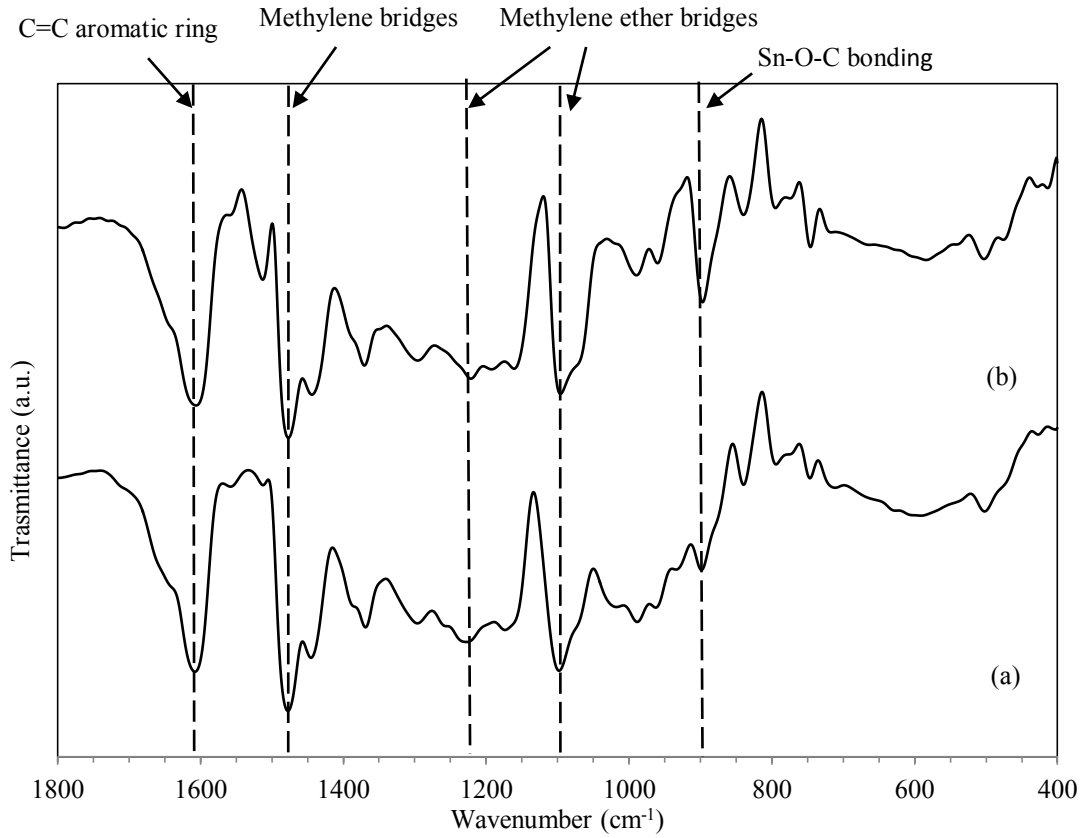

Figure E.1 FTIR spectrum of the precalcined composite prepared with Sn/F sol (a) and Sn/E sol (b).

Table E.1 FTIR signal ratio of the composite prepared with different solvent in tin sol.

Type of solvent	Signal ratio		
	Methylene ether bridge	Methylene bridge	Sn-O-C bonding
Formaldehyde	1.47	0.99	0.46
Ethanol	1.39	0.91	0.44

Nevertheless, the product which prepared by using ethanol has surface area larger than the product using formaldehyde as shown in Table E.2. This could be resulted from the time that spent through galation step of mixture prepared form Sn/E sol is greatly longer than mixture prepared from Sn/F sol. It allows the tin sol to homogeneously mix with rf gel, which results in more uniform interaction between tin sol and rf gel. Considering adsorption-desorption isotherm of both products, the result shows type IV isotherm which indicates mesoporous structure (See in Figure E.2). It can be concluded that type of solvent in the preformed tin sol does not affect formation of mesoporous tin dioxide.

Table E.2 Surface area and mean pore diameter of the obtained product prepared from different solvent in tin sol.

Type of solvent	Surface area (m^2/g)	V_p $cm^3(STP)/g$	Mean pore diameter (nm)
Formaldehyde	39.25	0.0811	4.82
Ethanol	50.42	0.1128	13.88

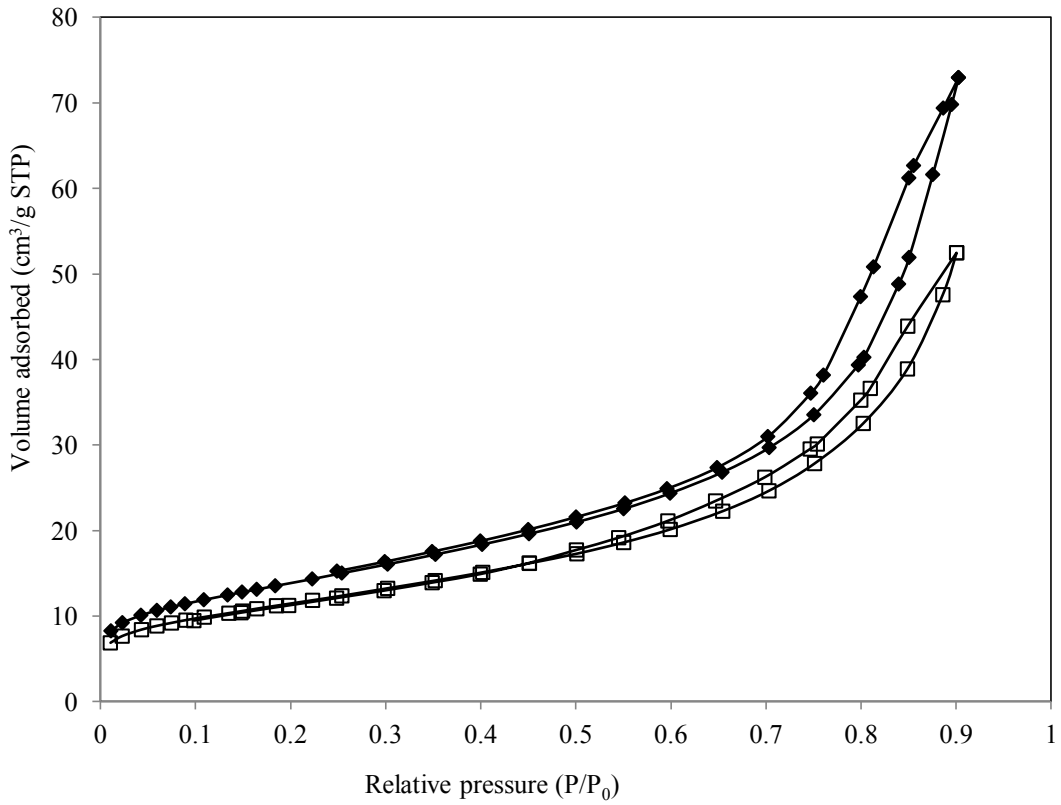

Figure E.2 N_2 adsorption-desorption analysis of tin dioxide product prepared with (□) Sn/F sol and (♦) Sn/E sol.

APPENDIX F

LIST OF PUBLICATION

1. Kornkamol Banjerdteerakul, Varong Pavarajarn “SYNT ESIS OF E SOPOROUS TIN DIOXIDE ASSISTED BY RESORCINOL/FOR A LDE YDE GEL”, The 3rd International Thai Chemical Engineering and Applied Chemistry conference, Khon Kaen, Thailand, October 17-18,2013.
2. Kornkamol Banjerdteerakul, Varong Pavarajarn “INCORPORATION OF RESORCINOL-FORMALDEHYDE GEL FOR THE FABRICATION OF E SOPOROUS TIN DIOXIDE”, CREN 2013, igashi-Hiroshima, Japan, November 25-26, 2013.

VITA

Miss Kornkamol Banjerdteerakul was born on March 5th, 1990 in Bangkok, Thailand. She received the Bachelor's Degree of Engineering with major in Chemical Engineering from Chulalongkorn University, Bangkok, Thailand in April 2012. She entered the master of Engineering in Chemical Engineering at Chulalongkorn University, Bangkok, Thailand in May 2012.